Extraterrestrial Mass Wasting: Comparing Landslides across the Solar System

Author: Tim van Meurs [6546013]
Supervisor: Dr. Tjalling de Haas
Second corrector: Prof. Dr. Maarten Kleinhans
Third corrector: Sharon Diamant MSc

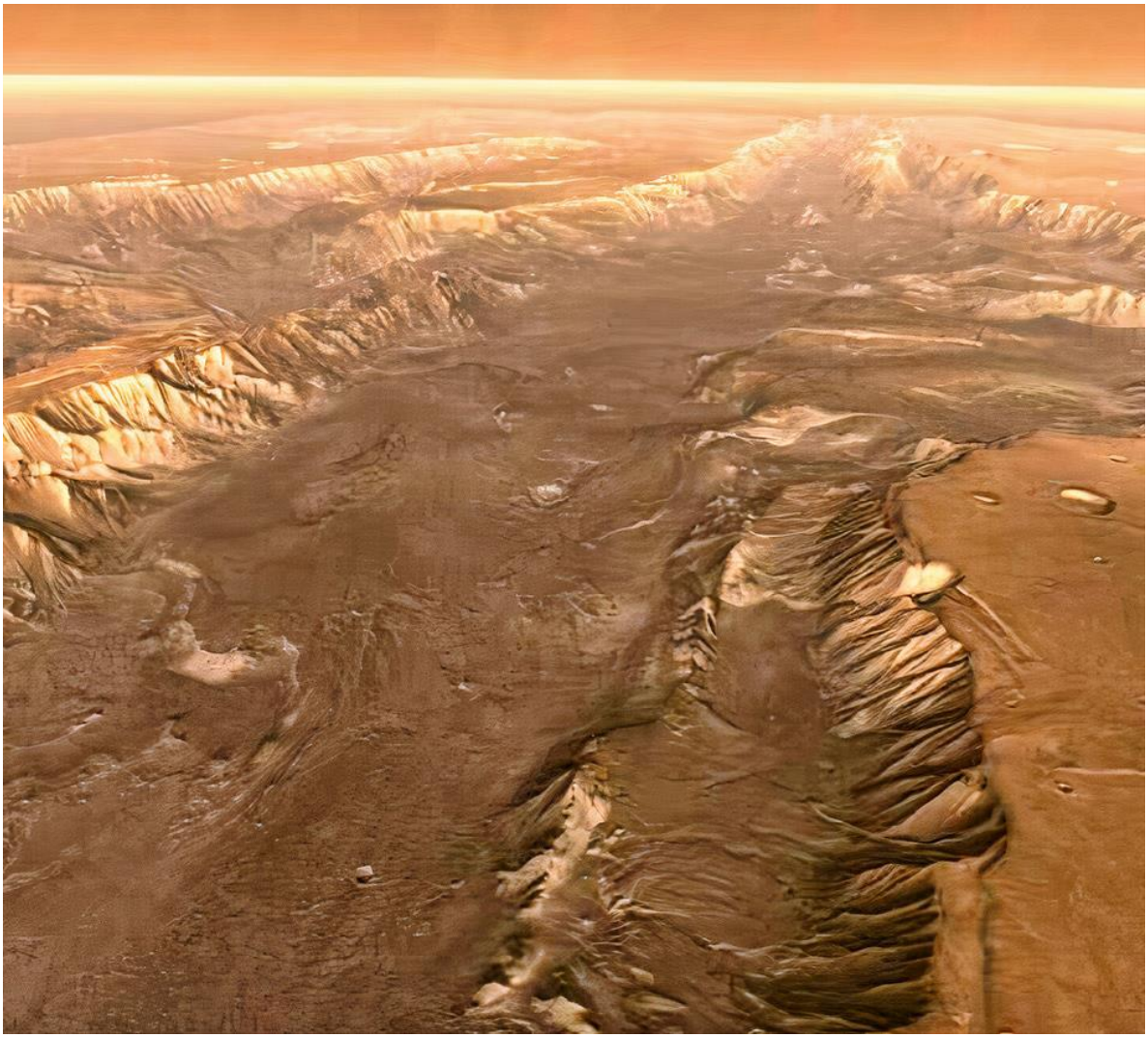

18-10-2024

Acknowledgements

I would like to sincerely thank my supervisor Tjalling de Haas for his support during this thesis project, his valuable insights during the meetings and the extensive feedback were very useful. I would also like to thank Sharon Diamant for the day-to-day supervision during the project, her helpful advice on the writing phase of the project and constant availability for a quick update or question. But most importantly, for her general enthusiasm for planetary and space science, which increased mine even more.

Abstract

Mass wasting, the downslope movement of material such as rock, earth, or debris under the influence of gravity, is a key geomorphological process observed not only on Earth but also across various rocky bodies in the Solar System. These movements occur through different mechanisms, including dry granular flows, liquid lubricated movements, or sublimation-driven processes. Despite numerous studies on extraterrestrial mass wasting, a comprehensive overview of these processes across different celestial bodies has been lacking. This review fills that gap by utilizing a specialized classification system to examine mass wasting features on the Moon, Mars, Mercury, asteroids Ceres and Vesta, and comets 67P and 9P. The analysis reveals that flow-type movements are the most prevalent, with more specific subclasses showing a more diverse distribution. Large slides and slumps are also widespread. Fall-type movements are less commonly identified, mainly due to their smaller size, as quality of surface data significantly influences the detection and identification of features. Morphological analysis of extraterrestrial mass wasting shows that fluidization of the moving material significantly influences the final morphology, especially runout length. Sublimation of volatiles is the most important fluidization agent, though in some rare cases, transient liquid water can cause flow lubrication. A deeper understanding of extraterrestrial mass wasting can provide valuable insights into the surface characteristics of rocky bodies, such as the presence of water ice and other volatiles. Moreover, understanding these processes can assist in identifying safe sites for future human exploration and settlement on the Moon and Mars.

Contents

Chapter 1 – Introduction

1.1 Background

Mass wasting is defined as the downslope movement of material such as rock, earth or debris under the influence of gravity, and it is one of the most common morphological processes. On the earth, mass wasting events occur frequently and can have enormous impacts on landscapes and communities, causing damage, economic losses and deaths (Pradhan & Siddique, 2019). Aside from Earth, mass wasting also occurs on other rocky bodies in the inner Solar System (Mercury (Aubry et al., 2021; Brunetti et al., 2015; Xiao & Komatsu, 2013), Venus (Malin, 1992)and Mars (Conway et al., 2019; Crosta et al., 2018; Dundas et al., 2019; Malin & Edgett, 2000; Quantin et al., 2004; Tesson et al., 2020)), as well as on asteroids (Duarte et al., 2019; Krohn et al., 2014; Otto et al., 2013; Parekh et al., 2021; Schmidt et al., 2017) and comets (Belton & Melosh, 2009; Lucchetti et al., 2019; Pajola et al., 2017; Steckloff et al., 2015). Gravity, though sometimes weaker than we experience on Earth, affects the material on the surface and causes mass wasting to occur. On these bodies, many forms of mass wasting have been observed and it is an ongoing process, with events happening constantly. On a long timescale, mass wasting can be considered the most important factor in shaping the landscapes of the rocky worlds in our Solar System.

On earth water is an important element in mass wasting processes. It is an important factor in the weakening of slopes. When water enters the soil, it gets in between the grains and the water pore pressure reduces the intergranular friction (Keller & DeVecchio, 2019). This leads to a decrease of the resisting forces. Water also brings additional loading onto the soil, increasing the driving forces due to gravity. When these driving forces eventually surpass the resisting forces, the slope becomes unstable and a mass movement can occur (Pradhan & Siddique, 2019). Different amounts of water can lead to varying types of mass wasting (Cruden & Varnes, 1996).

In the Solar System, it is very rare for liquid water to exist on the surface of rocky bodies. However, mass wasting features are observed with morphologies that suggest fluidized movement. Therefore, there must be an explanation for this behavior. There are three ways in which mass wasting material can be mobilized. These are dry granular flow, lubricated flow and sublimation driven flow. Although their names here indicate flow movement, these mechanisms are also involved in slide and slump-type movements. The different mechanisms are somewhat related to water content in terrestrial mass wasting, in the sense that they have a different degree of fluidization.

Dry granular flow describes the movement of granular material that is not fluidized by liquid or gaseous substances, but moves downslope under the influence of gravity. The movement is influenced by basal friction and intergranular friction. These types of movements generally form slides or small-scale flows (Senthil Kumar et al., 2013) . However, Krohn et al. (2014) found that dry granular flows can in some cases form more flow-like movements.

Lubricated flow is flow that is partly fluidized, but does not behave like a fluid completely. This can occur in several ways. Schmidt et al. (2017) found that for flows on the asteroid Ceres, ice grains within a flowing mass can start to melt, making the flow more mobile. De Blasio (2011) proposes lubrication due to melt as a possible cause for the reduction of basal friction, leading to longer runout flows. Another way lubricated flow can occur, is by the production of transient liquid water. Although very rare, it is possible for water to exist in liquid form in very specific temperature and pressure conditions. This is found to be possible on Mars (Hecht, 2002) and on Vesta (Scully et al., 2015). During the

residence time, before it vaporizes again, this water can theoretically lubricate flows. This partial fluidization due to lubrication of flow reduces the intergranular friction, and increases the mobility.

Sublimation driven flow is a type of flow that has been fluidized by gasses produced as a result of ice sublimation. This can occur when subsurface ice is heated by solar irradiance. The volume flux of the produced gas is so large, that the intergranular friction is decreased significantly (de Haas et al., 2019; Mangold, 2011). As a result, the material behaves like a fluid and can shape landforms that were otherwise impossible. In some cases, frictional heating between the grains of a flow can lead to even more sublimation. This mobilizes even more material, causing entrainment, which allows the flow to grow in volume and gain momentum (de Haas et al., 2019). Hugenholtz (2008) proposes a link between frosted granular flow, a rare type of flow on Earth where frost reduces intergranular friction, and fluidized flow by CO_2 vaporization in Martian gullies. Roelofs et al. (2024) showed in laboratory experiments under Martian conditions that flows experiencing sublimation of CO_2 particles in the material display a high degree of fluidization. These flows were found to exceed flow velocities 2 – 3 times higher than dry granular flows.

Whether or not volatile substances play a role in the mass wasting process at a certain location is an important distinction to make. Not only can this influence the mobility of a movement and therefore determine the morphology and extent of a feature, but it also reveals information about the contents of the subsurface (Crosta et al., 2018). The presence of volatile substances such as CO_2 and H_2O in the subsurface can be revealed in the form of these mass wasting events. A good understanding of how these mass wasting processes work can therefore aid in the search for water (-ice) or other important resources on rocky bodies in the Solar System (Hecht, 2002; Orosei et al., 2020; Schmidt et al., 2017; Scully et al., 2015).

1.2 Available research

Mass wasting on Earth is studied extensively. Using observations from satellite data with high spatial and temporal resolution, drone observations, ground-based photo and video footage, and field research valuable data can be gathered. Thanks to all these methods, we know a lot about how mass movements occur and what effects they can have on their surroundings. However, this wide range of research methods is not available for extraterrestrial mass wasting. For these events, only satellite data can be used to observe the resulting morphology. Fortunately, weak erosional forces on rocky bodies with no atmosphere allow many features to be preserved for a long time, making studying mass wasting features easier. The difficult part is collecting high-resolution observations. All available planetary data comes from space missions that are sent to a specific target, carrying scientific instruments. Collecting this data from bodies far away is a much more complex task compared to data from Earth orbit or surface observations. Factors like orbit height, spacecraft capabilities and technological advancement at the time of launch all influence the quality of imagery data gathered from a celestial body. Appendix A1 gives an overview of the image quality as well as elevation data quality of all bodies discussed in this review. Appendix A2 contains a description of the space missions relevant to the collection of this data, including information on the cameras and sensors used.

During early decades of research on extraterrestrial mass wasting, only large-scale implications of mass movements could be found, like modified or degraded craters (Moore et al., 1999; Schultz & Gault, 1975). Later, the identification of individual features and their attributes became possible, allowing for more detailed hypotheses on their formation (Malin & Edgett, 2000). Now, more data with increasing quality is being collected by satellites across the solar system, allowing mass movements to be studied in higher resolution. Research is done on many different scales, ranging from an entire celestial body (e.g. Conway et al., 2019), to a specific region like Valles Marineris on Mars (e.g. Quantin et al., 2004),

or even a single impact crater (de Haas et al., 2019). This is visible in the maps in appendix A3. Especially on Mars, where the majority of data points are located in Valles Marineris, while the rockfalls identified by Tesson et al. (2020) are concentrated around 60° to 120° east. Sometimes, findings are compared to mass wasting on Earth (e.g. Brunetti et al., 2015). And in some cases, two bodies are discussed in one study (Brunetti et al., 2015; Parekh et al., 2021). An overview of mass wasting processes on all rocky bodies in our solar system, however, has not yet been made. Comparing the characteristics and behavior of such processes between all these different worlds, rather than only to the Earth, could provide useful insights into what processes are important in their triggering and movement.

1.3 Relevance

Although the conditions are wildly different on all rocky worlds orbiting our Sun, the basic physical principles that guide mass wasting processes are the same, namely the downward movement of material along a slope is forced by gravity. However, there are countless ways in which the movement can vary. The triggering, erosion or incision, entrainment, mobilization, and deposition of a mass wasting event can all be influenced by local conditions and play an important role in how the feature takes shape and how it is preserved over time. Mass wasting features, their morphology and mobility in an environment can therefore tell us a lot about the conditions and the materials at the location (Aubry et al., 2021; Crosta et al., 2018). This way, we learn more about what it is like on the surface of our planetary neighbors.

Morphological features identified on other worlds often share similarities with those found here on Earth, like the shape of a landslide deposit or the presence of lateral levees along debris flows. The mechanisms behind their formation are therefore thought to be similar as well, but this is not necessarily the case. For instance, the formation of gullies on Mars was initially linked to liquid water (Malin & Edgett, 2000), because that is how gullies form here on Earth. Now we know that there are other ways in which these features can form, like dry granular flow (Krohn et al., 2014), or sublimation driven flow (de Haas et al., 2019; Roelofs et al., 2024). If we truly understand how the observed features form and if certain substances play a role in this formation, we can learn a lot about the presence of these minerals on the surfaces of celestial bodies.

Furthermore, if we envision a future in which humans will embark on long-term missions to the Moon, Mars or beyond, there will have to be permanent bases on these locations. If humans are going to settle on an unknown world, it is important that this will be at a safe location. We know the damage mass movements can inflict here on Earth, so a deep understanding of extraterrestrial mass wasting and the underlying mechanisms is therefore crucial to future astronaut safety.

1.4 Research aims

This thesis aims to create an overview of all mass wasting activity happening on a wide selection of rocky bodies in our solar system. The bodies discussed in this review are the Moon, Mars, Mercury, asteroids Ceres and Vesta, and comets 67P and 9P. Mass wasting occurring on the surfaces of these bodies is investigated and classified so that a clear overview can be made showing what processes can be observed on the different worlds. Furthermore, the mechanisms responsible for the triggering and the overall motion of the wasting material are discussed. By investigating a wide range of bodies, and the differences and similarities between them, this review aims to make a holistic overview of mass wasting in the solar system in general. The main research questions are:

1. What types of mass wasting have been identified on different rocky bodies in the Solar System?
    - Can these be classified using Earth-based classification?
    - How do mass wasting features of the same class differ on various bodies?
2. What are the main driving factors in extraterrestrial mass wasting?
    - Which factors precondition slope instabilities?
    - What are important triggering factors?
    - Where and how does fluidization influence mass wasting mobility?
    - What is the role of volatiles on mass wasting on the studied bodies?

Chapter 2 – Classification

2.1 Classification of mass wasting types

Cruden & Varnes (1996) propose a mass wasting classification strategy consisting of six types of movement and three types of material that together form the basis for describing all mass wasting. Additional information regarding the activity, rate of movement and moisture content of the landslide can be used to further describe the feature in more detail. The use of the word landslide as a general overarching term for mass wasting processes is not uncommon, although it can certainly be confusing as it hints at the sliding movement type (Shanmugam & Wang, 2015). Therefore, the terms mass wasting or mass movement will be used here to indicate the general process.

Due to water or moisture being mostly absent in liquid form in the extraterrestrial bodies discussed in this research (see chapter 3), the moisture content in the movements is left out of the classification. The activity and rate of movement are left out as well, due to the inability to measure the speed of the processes on bodies other than Earth (Shanmugam & Wang, 2015). Below, five main movement types proposed by Cruden & Varnes (1996) are discussed. Their definition is given, along with attributes of extraterrestrial features of this kind of movement.

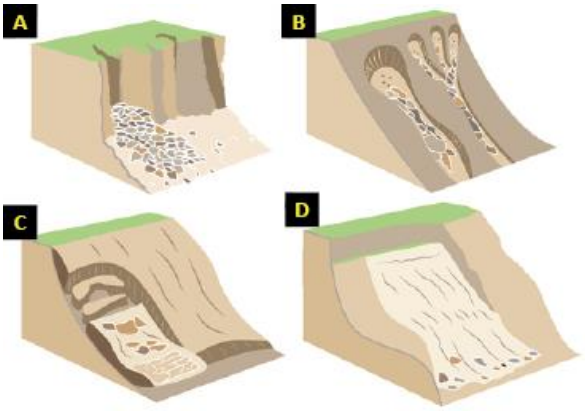

Figure 1: Illustrations of movement types. A) Fall. B) Flow. C) Slide. D) Slump (Image credit: British Geological Survey: https://www.bgs.ac.uk/discovering-geology/earth-hazards/landslides/how-to-classify-a-landslide/).

2.1.1 Fall

Falls are described as a detachment of a block of material from a steep slope, followed by rapid displacement of the material by falling, bouncing and rolling (see Figure 1). Sliding movement over an underlying slope moves the block away from the parent cliff and can create a trail in the soil (Cruden & Varnes, 1996). The main way that fall-type movements are found across the rocky bodies in our Solar System, is as rockfalls. These mostly occur on the steep, almost vertical, cliffs of impact crater rims. Rocks and boulders detach from the parent cliff and fall onto the slope below. Here, a talus cone can form (Pajola et al., 2017). It is also possible for boulders to bounce and roll away from the cliff and toward the crater floor. This can leave a trail of roll and bounce marks on the surface (Kokelaar et al., 2017; Tesson et al., 2020; Xiao et al., 2013). Compared to other types of mass wasting, rock falls are generally quite small in size (Tesson et al., 2020).

Common attributes found in extraterrestrial *falls* are (see also Figure 3)(Kokelaar et al., 2017; Pajola et al., 2017; Tesson et al., 2020; Xiao et al., 2013):

- Talus cone / apron of debris below ridge.
- Longitudinal tracks downslope, along with bounce marks or ‘pit chains’.

- Boulders are present at the bottom of the slope.

2.1.2 Flow

Flows are a type of mass wasting where the detached material is non-cohesive and behaves as a fluid, generally moving rapidly downslope (see Figure 1). Intergranular movement is the dominant type of motion and there are no stable shear surfaces. Flows can often originate from slide-type movements that lose cohesion, take up water or achieve high velocities. The volume of the flow can increase during an event due to material gained by entrainment. Important sub-types of flow include channelized and open-slope flows, indicating whether the flow follows a pre-existing path or flows freely along a slope. In addition, avalanche and creep are two subclasses based (partly) on velocity. The former being a large, extremely rapid (open-slope) type of flow and the latter an extremely slow flow. Finally, in extraterrestrial settings, ejecta flows formed around impact craters are an important subclass. These sub-types are discussed below (Cruden & Varnes, 1996; de Haas et al., 2019; Shanmugam, 2015).

Common attributes found in extraterrestrial *flows* are (see also Figure 3)(Conway et al., 2019; Crosta et al., 2018; Kokelaar et al., 2017; Krohn et al., 2014; Otto et al., 2013; Parekh et al., 2021; Xiao et al., 2013; Xiao & Komatsu, 2013):

- Bulbous front / terminal ridge.
- Parallel striations in the flow direction.
- Marginal levees.
- Lobate or finger-like frontal deposits* on moderate slopes.
- Sheet-like debris fans or aprons on low slopes.
- Boulders are rare.
- Multiple cycles of erosion and deposition by flows cause evolution of the feature.
- Tributary organization possible.

* Kokelaar et al. (2017) makes the distinction between lobate and finger-like frontal deposits based on the length to width ratio of the deposit. If *L:W* is larger than 1.5 the deposit is finger-like and if *L:W* is smaller than 1.5 it is lobate.

Flows can be subdivided into different types. Two subtypes also present in the classification by Cruden & Varnes (1996), are creep and avalanche. Here, these classes are adopted as important subclasses. A distinction between channeled flows and sweeping flows is also introduced, based on the type of interaction with local topography. Avalanche and creep features are classified based on velocity of movement. And finally, ejecta flows are crucial movement types in extraterrestrial context. On cratered bodies, these features are abundant and distinguishable from other types. Below, these subclasses are described, and their attributes are listed.

Avalanche

Although an avalanche is a part of the flow-type mass movement class, it can be advantageous to include it as a class of its own. Cruden & Varnes (1996) describe avalanches as large, extremely rapid, open-slope flows. Avalanches are identified on multiple bodies in the Solar System (Crosta et al., 2018; Kokelaar et al., 2017; Otto et al., 2013; Quantin et al., 2004; Xiao & Komatsu, 2013). Because involvement of liquid water in large scale flows such as avalanches, this class only contains dry granular avalanches and sublimation-driven avalanches. Although velocity of the avalanche cannot be observed Shanmugam & Wang (2015), avalanches typically have longer runout deposits which can be linked to high velocity events (Crosta et al., 2018). Important morphological distinctions between flows and avalanches in this classification are (see also Figure 3)(Crosta et al., 2018; Cruden & Varnes, 1996):

- Large size, high volume.

- Long runout.
- Open-slope flow, so it does not follow local topography.

Creep

Varnes (1978) mentioned the term creep as a type of extremely slow movement, occurring in both rocky material (called deep creep) as well as soils. The most important distinction is the velocity of the flow, so the movement type can exist in various materials and circumstances. The problem with identifying creep on rocky bodies other than Earth, is that direct velocity measurements are not possible (Shanmugam & Wang, 2015). Therefore, classification is based on attributes that indicate slow movement, like gentle slopes and relatively large areas that flow as one mass. Distinctions from other flow types can be made based on the differences in morphology of the deposits (Xiao et al., 2013). Key attributes for creeps are the following (see also Figure 3) (Kokelaar et al., 2017; Otto et al., 2013; Xiao et al., 2013).

- Extensive area.
- Convex shape upwards.
- Transverse ridges ("elephant hide").
- Gentle slopes.

Channeled flow

When the material in a flow is concentrated by local topography, incision or other factors, it is considered a channeled flow. This does not necessarily mean that a channel is created by the flow itself by incision, but it is a possibility (Senthil Kumar et al., 2013). These types of flow are closely correlated to gully morphologies, which are described as alcove-channel-fan systems in which flow-type movements take place that shape the landform (Conway et al., 2019). The frequently mentioned 'spur and gully' morphology is also related to this type of channeled flow (Krohn et al., 2014). Some common attributes for channeled flow features are (see Figure 3)(Conway et al., 2019; Kokelaar et al., 2017; Krohn et al., 2014; Xiao et al., 2013):

- Spur or alcove .
- Channel or chute.
- Depositional fan.
- Marginal levees.
- Concentrated flow, follows local topography.

Sweeping flow:

Flows where the material is not concentrated, but rather flows downslope along a wider area are classified as sweeping flows. These flows do not form channels or debris aprons. Rather, the material is deposited in thin sheets along the width of the failure slope. Sweeping flows often have long runouts and do not follow local topography, which can be explained by relatively high velocity (Xiao et al., 2013). Common attributes of sweeping flows are (see Figure 3)(Schmidt et al., 2017; Xiao et al., 2013):

- No flow concentration, constant width.
- Sheet-like deposits.
- Not affected by local topography.

Ejecta flow:

When considering mass wasting on celestial bodies, flows directly related to meteorite impacts have to be included. Ejecta flows are a special kind of mass movement, as they are unique in material type, location and movement characteristics. This is why they are regarded as a separate subclass of flow. These flows occur exclusively in ejecta blankets that surround impact craters. This means that the flow

material is always ejecta material, which is often fine-grained (Xiao & Komatsu, 2013). These flows are always directed outward from the crater rim and as a result, they can cover extensive areas around the crater. Schmidt et al. (2017) found that these types of flows can cover up to 20% of the crater rim. Common attributes of ejecta flows are (see Figure 3)(Crosta et al., 2018; Schmidt et al., 2017; Xiao & Komatsu, 2013):

- Outward from crater rim.
- Constant thickness.
- Sinuous or semicircular edges.

2.1.3 Slide (translational)

A slide is the shear-surface movement of a mass of material along a generally planar surface of rupture, which can grow larger from an initial failure surface (see Figure 1). A slide moves translationally downslope, with little to no intergranular movement and with the surface layer remaining on top. While there is no internal deformation of the sliding mass, surface cracks may form. The sliding mass can exceed the rupture surface, sliding onto the original slope below (Cruden & Varnes, 1996; Shanmugam & Wang, 2015).

Common attributes found in extraterrestrial *slides* are (see Figure 3)(Brunetti et al., 2015; Kokelaar et al., 2017; Krohn et al., 2014; Otto et al., 2013; Parekh et al., 2021; Quantin et al., 2004; Xiao et al., 2013):

- Eroded scarp.
- No (spur and) gully morphology or boulders.
- Slight compression or extension features.
- No large transverse features.
- Lobate tongue or elongated lobes at the base.

2.1.4 Slump (rotational slide)

A slump is described as a mass of material sliding downslope across a curved concave surface of rupture with relatively little deformation (see Figure 1). This type of movement is also called a rotational slide. The slump generally consists of cohesive material that detaches as one block when the slope is sufficiently steep (Varnes, 1978). Due to the rotational shear surface movement, the surface tilts backwards in upslope direction. The head of the slump block moves downwards following the failure surface, while the lower part moves over the end of the rupture surface. This forms the toe, which can be elevated due to the concave shape of the rupture surface (Cruden & Varnes, 1996).

Common attributes found in extraterrestrial *slumps* are (see Figure 3)(Brunetti et al., 2015; Crosta et al., 2018; Kokelaar et al., 2017; Krohn et al., 2014; Otto et al., 2013; Parekh et al., 2021; Xiao et al., 2013).

- Steep, almost vertical scarp that is often curved.
- Concave or spoon-shaped cross-section.
- Tilted back block, with generally little deformation.
- Transverse features may include ridges and cracks.
- Generally large in volume, with thick deposits over a short distance.

2.1.5 Spread & topple

A spread is described as an extension of a cohesive mass of material over an underlying layer of soft material. Subsidence into the softer layer is normal during this process. Unlike slides and slumps, there is no intense shear surface. Rather, there is a flowing layer of a certain thickness along which the

movement takes place. This type of movement is often linked to water-related processes like liquefaction (Cruden & Varnes, 1996). Although a spreading of material is observed frequently in extraterrestrial settings, this type of mass movement consisting of two layers is not found on other bodies except Earth. The observed spreading is a result of a flowing or sliding motion in downslope and lateral direction, forming debris aprons or fans. In these cases, an underlying layer of soft material is not the cause for this behavior and thus the term spread cannot be used as a classification.

Cruden & Varnes (1996) describe a sixth type of movement: topple (see Figure 2). Toppling describes the rotational detachment of a mass of material from a slope. This type of movement can lead to falls or slides. Due to the similar behavior of the detached material in topples and falls, Xiao et al. (2013) did not separate these two movements. And since there are very few cases of extraterrestrial mass wasting classified as this type, the topples are left out of this overview.

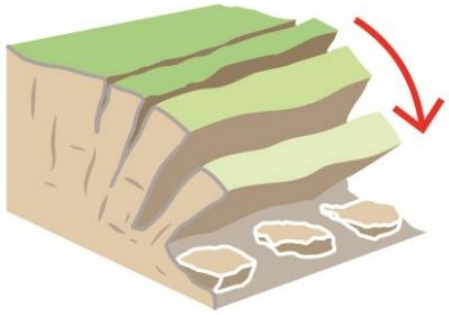

Figure 2: Illustration of a topple-type movement (Image credit: Brittish Geological Survey: https://www.bgs.ac.uk/discovering-geology/earth-hazards/landslides/how-to-classify-a-landslide/).

2.1.6 Intermediate classes

In the end, mass wasting classification is somewhat arbitrary so there will always be features that do not fully fit into one category. The morphology is dependent not only on the movement type but also on the material, geological and physical context, and timescale (Duarte et al., 2019; Xiao et al., 2013). This can cause features to share attributes from two or more of the before-mentioned classes. This can also be the case for features at different scales, e.g., small-scale slumps may look similar to debris flow deposits (Xiao et al., 2013). Also, behavior of a mass movement can vary. A generally incoherent flow can sometimes act as a more cohesive mass (Shanmugam & Wang, 2015). These inconsistencies can make strict classification difficult, and it can therefore be useful to use intermediate stages. For example, Crosta et al. (2018) describe intermediate characteristics of features between slumps and flows as well as features between rock avalanche and ejecta features. When expanding a dataset of flows on Ceres using a predetermined classification, Duarte et al. (2019) found that most of the features actually had an intermediate morphology between the classes.

Another way such an intermediate class can be useful is in a situation where a mass wasting event of one type gradually transitions into another. Slumps and slides can transform into flow-type movements due to a loss of cohesion, an increase in velocity, an increase in water content or a combination of factors (Crosta et al., 2018; Kokelaar et al., 2017; Varnes, 1978). Varnes (1978) initially stated that movements that transform into another type are classified as ‘complex’ movements. However, Hungr et al. (2014) argued that almost every mass movement is complex to a degree. Instead, the primary and secondary types of movement should both be mentioned.

Numerous other classes are used by authors that are only relevant to their studies. They can be used to compare features based on specific, research-related qualities. For instance, Quantin et al. (2004), made a distinction between chaotic and structured landslides and classified these further based on the presence of debris aprons. This is an example where classes are created to incorporate more detail (zooming in). Another way classes can be introduced is to group multiple features (zooming out). Otto et al. (2013) introduced a class called combining various types of mass wasting that all occurred within impact craters, fittingly called intra-crater mass wasting. Features classified as such will not be included in this research or will be reclassified according to the attributes discussed above.

2.2 Scale limitations

The mass wasting features discussed in this chapter are observed using imagery captured by satellites orbiting the rocky bodies. This satellite imagery is often of high enough quality that landforms can be identified, and features can be used to classify mass wasting deposits. However, this is not always the case. Appendix A2 gives an overview of relevant space missions sent to the bodies discussed in this review. The focus of the mission, the overall capability of the spacecraft and the advancements in camera technology at the time of launch are some factors that can influence the image data gathered by the mission. As a result, the resolution of image data can vary significantly between target bodies and between missions. Appendix A1 shows an overview of the resolution of the available imagery of the Moon, Mars, Mercury, Ceres, Vesta and comets 67P and 9P. This table shows that Mercury has the lowest image quality out of all bodies. With a resolution of 166 m/pixel, only very large features can be identified, and it can be difficult to see subtle differences needed for correct distinction between slide and slump. On the other hand, very high-resolution images are available of the Moon (0.5 m/pixel, local mosaics) and Mars (0.3 m/pixel, local images). These images make small scale observations of mass wasting events possible, like the identification of individual boulders. For Ceres and Vesta, global mosaics have been made on both high-altitude mapping orbit (HAMO) and low altitude mapping orbit (LAMO), resulting in different resolutions (Russell & Raymond, 2011)(see appendix A2 for more detail). The LAMO data has a resolution of 35 m/pixel for Ceres and 20 m/pixel for Vesta. This allowed for the identification of slumps, slides and flows smaller than a kilometer in length (Parekh et al., 2021).

Besides the visual interpretation of mass wasting features, poor data resolution can inhibit the use of elevation-related information such as fall height or slope, which is useful for classifying a feature or determining geometry and flow characteristics. For example, slumps have a characteristic tilted back head which makes accurate elevation data helpful in the classification process. In most cases, the resolution of elevation models is lower than that of the surface imagery (see appendix A1: Imagery and resolutions). Elevation data with a resolution too coarse compared to the feature size is a limitation in the measurement and quantification of mass wasting morphology (Parekh et al., 2021).

Low resolution imagery can limit the identification of mass wasting features, and it influences what types are identified. If only very large features are visible, this creates a bias on what types of mass wasting are identified on that body. Slides occur in a wide range of sizes (Brunetti et al., 2015) and slumps are generally quite large (Xiao et al., 2013), so these types are likely the first features to be observed. Flows and especially falls are typically much smaller in size and therefore require higher image quality to be identified. Avalanches are an exception, since these are extremely large flows.

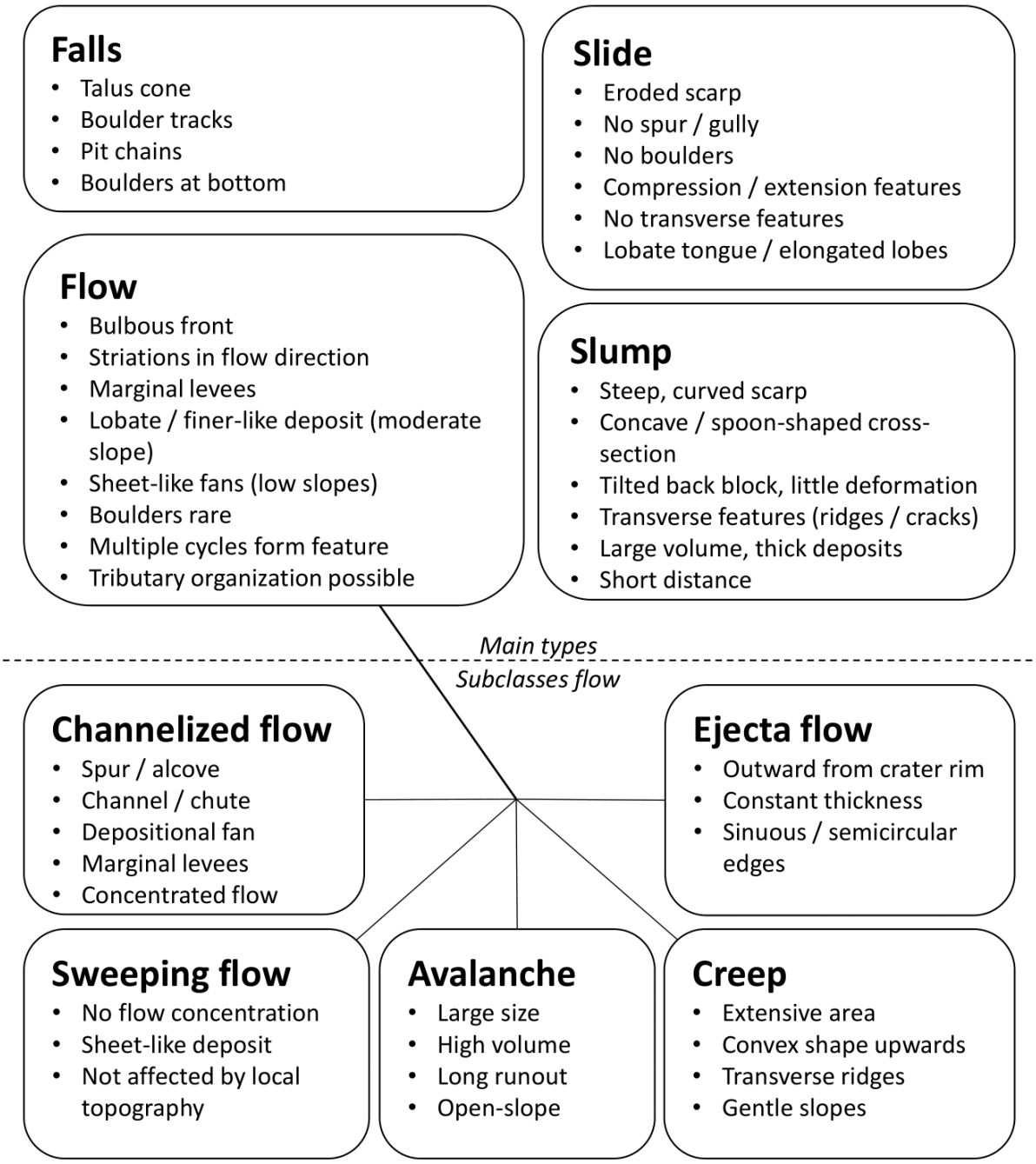

Figure 3: Overview of main mass wasting types and subclasses of flow-type movements. Per class, important attributes used in classification are given.

Chapter 3 – Mass Wasting on Rocky Bodies

3.1 All bodies compared

In this chapter, we examine the different types of mass wasting that are present on each rocky body. This is done using the classification discussed in Chapter 2. Using the same definition of movement types everywhere makes it possible to compare the bodies. Furthermore, it allows for a clear overview of observed mass wasting processes around the Solar System. Table 1 shows this overview where in the first half of the table, the presence of the main movement types is displayed as falls, flow, slides and slumps. And in the second half, the subclasses of flow-type movements are shown.

This table shows that on the Moon and Mars, all four main movement types are present, but the types of flow that occur are different. Only two of the main movement types are observed on Mercury, namely flows and slides. On Ceres and Vesta, no falls have been identified so far but flows, slumps and slides are all present. Though, the types of flow on these asteroids are different. On comets, falls and flows have been found to occur on the surface.

Table 1 also shows significant differences in flow types observed on the bodies. For example, avalanches are only identified on Mars thus far.

Table 1: Movement types identified on each body. The main classes used by (Cruden & Varnes, 1996) are shown in the top half as the 'Main classes', and important subclasses of the flow type are shown below.

		the Moon	Mars	Mercury	Ceres	Vesta	Comet 67P	Comet 9P
Main Classes	Fall	x	x				x	
	Slump	x	x		x	x		
	Slide	x	x	x	x	x		
	Flow	x	x	x	x	x		x
Subclasses (flow)	Avalanche		x					
	Creep	x				x		
	Channeled flow	x	x	x		x		
	Sweeping flow	x			x			
	Ejecta flow		x	x	x			

3.2 Moon

3.2.1 Conditions on the Moon

The Moon is the closest rocky body to Earth. Its surface can be divided into two types: the light-colored, older highlands and the younger lowlands, or maria, with their recognizable darker color. The highlands consist of anorthosite rocks and have been subject to, and shaped by, meteoroid impacts during the 'late heavy bombardment' before 3.8 billion years ago (Kokelaar et al., 2017; Xiao et al., 2013). The lower-lying maria consist of basaltic rocks and lava flows, formed between 3.8 and 2.5 Ga and possibly as late as 1 Ga. Due to this younger age, these areas have a lower crater density compared to the highlands. After the late heavy bombardment, volcanism and meteoroid impacts are the main active surface processes. And since 1 Ga, volcanism has stopped and impacts alone shape the surface (Xiao et al., 2013).

The surface of the Moon is covered with loose rocky material called regolith. Fragment sizes can range from tens of meters to a few micrometers, although most of the material is smaller than 1 mm, making it a fine and often powder-like substance (Housen & Wilkening, 1982; Kokelaar et al., 2017). The low gravity of 1.62 m/s^2 affects the angle of repose and the stability of this regolith (Kleinhans et al., 2011). The static angle of repose is increased, and the dynamic angle of repose is decreased, although the effect is found to be minimal on the Moon (Kokelaar et al., 2017). The surface is depleted of crustal volatiles (Brunetti et al., 2015; Xiao et al., 2013), but in permanently shadowed regions on the poles, water ice is present in the subsurface (Kokelaar et al., 2017). This, combined with the absence of liquid water and an atmosphere, leads to a high preserving capacity of lunar morphology because no erosion takes place, except the degradation by mass wasting (Brunetti et al., 2015; Kokelaar et al., 2017; Xiao et al., 2013).

3.2.2 Lunar mass wasting

As shown in Table 1, all four of the main movement types have been identified on the Moon: falls, flows, slides and slumps. Additionally, some flow subtypes can be distinguished. Below, these movements are described. The global distribution of Lunar mass wasting is visualized in the map in appendix A3.1. On this map it can be seen that the majority of observations are done in the maria regions, and less features are found in the highlands.

Fall

On the Moon, fall-type movements have been identified by both Kokelaar et al. (2017) and Xiao et al. (2013). The falls generally occur on steep slopes where the rock is fractured by impacts and are characterized by longitudinal trails originating from, or just below, the crater rim. Usually, boulders of varying sizes can be found at the end of these trails near the bottom of the crater. The trails are not always a continuous line formed by rolling but can also be chains of pits formed by bouncing (Xiao et al., 2013). Smaller material can be entrained by boulder movement and is deposited closer to the source area since larger grains have more momentum to transport them further. This distribution leads to a longitudinal sorting of the displaced material (Kokelaar et al., 2017).

Flow

Flows on the moon can be subdivided based on flow concentration. Xiao et al. (2013) identified both channel forming flows and sweeping flows. Channel forming flows generally have a classic gully-like morphology including, in a downslope direction, an alcove, a channel and a depositional fan (Senthil Kumar et al., 2013; Xiao et al., 2013). Some flows can even incise in bedrock (Senthil Kumar et al.,

2013). Based on a comparison of the flow's albedo and that of the surrounding material, the flows likely consist of regolith or impact melt (Xiao et al., 2013). After detaching from the crater wall, the flows erode channels by pushing local rocks downslope. This is described by Kokelaar et al. (2017) as bulking of the flow, a property of flow-type movements that de Haas et al. (2019) found to be important to accurately model debris flows on Mars. Flows that reach gentle slopes form depositional fans, while flows that end on moderate slopes form lobate or finger-like frontal deposits (Kokelaar et al., 2017). Senthil Kumar et al. (2013) suggest that lunar flows are triggered by seismic shaking due to nearby impacts. They also found that small scale flows can originate from small impacts on the crater wall.

Sweeping flows are not very different from channel forming flows, they simply do not form channels. The flow is more spread out rather than concentrated, although this does not mean that wide sheets are always formed. Xiao et al. (2013) identified sweeping flows that likely formed from similar material as the channel forming slope mentioned previously, but mainly in smaller craters. These sweeping flows did not follow local topography, indicating fast movement, and their behavior implied strong fluidization (Xiao et al., 2013). In both channel forming flows and sweeping flows, the material did not reach the crater floor, but was rather deposited on the walls. Many flow features are smaller than for example slides or slumps, so their deposits will not always reach the flat area of the crater floor.

Creep features are identified on all terrain types on the Moon. They are formed by a slow movement of regolith downslope, without there being a failure. This means that internal deformation dominates the movement. Kokelaar et al. (2017) suggest that the movement is triggered and sustained by small disturbances of the regolith by ground shaking due to either moonquakes or impacts. The movement results in relatively widespread areas with transverse ridges, often referred to as 'elephant hide' (Kokelaar et al., 2017; Xiao et al., 2013).

Slide

Slides on the Moon consist of relatively coherent slabs of regolith that slide downhill across a failure surface. Both rock slides and debris slides are found on the lunar surface (Brunetti et al., 2015; Xiao et al., 2013), distinguished by grain size and cohesion of the sliding mass. Rock slides are likely to form in impact melt sheets due to their unstable underlying slopes and their tendency to shatter on disturbance. Meanwhile, debris slides form in areas of highly fractured bedrock (Xiao et al., 2013). During the slide, the failure surface can grow in size and slight deformation of the slab might occur due to compression and extension. If the sliding mass loses cohesion and falls apart, the movement can transition into a flow-type movement (Kokelaar et al., 2017). The material deposited by slides can fill the crater floor so that a relatively smooth surface is formed.

Slump

Slump features on the Moon are generally found in younger craters. They are thought to form shortly after crater formation, while the material is still unstable. However, slumps are also found in older craters, as well as in tectonic scarps and volcanic rilles (Xiao et al., 2013). During the rotational movement, the mass deforms internally, forming cracks and folds and deposits can pile up at the foot. Similar to slides, slumps can transform into flow-type movements when cohesion is lost (Kokelaar et al., 2017).

3.3 Mars

3.3.1 Conditions on Mars

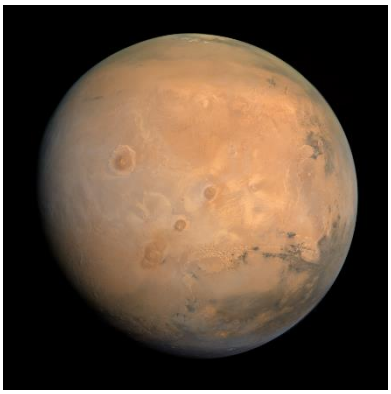

Mars is the closest planet to the Earth and is the only body discussed in this study that has an atmosphere. The gravitational acceleration on Mars is 3.73 m/s^2, 38% of what we experience here on Earth (Williams, 2024). With a surface pressure of around 6 mbar, it is a very thin atmosphere compared with o Earth, but still, it is sizable enough that it allows for aeolian processes (Tesson et al., 2020; Williams, 2024). These processes shape landforms like sand dunes, but can also degrade deposits of mass movements during regular storms, affecting their preserving capacity. The mean temperature on the surface is -63°, but it can vary significantly diurnally and throughout the long seasons of the Martian year, down to -87°C and up to 20°C (Crosta et al., 2018; Tesson et al., 2020; Williams, 2024).

Although liquid water is not thermodynamically stable under Martian conditions, a combination of factors can lead to scenarios where it can exist. The surface pressure is around the triple point pressure of pure water, 611.73 Pa, and the temperature can reach above the melting point so theoretically it can exist (Hecht, 2002). Higher pressures observed in low-lying areas, as well as salts on the surface, can make it easier for water to melt (Diez, 2018; Hecht, 2002). In areas with thin layers of water ice, when the sunlight heats the surface, melt can occur. And when this happens, both evaporation and refreezing happen at slow rates, allowing transient liquid water to exist (Hecht, 2002). Furthermore, water can also surface from aquifers. When at the surface, water generally has a residence time of up to a few hours, meaning that it is possible for liquid water to shape the surface (Conway et al., 2019; Hecht, 2002). Aside from surface water, a stable body of liquid water has been found underneath the south polar ice cap (Diez, 2018; Orosei et al., 2020). This ice cap, together with the northern one, contains most of Mars' water, stored as ice, which is stable under Martian conditions.

Another volatile substance found on the Martian surface is CO_2. The majority of the atmosphere consists of CO_2 gas, around 95% (Crosta et al., 2018; Williams, 2024). Due to the high temperature fluctuations throughout the day, a layer of CO_2 ice can deposit on the surface straight from the atmosphere when it is cold enough. Later, when temperatures rise again, this layer will sublimate back into the atmosphere. Because of the low atmospheric pressure, ice does not melt but sublimates instead. This diurnal CO_2 cycle only creates a thin frost layer of less than one mm thick (Tesson et al., 2020). Piqueux et al. (2016) suggest that areas with dusty, low thermal inertia are subject to CO_2 ice condensation at nighttime since diurnal temperature change is highest here. Though small, the CO_2 ice layer on and within the top soil layer inhibits the induration of the soil. The diurnal cycle of this CO_2 ice layer can even play a role in the triggering or enabling of surface processes, including mass wasting (Piqueux et al., 2016). There is also a seasonal CO_2 cycle. From the poles down to roughly 60° on both hemispheres CO_2 ice condensates from the atmosphere to form a seasonal frost layer (Piqueux et al., 2016; Tesson et al., 2020). This layer has been linked to gully activity (Conway et al., 2019; de Haas et al., 2019; Dundas et al., 2019).

3.3.2 Martian landforms

Surface types: Planitia(e), Planum (plana), Terra, Mons (montes): The surface of Mars can be subdivided into several geological regions. Planitiae (e.g. Hellas Planitia) are flat plains or lowland regions. These areas are relatively young and are less heavily cratered. Highland areas are generally called terrae (e.g. Arabia Terra). These areas have greater elevation and relief and are older than planitiae, with a more heavily cratered surface. Flat highland areas, or plateaus, are called plana, an

example of such a region is the Tharsis Planum. Finally, there are montes. Large (volcanic) mounds that act as recognizable features on the Martian surface. Examples are Olympus Mons, Elysium Mons and the Tharsis Montes.

Chasmata: Chasmata are large canyon-like features found all over the Martian surface. Their high elevation difference of up to 10 km and large sloping areas provide ample opportunity for mass wasting processes to take place. A large complex system of these chasmata together forms the iconic Valles Marineris area. Here many large slumps and slides dominate the slope morphology, and therefore much of the research on Martian mass wasting is conducted here (Crosta et al., 2018).

Gullies: The gully landform was first discovered on Mars by Malin & Edgett (2000). Gullies on the planet Mars get their name not from their terrestrial counterparts, but rather from their resemblance to spur and gully morphology. Conway et al. (2019) define Martian gullies as composite landforms containing an alcove, a channel and a depositional fan, as do (Conway et al., 2019; Dundas et al., 2019; Orosei et al., 2020; Roelofs et al., 2024). They form on relatively steep slopes of 20° to 30° or higher and can grow up to several kilometers in length. Gullies that originate from crater wall bedrock have the steepest alcove and depositional fan slopes. Older gullies may have experienced backfilling of the channels, erosion by wind or covering by other deposits. This can make them difficult to interpret correctly (Conway et al., 2019).

3.3.3 Martian mass wasting

As was the case on the Moon, all main movement types (fall, flow, slide and slump) are found on Mars (Table 1). Three different flow types have been identified. Channeled flow, avalanches, and ejecta flow. The global distribution of observed mass wasting features on Mars is visualized in the map in appendix A3.2, which shows that this is not an even one. The majority of observations are located within or around the Valles Marineris region and the adjacent outflow channels of the Circum-Chryse region.

Fall

Rockfalls on Mars have been identified by Tesson et al. (2020). These movements include the detachment of a block of material from its host cliff and the subsequent falling, bouncing and rolling until it finally lays still. On Mars, the location and frequency of rockfalls are related to latitude. Tesson et al. (2020) found that the highest frequency of rockfalls is found between 15° and 40° North and South, on the equator-facing side of impact craters. In equatorial regions, rockfalls are most common on North and South facing slopes. These slopes experience the most thermal stresses due to daily temperature changes, which weakens the cliffs. Furthermore, Tesson et al. (2020) found that most blocks detach around 50 m from the crater rim and 88% of rockfalls originate from slopes steeper than 32°.

Flow

Multiple types of flow are found on the Martian surface, as shown in Table 1. By far the most investigated are the channeled flows and the associated gully morphologies, but avalanches and ejecta flows are also found.

The images captured by the HiRISE instrument on the Mars Reconnaissance Orbiter have a resolution of up to 0.3 m/pixel, which provides extraordinarily detailed data of the Martian surface. Thanks to this high-quality data, surface activity on a much smaller scale can be investigated. For example, gullies have been found all over the planet's surface. These gully morphologies were first discovered in the year 2000 (Malin & Edgett, 2000), and there have been many theories about their formation (Conway et al., 2019). These include dry granular flow, partially wet flows such as Earth-like debris flows, and fluvial flow. Conway et al. (2019) concluded that no single mechanism is responsible for gully

formation. Mechanisms based on liquid water flow require very specific pressure and temperature conditions so are unlikely to cause widespread gully formation now, though this can explain historic gully formation. Dry granular flows are a more likely formation mechanism because they can behave as a fluid (Krohn et al., 2014). However, to achieve the observed morphology, these flows must have been fluidized. And since CO_2-ice is abundant in Martian regolith, the flows are most likely fluidized by CO_2 sublimation. This is also supported by the seasonal CO_2 cycle (Conway et al., 2019; Dundas et al., 2019). Despite the different formation mechanisms of gullies, they are formed by a flow-type motion, with a channel morphology as a result. Therefore, gully landforms can be interpreted as channeled flow-type mass wasting.

As discussed in Chapter 2, avalanches are very large, high-velocity flows. This type of long runout, high volume mass movement is found to be common in Martian impact craters and chasmata, although few are found at higher latitudes (Crosta et al., 2018). They are very variable and can have extremely long runout lengths, explained by a relatively high mobility. Although velocity of Martian mass wasting cannot be measured directly, Quantin et al. (2004) did find certain morphologies that indicate high velocities during the flows. This high velocity, along with the large volume, allows these Martian features to be classified as avalanches.

Crosta et al. (2018) mention ejecta flows as an intermediate class with rock avalanches, not as a class of mass wasting on its own. Although this may indicate that their presence is less obvious or noteworthy compared to avalanches, it does mean that this type of movement occurs on Mars. These movements are in many ways similar to other flow-like mass movements like avalanches, but they occur in ejecta blankets. The elevation difference from the crater rim outward is much less compared to towards the crater center, so the slopes are generally gentle. The runout distance of ejecta flows on Mars can be very large, despite their gentle slopes and moderately high drop height. The location and direction of ejecta flows are also influenced by the initial velocity of the ejected material (Crosta et al., 2018).

Slide

Large landslides on Mars have been identified and measured by Quantin et al. (2004). This study focused on the Valles Marineris region, where chasmata provide extreme topography and very long and steep slopes. An original classification was used in this study based on the structure of the deposit, and a careful reclassification was made based on the characteristics discussed in Chapter 2. The features were subdivided into slides, avalanches, and a few slumps. The slide type was mostly found along the wide slopes of Valles Marineris and showed rough deposits downslope of a tectonic structure, where the material detached from. The slides were found to have relatively high mobility, which is possibly related to the volatiles in the pore spaces (Quantin et al., 2004).

Slump

Similar to the slides, large slump features are also found in the Valles Marineris region of Mars. Crosta et al. (2018) identified many mass wasting features, including large slumps. These have a large volume and a relatively short runout length. The slump block detaches from the slope and leaves behind a curved scarp. It then slides down, and the head of the block tilts backwards. Sometimes secondary failures create a stepped surface. Crosta et al. (2018) also found that large slumps often transition into flows when the slump block loses cohesion. In such a case the runout of the now complex movement is much larger than that of a simple slump feature.

3.4 Mercury

3.4.1 Conditions on Mercury

Mercury is the closest planet to orbit our sun. It is a rocky metal world without an atmosphere (Blewett et al., 2011; Brunetti et al., 2015; Pokorný et al., 2021). Volcanism was an important and widespread surface-altering process on the planet, but geological activity is thought to have stopped a long time (Blewett et al., 2011). Its surface is subject to space weathering in the form of bombardment by micrometeoroids and solar wind sputtering, the latter of which has a large impact due to the planet's proximity to the Sun (Blewett et al., 2011). The amount of meteoroid material hitting Mercury is fairly high compared to other bodies, with a mass flux of 5 times and 50 times the amount of the Moon and Ceres, respectively (Pokorný et al., 2021). Although it was long thought that Mercury contained little volatile material, high abundances of volatile elements have been found and their presence has been linked to hollows (see section below) and mass wasting (Aubry et al., 2021; Blewett et al., 2011; Xiao & Komatsu, 2013). It is thought that unstable volatiles can form a tenuous exosphere around the planet (Pokorný et al., 2021), but the solar winds make it difficult for this to be stable for long.

3.4.2 Notable Mercurian Landforms

Hollows are a landform unique to Mercury. They are shallow, rimless depressions with bright interiors and bright halos, (elongated) circular in shape. A study by Blewett et al. (2011) found the average depth and radius to be 44 m and 137 m, respectively. They are found all over the planet and are found mostly in clusters within impact craters. Possible causes of these hollows are volcanism, explosive outgassing, collapse into a subsurface void and loss of volatile-rich material through sublimation, the last of which is the most likely. As the volatile material sublimates, the slopes fail, and depressions emerge. Lucchetti et al. (2021) proposed that a layer of volatile-rich material formed during the differentiation of impact melts is responsible for hollow formation. This is in line with the findings of Blewett et al. (2011), who linked the rounded outlines and flat floors to a radial growth limited by a resistant base. The resistant base might be the end of the volatile-rich layer. Hollows on south-facing crater rims suggest a correlation with peaks in diurnal temperature (Blewett et al., 2011). Finally, the resemblance to the Martian terrain formed by CO_2 sublimation also supports this hypothesis.

3.4.3 Mercurian mass wasting

Although mass wasting events on Mercury are poorly studied, we know they occur on a global scale. Sliding features in large impact craters have been identified all across the planet, while different types of flowing movement are also found but are less common (Table 1). The global distribution of Mercurian mass wasting is visualized in the map in appendix A3.3.

Flow

Multiple flow features have been identified on Mercury. A survey by Aubry et al. (2021) found several landforms on the surface that are linked to slope processes. One of these features was 'spur and gully morphology', featuring a debris apron downslope. This morphology is also seen on the Moon, Mars and Vesta and the movement that formed it can be classified as a flow (Conway et al., 2019; de Haas et al., 2019; Krohn et al., 2014; Xiao et al., 2013). The flow features were only found in fresh craters. Similarly, lunar slumps were found mostly in young craters, and this was linked to the unstable nature of fresh crater slope material (Xiao et al., 2013). Malliband et al. (2019) found similar features with an alcove, a chute and a fan and described them as erosion-deposition systems. These features are

characterized by a high relative albedo and their formation is linked to sublimation processes (Malliband et al., 2019).

Xiao & Komatsu (2013) found ejecta flows around impact craters on Mercury. These flows originate on the outward side of the crater rims and cover large areas. The outflow areas are found to have constant thickness and rough surfaces. The flows can have a tongue-like shape with semicircular edges or a plateau-like shape with sinuous edges. The flat and widespread shape of these flows implies high mobility. Although difficult to measure with high certainty, Xiao & Komatsu (2013) found the mobility of the material to be comparable to similar features on other bodies. This means that fluidization does play a role in these ejecta flows. This is also supported by the fact that volatile material was found on the bottom of some of the parent craters, indicating that these were present in the target surface.

Slides

Landslides within impact craters are common features on Mercury. Brunetti et al. (2015) listed 58 features spread over 38 craters, distributed relatively evenly over the planet. The large amount of meteoroid impacts causes there to be a lot of highly fractured rock on the surface, subject to sliding. Schultz & Gault (1975) proposed that impact-generated seismic shaking on Mercury and the Moon can trigger mass movements. This shaking can also fluidize the loose material to aid the movement. This combined with the abundance of fractured rocks explains why the slides are common and exist in many sizes. Brunetti et al. (2015) found slides with a size range of 9 to 245 km^2, although smaller slides are likely also present. These, however, are difficult to identify due to image quality.

3.5 Ceres

3.5.1 Conditions on Ceres

With a diameter of 950 km, Ceres is the largest object in the main asteroid belt between Mars and Jupiter and is considered a dwarf planet (Schmidt et al., 2017; Williams, 2016). It has an average temperature of -105 °C on the surface and its gravity is 0.26 m/s^2 (Williams, 2016). The subsurface of Ceres contains water ice, and this is most abundant and shallow in the polar regions (Parekh et al., 2021; Schmidt et al., 2017). Especially in permanently shadowed regions, water ice can be retained because no sunlight can cause sublimation (Pokorný et al., 2021). Although the mass influx of meteoroids is much smaller compared to inner solar system bodies such as Mercury and the Moon, meteoroid impacts occur over the entire surface. This means that in the permanently shadowed regions, meteoroid impacts can still generate heat and therefore cause volatile loss (Pokorný et al., 2021). The sublimation of volatile water from the surface produces a thin water exosphere (Pokorný et al., 2021), and this process is thought to play a role in the lubrication of mass wasting (Parekh et al., 2021). Cryovolcanic processes also play an important role on the Cerean surface (Parekh et al., 2021).

3.5.2 Cerean mass wasting

On Ceres, multiple movement types have been identified (see Table 1). Large slumps and slide movements play important parts in the degradation of impact craters (Parekh et al., 2021). Flow-type movements have also been found on the asteroid, which are found to be much more common (Parekh et al., 2021). These have been subdivided into three different types, which were reclassified to fit into the classification scheme of this study. These features were first categorized by Schmidt et al. (2017). The features are found all over the asteroid, and their context in terms of surrounding geology and age are wildly different. As a result, and this is the case for many mass wasting classifications, many of the flow features can be seen as intermediate between two flow types (Duarte et al., 2019). The global distribution of Cerean mass wasting is visualized in the map in appendix A3.4. This map shows that the majority of mass wasting features are flows, while slides are less frequent and even less slumps have been identified.

Flow

The first flow type described by Schmidt et al. (2017) are large, voluminous flows that form after a crater wall failure. These flows typically occur on steep slopes, in high latitudes craters, roughly above 50°. The distinct 'rolled' morphology of these types of flow indicates that deformation occurs. This can be explained by the ice content in the material, making it easier to overcome the grain friction (Schmidt et al., 2017). Duarte et al. (2019) found that these types of flows have a low efficiency in transporting material. Despite the steep slopes, the flow does not reach very far, which indicates relatively low mobility. They also concluded that there was no strong relationship between the mobility and the runout length. This means that fluidization of the flows by subsurface ice does have an effect, since otherwise there would be a clear connection between the two.

The second flow type is characterized by long, thin sheets of material flowing along gentle slopes (Schmidt et al., 2017). Duarte et al. (2019) also found that these types generally have a shallow failure. Despite the gentle slopes, these flows can have long runout lengths. This can be explained by lubrication of the flow by ice. This can happen at temperatures close to the surface temperature of Ceres. Frictional heating of ice grains in the flow material can cause them to become slippery or even melt, reducing basal friction and allowing the flow to travel long distances (Schmidt et al., 2017). Based

on the classification characteristics discussed in Chapter 2, this type of flow can be reclassified as sweeping flow. Because of its wide and flat morphology, and the fact that the flow is not concentrated but spread out.

The last flow type described by Schmidt et al. (2017) is wide sheeted flows of smooth material that flow outward from the crater rim. These flows are related to ejecta blankets and either due to the ejecta being deposited during the formation of an impact crater or form in existing ejecta blankets. Duarte et al. (2019) and Schmidt et al. (2017) propose that these flows are fluidized by ice within the material, mainly due to their long runout and gentle slopes. These flows can be reclassified as ejecta flows, based on the characteristics discussed in Chapter 2, as well as their direct link to ejecta materials.

Slump

Slump features are often the largest type of slope movement on Ceres in terms of volume and are predominantly found in large impact craters (Parekh et al., 2021). The material is relatively cohesive, causing it to slide down as a block rather than loose material. A special instrument on NASA's Dawn spacecraft found certain materials on the surface that could explain the cohesiveness of the regolith and therefore the presence of slumps (Parekh et al., 2021). The locations of slumps also correlate with the latitude range in which water ice is found down to several meters deep in the subsurface. Many large slump blocks on Ceres have secondary slumps, causing a sort of stepped morphology with multiple heads. Examples of such features are the ones found in the Toharu crater, which contains two failure surfaces (Figure 4).

Slide

In contrast to slumps, Cerean slides are not cohesive and form loose material. The relatively high abundance of water ice on the surface favors slumping or flowing behavior, but in the mid-latitudes of Ceres, the ice layer is deeper and there is a lower ice content on the surface. This region is also where most Cerean slides are found. Parekh et al. (2021) propose that the dry, non-cohesive material here provides more favorable conditions for the formation of slides. After detaching from the crater wall, the mass slides downslope and eventually deposits on flatter areas. During a slide, the failure surface is exposed, and the material spreads out laterally. This can cause some deformation of the material (Parekh et al., 2021). Boulders are also found at the bottom of slides, showing the transport capacity of these movements, as well as the difference in travel distance between grain sizes.

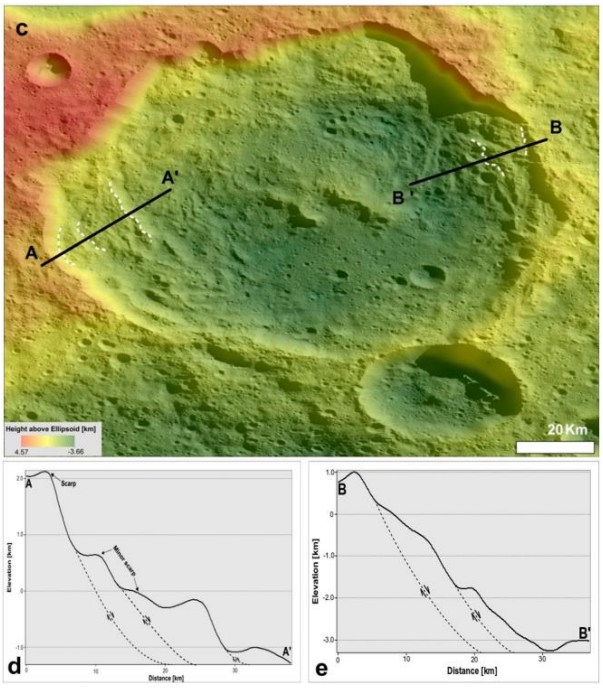

Figure 4: Toharu crater on Ceres, with two slump features. Cross sections show stepped morphology as a result of secondary failure (figure 1 from (Parekh et al., 2021))

3.6 Vesta

3.6.1 Conditions on Vesta

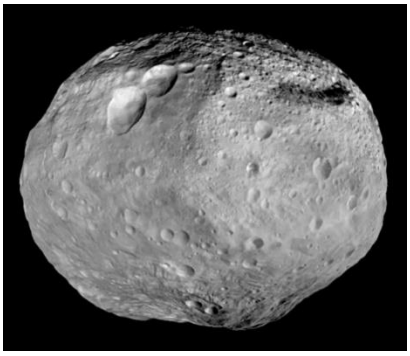

Vesta is the second largest object in the asteroid belt and can be classified as a planetesimal or a protoplanet (Otto et al., 2013; Parekh et al., 2021; Scully et al., 2015). It is not a perfectly spherical body, but rather an irregular ellipsoid. (Preusker, Scholten, et al., 2012) determined the best-fit ellipsoid dimensions to be 286.3 x 278.6 x 223.2 km. Its small size results in low gravity, which allows for a large elevation range of -22 km to +19 km relative to a reference spheroid (Otto et al., 2013). Due to elevation and density variations, the local gravity can vary significantly (Figure 5). The average gravitational acceleration of 0.22 m/s^2 can be altered by 20%, 1% and 0.3% by elevation difference, density variations and centrifugal effects, respectively (Otto et al., 2013). Vesta is a relatively dry body, it has very low volatile content due to extensive heating and dehydration (Parekh et al., 2021). A recent study, however, suggests that water ice does occur in the subsurface and even leads to transient flowing water (Scully et al., 2015). On the surface of the asteroid a granular-like, brittle regolith can be found. The layer of regolith is deeper compared to larger rocky bodies in the inner solar system ((Housen & Wilkening, 1982; Parekh et al., 2021).

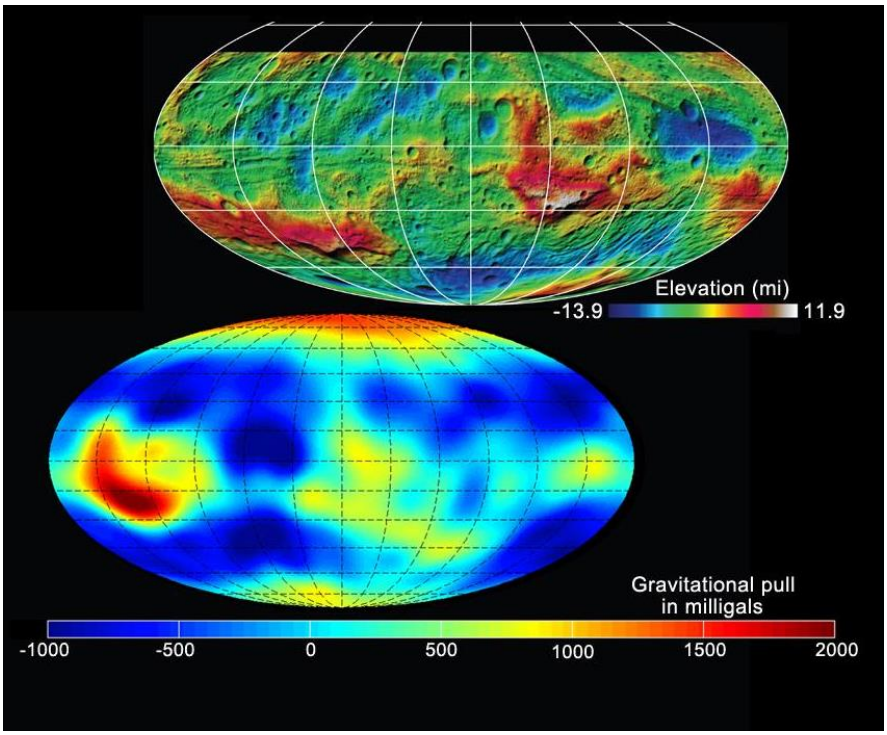

Figure 5: Elevation relative to reference ellipsoid and gravitational variations. (Image credit: NASA/JPL-Caltech/UCLA/MPS/DLR/IDA, source: https://www.jpl.nasa.gov/images/pia15604-shape-and-gravity-of-vesta)

3.6.2 Notable features on Vesta

The most important feature of Vesta is the giant impact basin Rheasilvia. This roughly 500 km diameter crater covers most of the south pole region of Vesta and is the most geologically active region of the asteroid (Otto et al., 2013; Parekh et al., 2021). The extreme topography of the 35 km high rims and 20 km high central peak provides good conditions for mass wasting. The eastern rim of Rheasilvia, an area called Matronalia Rupes, is a good example of this (Krohn et al., 2014; Otto et al., 2013).

Another noteworthy feature found on Vesta is so-called 'pitted terrain' (Figure 6). This can be described as a surface that contains clusters of many small pits, and it is found on the bottom of impact craters. Such terrain is formed by impact-induced devolatilization and subsequent outgassing of the produced vapor. This can happen when there are ice deposits deep in the subsurface when an impact occurs. During crater formation, the ice is heated up and sublimation causes outgassing through the regolith, which in turn forms the pits on the crater floor (Scully et al., 2015).

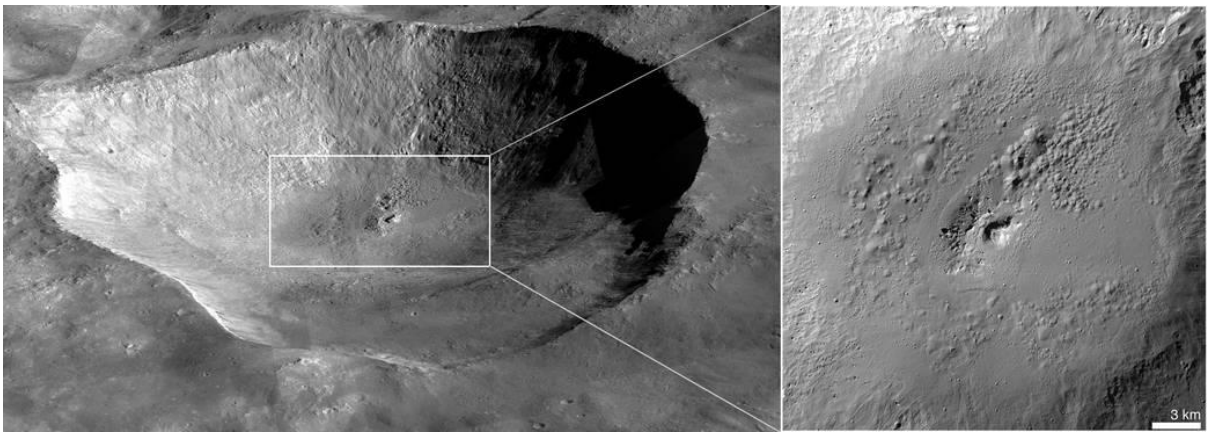

Figure 6: Pitted terrain in Marcia crater on Vesta (Image credit: NASA/JPL-Caltech/UCLA/MPS/DLR/IDA/JHUAPL) (source: https://www.nasa.gov/image-article/most-spectacularly-preserved-pitted-terrain-vesta/)

3.6.3 Vestan mass wasting

On Vesta, slumps, slides and flows are found (Table 1). Slumps are mostly found in large craters, while flows and slides are found mostly in smaller craters. Slides are also the most common mass wasting feature on the asteroid (Parekh et al., 2021). The global distribution of Vestan mass wasting is visualized in the map in appendix A3.5. This map shows that slides are the most common mass wasting feature, closely followed by flows, while only a few slumps have been found.

Flow

Scully et al. (2015) found two types of gully systems on Vesta: linear and curvilinear. Linear gullies are straight and non-intersecting, while curvilinear systems consist of interconnected curved gullies that form a drainage network. These gully systems are mainly found on the fresh slopes of younger (meaning 100s Ma (Scully et al., 2015)) craters as well as on steep slopes outside craters. This has to do with the unstable nature of the material after crater formation (Xiao et al., 2013), but also with the fact that gullies in older craters have been subject to processes like infilling for a long time (Scully et al., 2015). Linear gullies are formed not by eroding flow, but by the intersection of talus deposits. These are therefore likely caused by dry granular flow, similar to lunar gullies (Scully et al., 2015; Senthil Kumar et al., 2013). The curvilinear systems are formed by transient liquid water, which is possible when subsurface deposits of water ice are melted by impact heat. Slowly evaporating, the water flows down the crater slope, carrying regolith with it. As a result of these flows, the curvilinear gully system is formed (Scully et al., 2015). Following the classification scheme discussed in Chapter 2 – Classification, this type of movement can be reclassified as channel-forming flow. One other subclass of flows, creep, has been found on Vesta. No features have been identified that can be classified as sweeping flows or avalanches.

Otto et al. (2013) identified creep-like mounds of various sizes on Vesta. These features have curved shapes and form clusters, indicating a larger slope process is responsible. This type of movement takes place at the rim and the peak of the large Rheasilvia basin, as well as near young craters where they are also found in ejecta material. These locations imply that Vestan creep occurs in highly fractured materials (Otto et al., 2013). The formation of the creeps can be explained by compaction due to seismic shaking. This can be caused by shock waves from impacts propagating to the regolith, similar to what Schultz & Gault (1975) proposed happens on Mercury and the Moon.

Slump

Slumps on Vesta generally originate in large craters and consist of cohesive material. Slumps form in high sloping terrain, since this can trigger large blocks to detach from the host material at once. The high elevation range and low gravity of Vesta, predominantly in the southern hemisphere, can result in very steep slopes, making it a good environment for slumps to form (Parekh et al., 2021). Similar to slumps on Ceres, large Vestan slumps have multiple heads within one block. A prime example of a large slumping block is in the Matrinolia Rupes region. This region has extreme topography and therefore allows for large slope movements. Here, a particular slump feature covers an area of 600 km^2 and has multiple ridges, forming a step-like pattern of secondary slump blocks (Krohn et al., 2014).

Slide

Slides on Vesta are found in granular material that is not cohesive. This type of material is abundant on Vesta because it is a relatively dry body. This type is therefore the most common movement found on Vesta (Parekh et al., 2021). After detaching, the loose material forms a large mass, slides downslope

and laterally spreads out, causing deformation. Multiple slides can overlap each other when they deposit on crater floors (Parekh et al., 2021).

3.7 Comet 67P / Churyumov-Gerasimenko

3.7.1 Conditions on Comet 67P

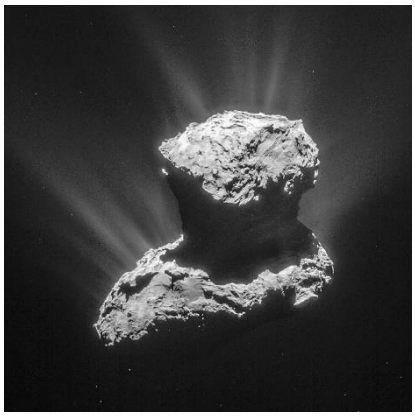

The comet consists mostly of dust and ice. It has a very unusual shape, looking like two merged semi-spherical objects. It is a fairly small object, only 4.4 km by 4.1 km in size. There is no atmospheric pressure on the comet and temperatures can range wildly due to its orbit. Simulations by Pajola et al. (2017) result in 100 K – 340 K. The comet is rich in CO_2-ice, and similar to the Martian CO_2 cycle, there is a seasonality in the abundance of CO_2 on the surface. In periods of increased illumination, the amount of CO_2 drops significantly (Filacchione et al., 2016).

3.7.2 Mass wasting on Comet 67P

Comets, due to their orbits and small size, are difficult to observe and even more difficult to reach. Therefore, their surfaces are studied very little compared to the larger rocky bodies in our Solar System. Nevertheless, the Rosetta mission managed to reach Comet67P and investigate the surface.

Fall

Pajola et al. (2017) discovered the collapse of a large cliff on the comet's surface. The Aswan cliff was observed with cameras on board the Rosetta spacecraft before and after the collapse. The steep cliff had retreated and below, a talus cone had formed with identifiable boulders. It was estimated that the material consisted of boulders ranging from 0.5 to 10 meter in diameter. Due to the steep cliff and the deposited material being large boulders, this mass wasting feature can be classified as a fall-type movement. Pajola et al. (2017) propose that diurnal temperature fluctuations caused gradual degradation and eventual failure of the cliff. An outburst happened around the same time and was linked to the cliff collapse. After analyzing the volume of the original cliff and deposited material, it was concluded that some of the cliff material was shot into space as the outburst (Pajola et al., 2017).

Lucchetti et al. (2019) also identified multiple deposits on the comet's surface and called them landslides. Large volumes of rock and debris were observed beneath cliffs. Large boulders were also described to have been transported further away by bouncing or rolling. The smaller material remained close to the host cliff, forming talus deposits. Based on the classification system proposed in chapter 2 (see Figure 3), these features can be classified as rockfalls. They cannot be seen as slide-type movements, because they mostly consist out of loose material and do not resemble a sliding mass. Furthermore, the high abundance of large boulders prohibits this classification.

3.8 Comet 9P / Tempel 1

3.8.1 Conditions on Comet 9P

Like comet 67P, this comet's nucleus is mostly made up of ice and dust. It too has no atmosphere and extreme temperature ranges.

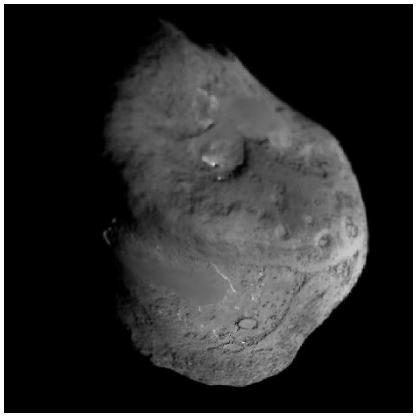

3.8.2 Mass wasting on Comet 9P

On comet 9P, outbursts of material are also common, caused by the sublimation of ices in the interior. These are not only caused by direct heating by the sun, but rather by thermal stresses from the high diurnal temperature fluctuations (Belton & Melosh, 2009).

Flow

Belton & Melosh (2009) investigated the striking smooth surfaces on the comet and linked these to the sources of the outbursts. It was concluded that outbursts of CO_2 can locally fluidize the surface material for up to 20 hours. Dust on the comet's surface fluidized by this sublimating gas can then flow down local topography under the influence of gravity. Eventually, when the gas pressure drops, the movement stops and a terminal scarp is formed (Belton & Melosh, 2009). Although this type of flow is different than has been identified on other bodies and does not match the same morphological attributes, it can be classified as a flow-type movement because it concerns fluidized movement.

Chapter 4 - Quantitative and morphological analysis

4.1 Comparing morphology

In the previous chapter, the various mass wasting types found on the surfaces of the celestial bodies were described. In this section, the morphologies of these features are compared between each body. Similarities and differences in the shape and size will be discussed for each of the movement types and this will be placed in the context of their respective host bodies.

4.1.1 Falls

Fall-type movements are mostly similar in morphology because the deposited material are often large boulders that have been transported downslope. However, there can be differences in how this leaves a mark on the surface. If boulders bounce very high, they can leave pit chains on the surface like in Figure 7A (pits indicated with numbers 2), while if they have a more rolling motion, they leave a trail like in Figure 7B (Kokelaar et al., 2017; Tesson et al., 2020). The rock fall found on comet 67P however, has a very different morphology. Here, a large volume of material was detached from the cliff and formed a talus cone beneath it, consisting of large and small boulders and rocks (Pajola et al., 2017). Therefore, the amount of detached material and the distance traveled can have a big impact on the resulting morphology.

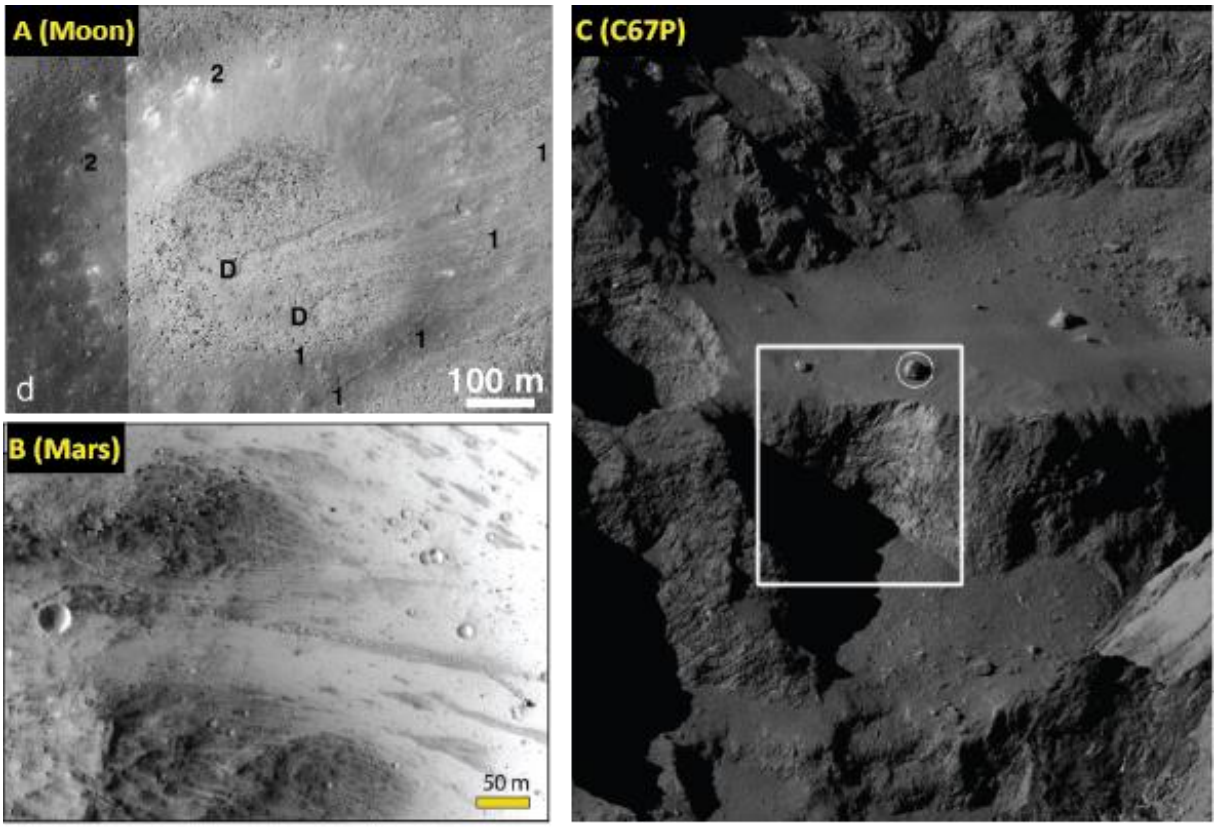

Figure 7: Examples of fall-type movements. A) Bottom of a lunar crater, with rockfall tracks indicated by numbers 1 and 2 (figure 3d from Kokelaar et al. (2017)). B) Bounce – and roll marks left by a detached boulder on Mars, downslope movement is to the right and the boulder is seen at the end of the trail (figure 2a from Tesson et al. (2020)). C) Cliff after rockfall, with talus cone and boulders beneath, circled boulder is just above the cliff edge (figure 2c from Pajola et al. (2017)).

4.1.2 Flows

As discussed in Chapter 2, flows can be subdivided into different types. In this section, all these subclasses are discussed and the morphology associated with them is compared between bodies. Not all flow features however fall into those subcategories, because they lack certain key attributes to be

classified as a specific type or because they are too intermediate. These are just called flows and are shown in Figure 8.

These flows are very diverse and can share attributes of multiple flow subclasses. For example, separation of fine and coarse material, as seen in Figure 8A on the moon, where fine material is found in the center while larger grains are pushed to the side (Kokelaar et al., 2017). This is known as kinematic sieving and mainly occurs in channeled flows, but when there is no flow concentration it cannot be classified as channelized flow. Lateral levees are also common in flows, as shown in Figure 8B on Ceres (Duarte et al., 2019). Another important difference between flows is the shape of the terminal ridge. Some features are found to have no clearly defined terminal ridge like in Figure 8C, while others have finger-like or lobed frontal deposits (Figure 8A and Figure 8B, respectively). The flow found on comet 9P by Belton & Melosh (2009) also does not fit into a subclass of flows. The smooth terrain it forms is unique to comets and is difficult to compare to other bodies.

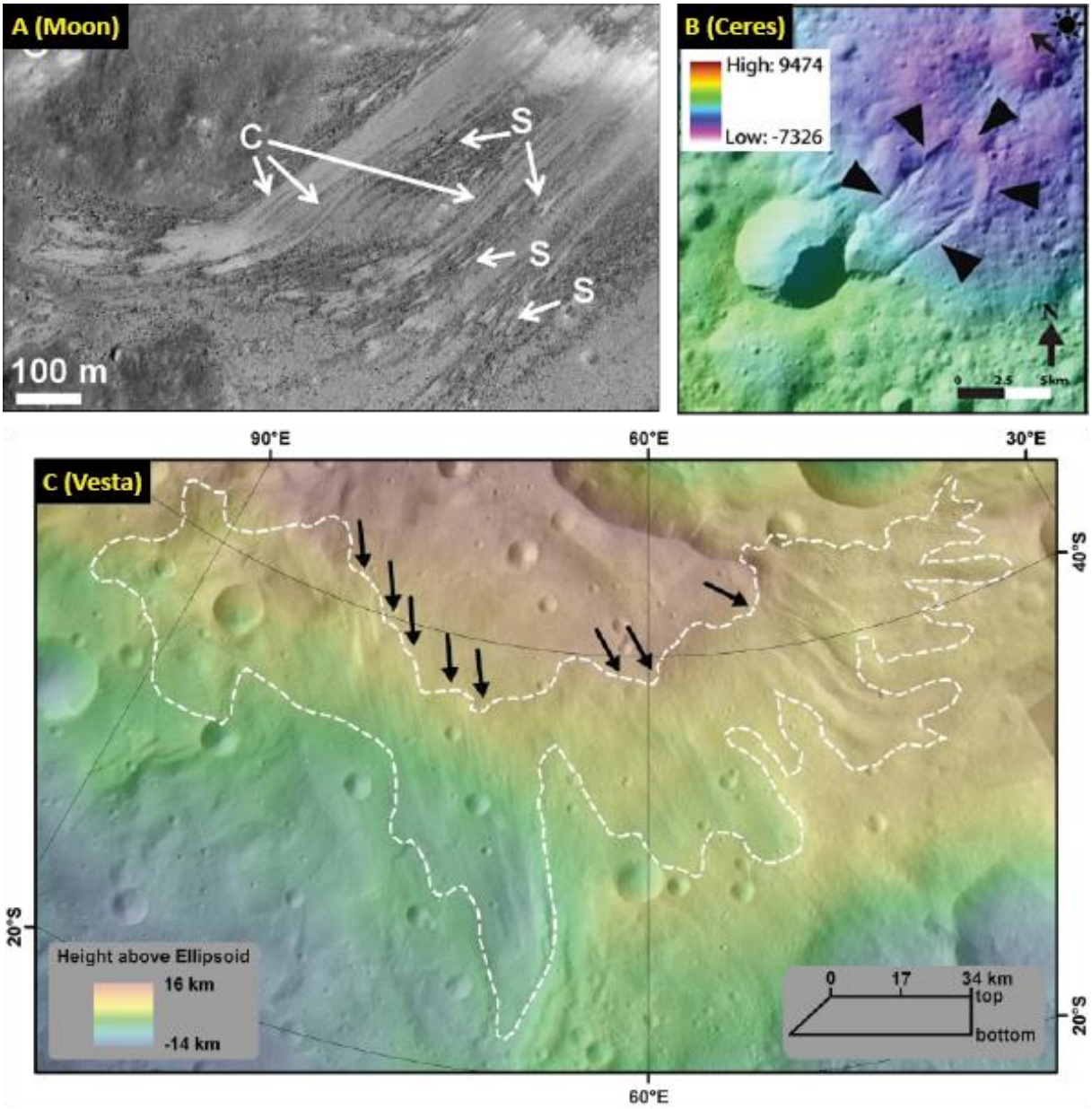

Figure 8: Examples of flows. A) Flow on the moon, depositional lobes at the bottom (figure 4c from **Kokelaar et al. (2017)***. B) Flow on Ceres, outward from crater rim down to a lower lying area. Black arrows indicate flow margin, and legend is given below the image (figure 2a from* **Duarte et al. (2019)***). C) Flow features on*

Vesta, down the steep slopes of the Matrinolia Rupes region, flow area is indicated with white lines and flowlines can be seen (figure 5 from Otto et al. (2013)).

Avalanche

So far, avalanches have only been found on Mars, so these features cannot be compared to similar movements on other bodies. Figure 9 shows an example feature. The long runout and large scale are visible, and the bulbous front shows a clear lobate shape.

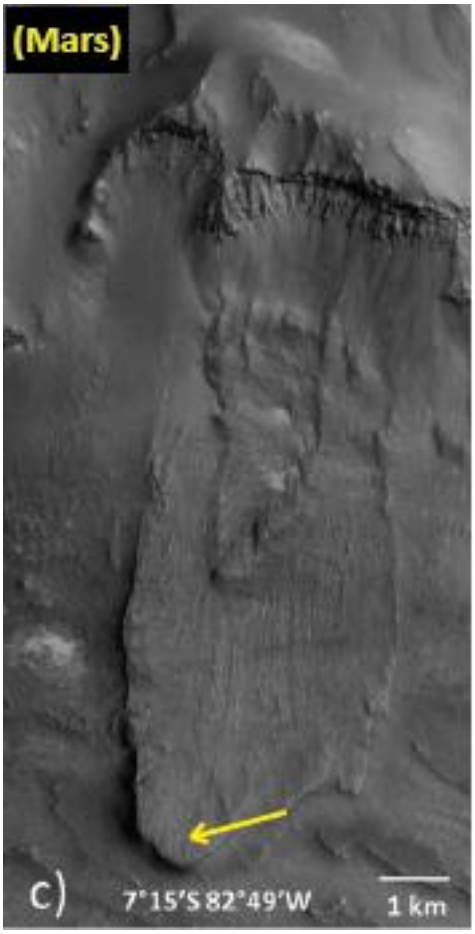

Figure 9: Example of a Martian avalanche, with long runout a bulbous front, indicated with a yellow arrow (figure 4c from Crosta et al. (2018)).

Creep

Creep-like movement has been identified on the Moon and Vesta. Examples are shown in Figure 10. The most important difference between creep on these bodies is the shape of the features that are stretched perpendicular to the slope. On the moon, these are straight ridges (Kokelaar et al., 2017; Xiao et al., 2013), while on Vesta curved mounds are the key morphology related to creep (Otto et al., 2013). The key similarity between these two bodies is that the creep concerns a large spread-out area, on which these identifying features are found.

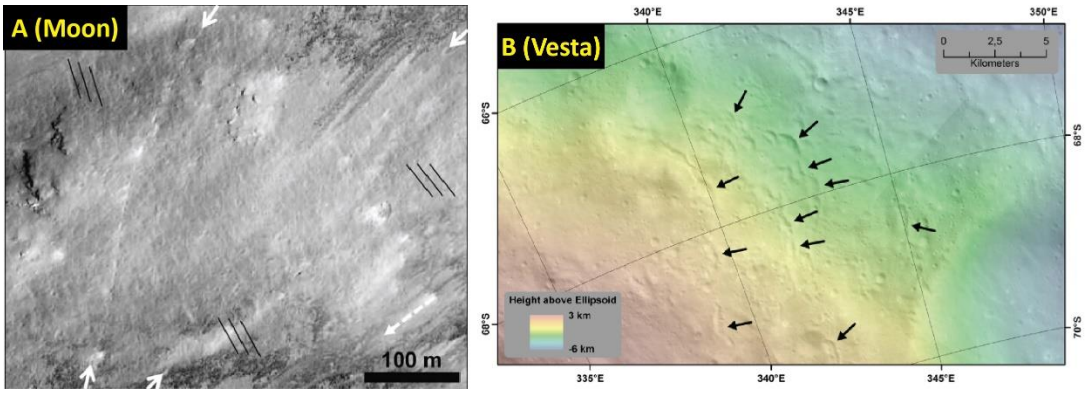

Figure 10: Examples of creep. A) Creep features on the Moon, with slope perpendicular ridges. Also, a boulder trail is indicated with white arrows (figure 3b from Kokelaar et al. (2017)). B) Creep on Vesta semicircular ridges indicated with arrows (figure 6 from Otto et al. (2013)).

Channeled flow

Channeled flow is the most common type of flow and has been identified on the Moon, Mars, Mercury, and Vesta as displayed in Figure 11. Notably, no examples of channelized flow have been found on Ceres, while its high volatile content and generally abundant surface activity would suggest this type of flow to be present.

The most important similarity between the channeled flow features across the different bodies is that gully morphology is almost always present. As discussed in Chapter 3, the alcove-channel-fan morphology is closely linked to this type of movement (Conway et al., 2019). An important difference between these morphologies is that in some cases the flow concentration (which is an important attribute for classification as channelized flow, see Chapter 2) is caused by the local topography (Senthil Kumar et al., 2013) and in other cases the moving material creates a lower point for other material to flow towards, forming flow concentration on its own (Dundas et al., 2019). In Figure 11A, the flow is confined by the rocks, and this contributes to the channelization of the flow. Meanwhile, in Figure 11C and Figure 11D, no clear obstructions can be seen and the flow concentration happens on itself.

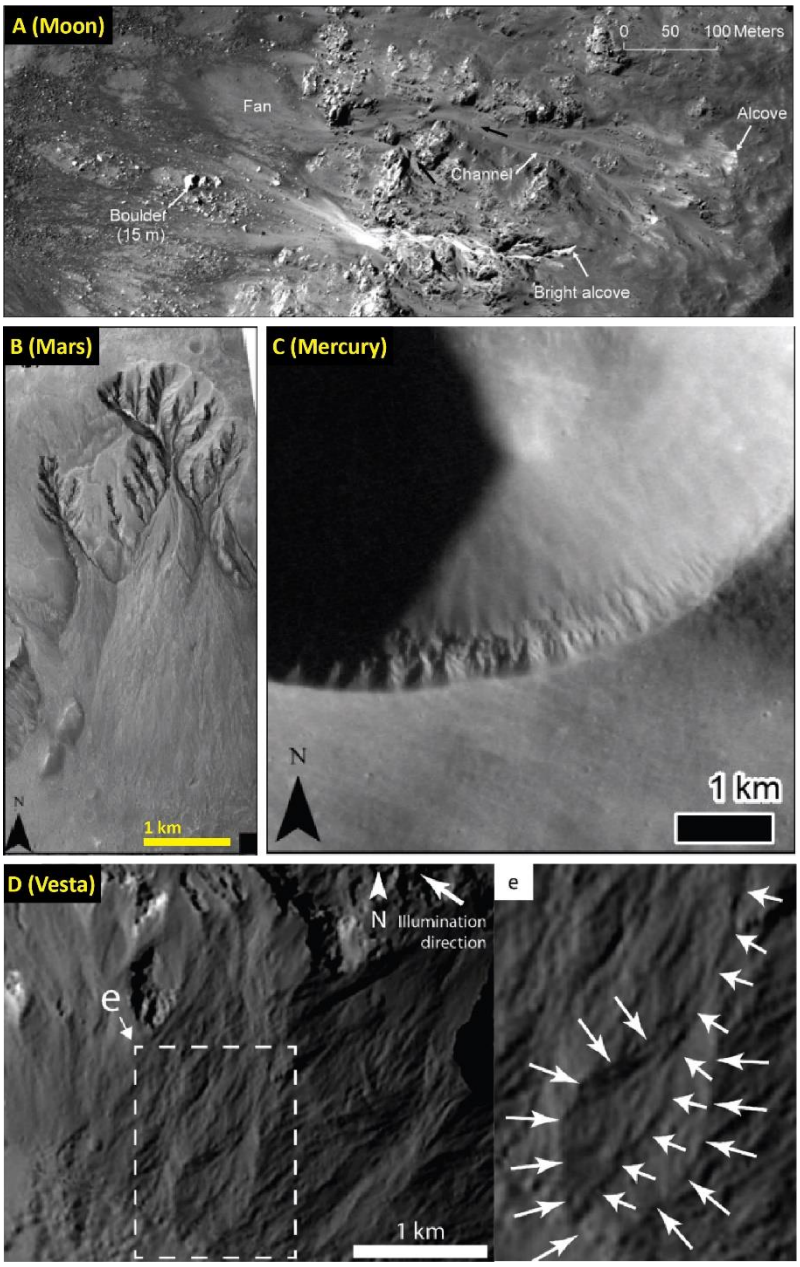

Figure 11: Examples of channelized flow. A) Flow on the Moon. A clear alcove, channel and fan are indicated on the flow, which traverses rocky local topography (figure 3c Senthil Kumar et al. (2013)*) B) Large gully on Mars, with clear alcove, short channel and depositional fan (figure 1j from* Conway et al. (2019)*). C) Flow features on Mercury, linked to spur and gully morphology. (figure 1e from* Aubry et al. (2021)*). D) Curvilinear gully on Vesta (figure 3d and inset e from* Scully et al. (2015)*).*

Sweeping flow

Sweeping flow features are found on the Moon and on Ceres. A similarity between sweeping flows on multiple bodies is that they are generally thin flows with long runouts. They are characterized by flow that is not concentrated but rather keeps a constant width or spreads out laterally. This is also an important difference in sweeping flow morphology. Xiao et al. (2013) found that sweeping flows on the Moon generally have a constant width while travelling downslope (see Figure 12A). Meanwhile, Duarte et al. (2019) found that these flows can form wide sheets that spread out laterally on Ceres (see Figure 12B).

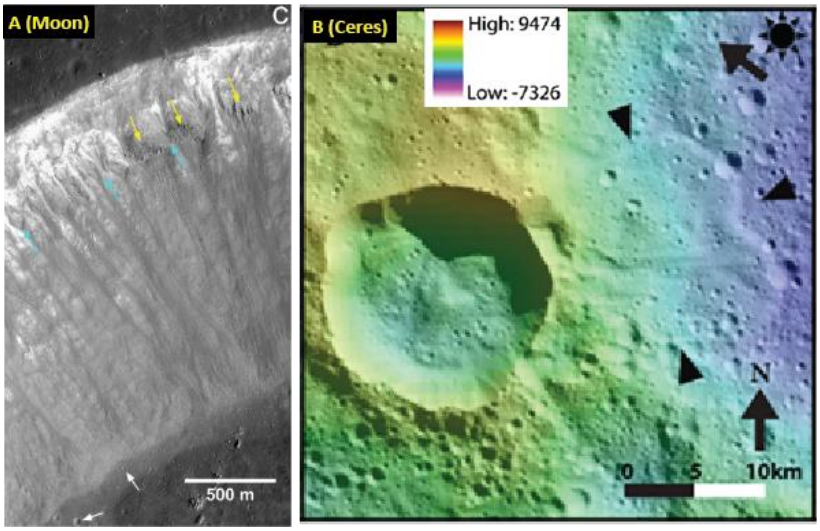

Figure 12: Examples of sweeping flows. A) Sweeping flow on a crater wall on the Moon, with constant width and no flow concentration (figure 4c from Xiao et al. (2013)). B) Sweeping flow into a large depression, forming a wide sheet with circular lobate edges (figure 2b from Duarte et al. (2019)).

Ejecta flow

Ejecta flows are found on Mars, Mercury and Ceres. These flows are directed outward from crater rims and generally have gentle slopes (Crosta et al., 2018). An important similarity between these flows is that they can reach very large distances resulting in a flat, spread-out morphology. This indicates that they have a relatively high mobility (Schmidt et al., 2017; Xiao & Komatsu, 2013). Another similarity is that they are often found along a large part of the crater rim. An important difference in ejecta flows is that they can either form as a direct result of the impact, due to the momentum of the ejected material (see Figure 13B and Figure 13C) (Schmidt et al., 2017), or they can occur later in the settled ejecta blanket (Crosta et al., 2018; Xiao & Komatsu, 2013), see Figure 13A. Another difference in morphology is that some flows have a more stretched-out shape like in Figure 13A, while others result in a wide sheet with sinuous edges like in Figure 13C.

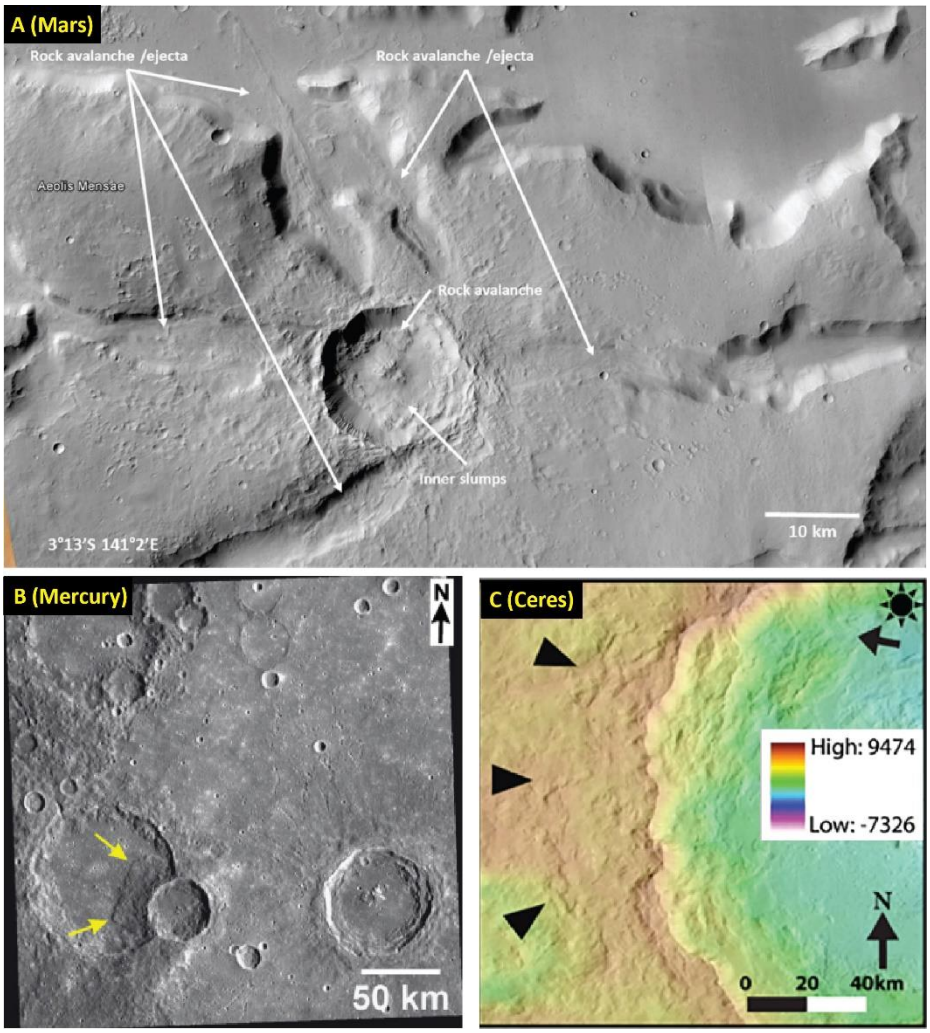

Figure 13: Examples of ejecta flows. A) Ejecta flows on Mars, as part of combined avalanche / ejecta flows. Here, flows happen at unstable areas in the ejecta blanket (figure 8 from Crosta et al. (2018)). B) Ejecta flow into an older crater on Mercury (figure 3d from Xiao & Komatsu (2013)). C) Ejecta flow on Ceres, with sinuous terminal ridges (figure 2c from Duarte et al. (2019)).

An important similarity in extraterrestrial ejecta flows is that they occur on relatively gentle slopes. This is because the slope outward from the crater rim is much less steep compared to the inside of the crater. Since the processes behind impact crater formation and the deposition of ejecta are similar across the Solar System (French, 1998).

4.1.3 Slides

Slides are a common mass wasting feature and have been identified on the Moon, Mars, Mercury, Ceres and Vesta. These features share a lot of similarities. They consist of large masses of non-cohesive material, which are deformed by compression and extension during the motion (Kokelaar et al., 2017; Parekh et al., 2021). Often, the material spreads out laterally, forming semicircular edges (Parekh et al., 2021). This can be seen in Figure 14D and Figure 14E. Important differences in slide-type movements are that they can occur at a wide range of scales (Brunetti et al., 2015). Also, the surface of the sliding mass can be smooth (see Figure 14A), or have ridges and bumps (Figure 14B and Figure 14C). Finally, an important difference in slides is the runout length. Some slides travel very far, like the ones in Figure 14C and Figure 14E that move down straight slopes, and others are confined by impact crater morphology, like in Figure 14A and Figure 14B. Runout length is also linked to volatile content in the slide material (Crosta et al., 2018).

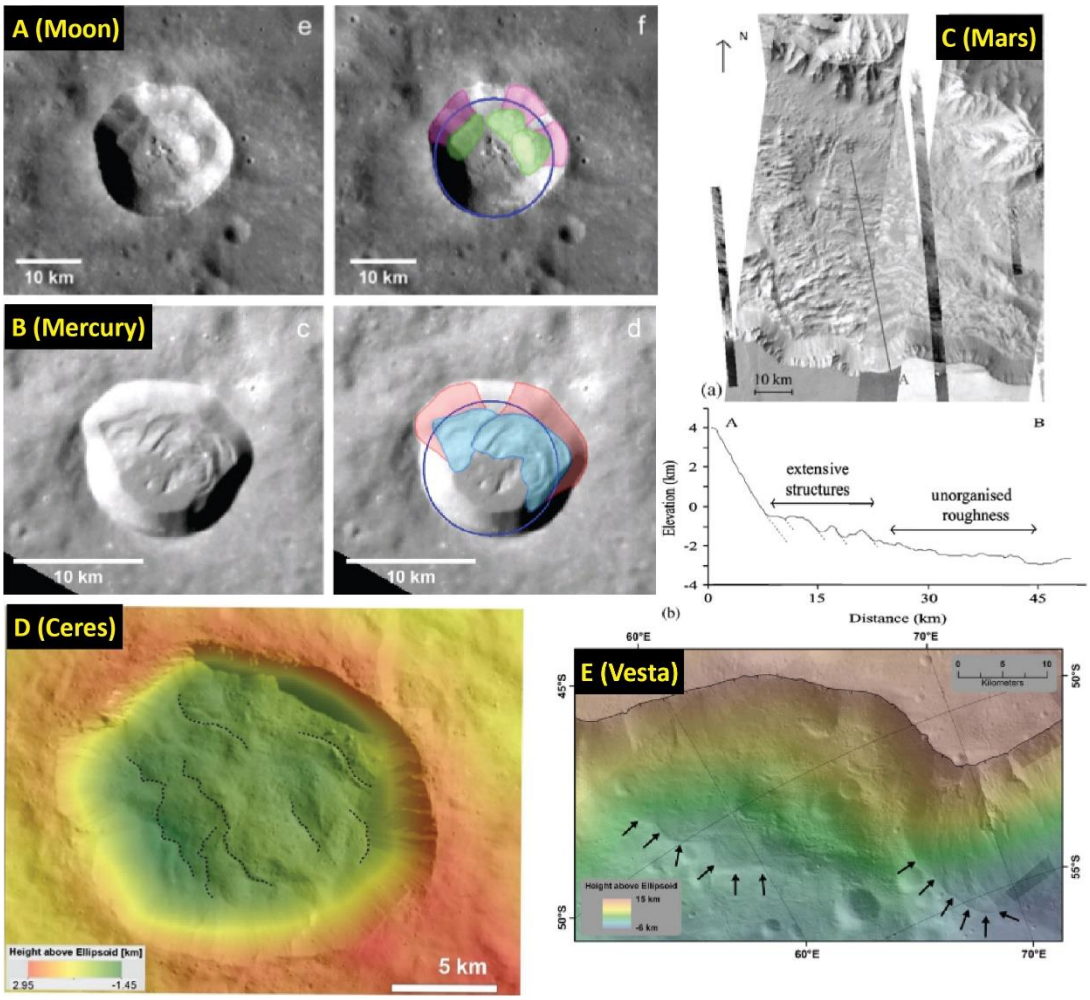

Figure 14: Examples of slides. A) Rockslides in a crater on the Moon, with deposit indicated in green, the scarp in pink and the original crater rim indicated with a blue line (figure 4e and f from Brunetti et al. (2015)). B) Rockslides in a crater on Mercury, with deposit indicated in blue, the scarp in red and the original crater rim indicated with a blue line (figure 4c and d from Brunetti et al. (2015)). C) Slide in a chasma on Mars with a cross-section (figure 2 from Quantin et al. (2004)). D) Slides in a crater on Ceres, with terminal ridges indicated with dotted lines (figure 2b from Parekh et al. (2021)). E) Slides along a slope in the Matrinolia Rupes region on Vesta, with terminal ridges indicated with black arrows (figure 11a from Otto et al. (2013)).

4.1.4 Slumps

Slumps are found on the Moon, Mars, Ceres and Vesta. These are generally very large features and are often linked to large impact craters (Crosta et al., 2018; Parekh et al., 2021). Despite their large size, they often have a small runout length, due to their rotational nature (Crosta et al., 2018). Another similarity is that in most slumps the primary slump block has a tilted back head as shown in the cross-section in Figure 15B. The most important difference between slumps found on these bodies concerns the secondary failure. Large slumps often have secondary slumps, forming a stepped morphology, like in Figure 15D (Crosta et al., 2018; Parekh et al., 2021). However, a secondary failure can also result in flows when the slump block loses cohesion (Crosta et al., 2018; Kokelaar et al., 2017). Such an example is shown in Figure 15C. While large slums become complex due to these secondary failures, smaller slumps like the one in Figure 15A, are generally simple, with only one slumping block (Parekh et al., 2021).

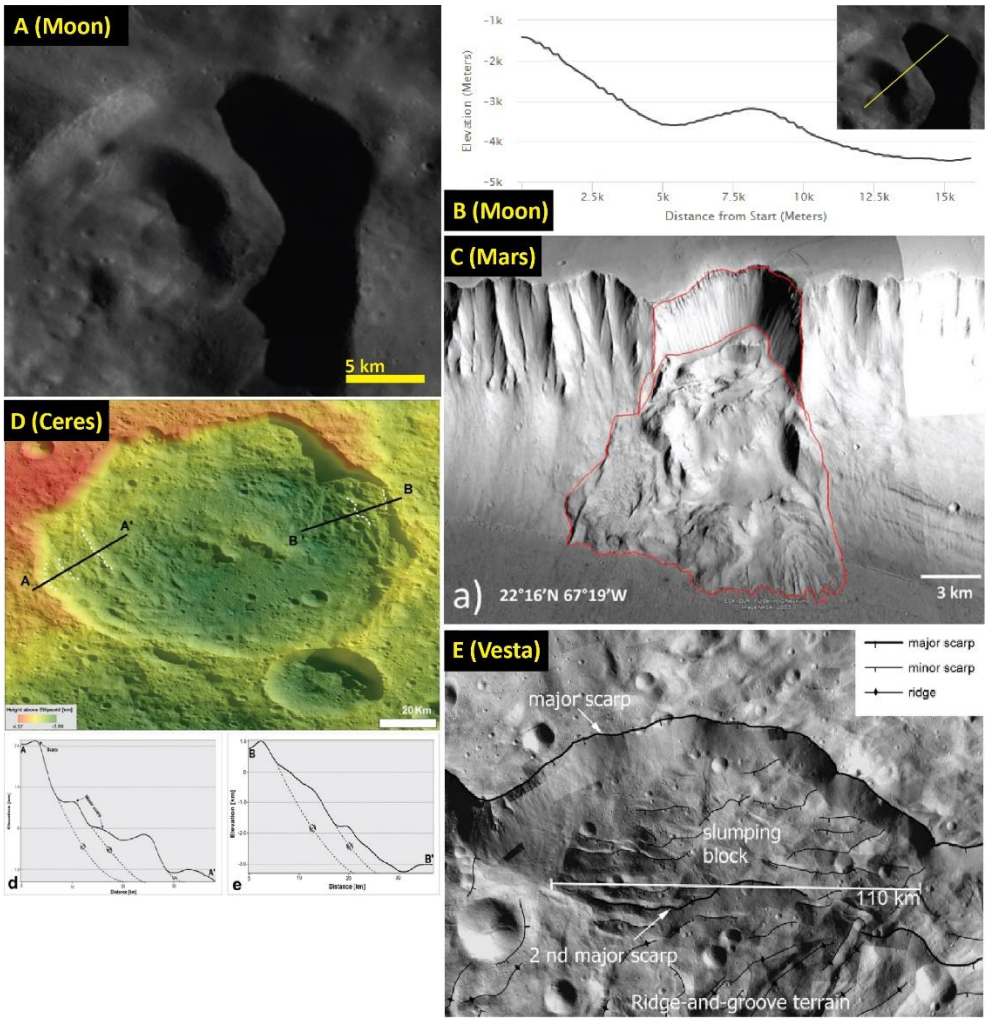

Figure 15: Examples of slumps. A) Simple slump in an impact crater on the Moon, with a cross-section given in B) (source: NASA Moon Trek). C) Large slump in the Valles Marineris region on Mars, with a curved scarp. This slump has transitioned into an avalanche and is therefore complex (figure 6a from Crosta et al. (2018)). D) Slumps in a large impact crater on Ceres, with accompanying cross sections showing the tilted back heads and secondary failure (figure 1 from Parekh et al. (2021)). E) Large slump feature in the Matrinolia Rupes region on Vesta with a curved main scarp and secondary failures (figure 16 from Krohn et al. (2014)).

Now we know something about how similar mass wasting features take shape on different bodies. However, comparing morphology alone does not give a complete picture. To better understand how these movements actually behave, we have to look at their mobility.

4.2 Mobility analysis

To understand and interpret the mobility of mass movements, quantitative data can be used. Maximum runout length *L* and the drop height *H* of a feature can be measured, depending on the availability of the elevation data. By dividing *H* with *L*, a friction coefficient can be calculated. This dimensionless parameter is used in many studies (Crosta et al., 2018; de Haas et al., 2019; Lucchetti et al., 2019; Parekh et al., 2021; Quantin et al., 2004; Schmidt et al., 2017) and can be used to compare the mobility of movements not only on multiple scales, but also between different bodies. In this section, the *H/L* values of most movement types are compared and discussed. Falls behave differently, so their mobility is not measured.

4.2.1 Falls

The mobility of falls is difficult to measure. The starting point of the motion is where the block detaches from the parent material. This mainly occurs near a crater rim, where the slope is steepest. Tesson et al. (2020) determined that 50 meters below the crater rim is the most probable source of detaching boulders, therefore, to a certain degree, the starting point is relatively easy to determine. However, to measure the runout length and the fall height, the final location of the block is required/needed. This can be difficult for multiple reasons. Most importantly, the deposited boulders can be very small. This means that high-resolution imagery is required to locate it. Then, the path of the boulder has to be determined to know the travel distance and direction. For this, the bounce or roll marks have to be identified, again requiring high-definition imagery. And finally, falls can trigger secondary mass wasting like flows or slides (Kokelaar et al., 2017; Xiao et al., 2013). When this happens, the movement becomes complex as the falling material is able to propagate further along the surface which renders this type of movement no longer as a rock fall

Another important aspect is that falls cannot really be expressed using mobility. Compared to the three other main movement types, falls are completely different in the way they behave. Firstly, falls generally consist of one single block of material instead of a granular mass (coherent or not) like the other types. Rather than moving over a failure surface where friction and gravitational pull interact, the material is detached once and then bounces and rolls downslope. This means that friction between the moving mass and the surface plays a smaller role. This makes the mobility, expressed as a friction coefficient, much less relevant to this type of slope movement.

4.2.2 Flows

Figure 16 below shows the mobility of flows found on Mars, the Moon, Ceres and Vesta. Here we see a large spread of the data points, both in feature size and in friction coefficient. The largest features are predominantly Martian avalanches. Martian debris flows are also among the smallest features, with lengths of around 700 m. The lunar flows are not as extreme, with intermediate lengths. For Ceres and Vesta, much more data was available. Vestan flows are somewhat smaller and have some variability in their mobility. Flows on Ceres show the highest variation in mobility, with friction coefficients ranging from 0.001 up to 1.67. This causes most of the data spread of all flows. The data shows that out of all movements, the lowest friction coefficient, and therefore the highest mobility, is found in these Cerean flows.

Apart from the mainly Cerean outliers, most flows are located in the central cluster. Despite the overall spread, the data shows a general downward trend. For features with longer runout distances, the friction coefficient is lower. This means that they have a relatively lower fall height for the travelled distance.

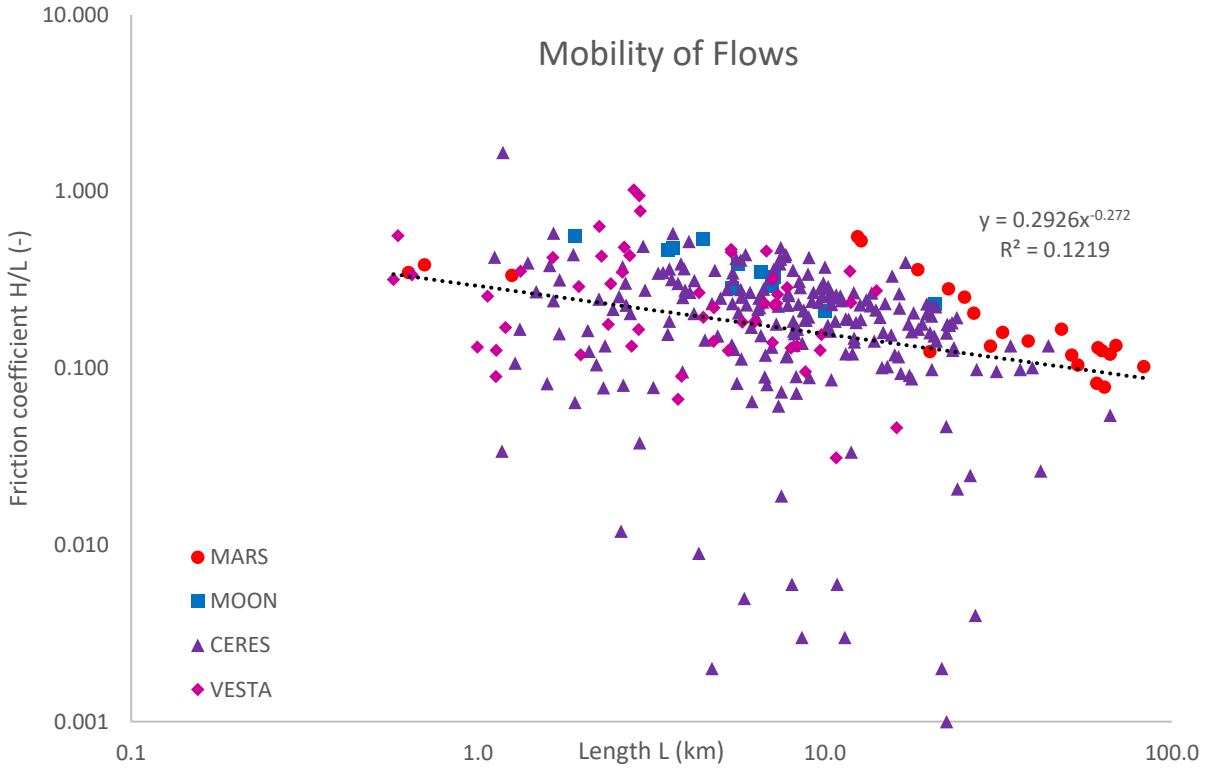

Figure 16: Mobility of flows shown by the dimensionless friction coefficient H/L plotted over runout length L in a log-log plot.

4.2.3 Slides

Figure 17 below shows the mobility of slides found on Mars, the Moon, Mercury, Ceres and Vesta. The data points are somewhat clustered for the Moon and Mars. For Mercury, there are little data points, and they are spread out / less concentrated. The measured Mercurian slides have similar lengths as lunar slides, but they seem to have a lower friction coefficient. The data for Ceres and Vesta, similarly to the flow data in Figure 16 shows a larger spread than the other bodies, in both length and mobility. The slides on these asteroids, especially on Ceres, are shorter compared to the other bodies. Nevertheless, the same downward trend in friction coefficient can be seen in the data. The trend line through all data shows a negative trend with a similar slope as the flow data.

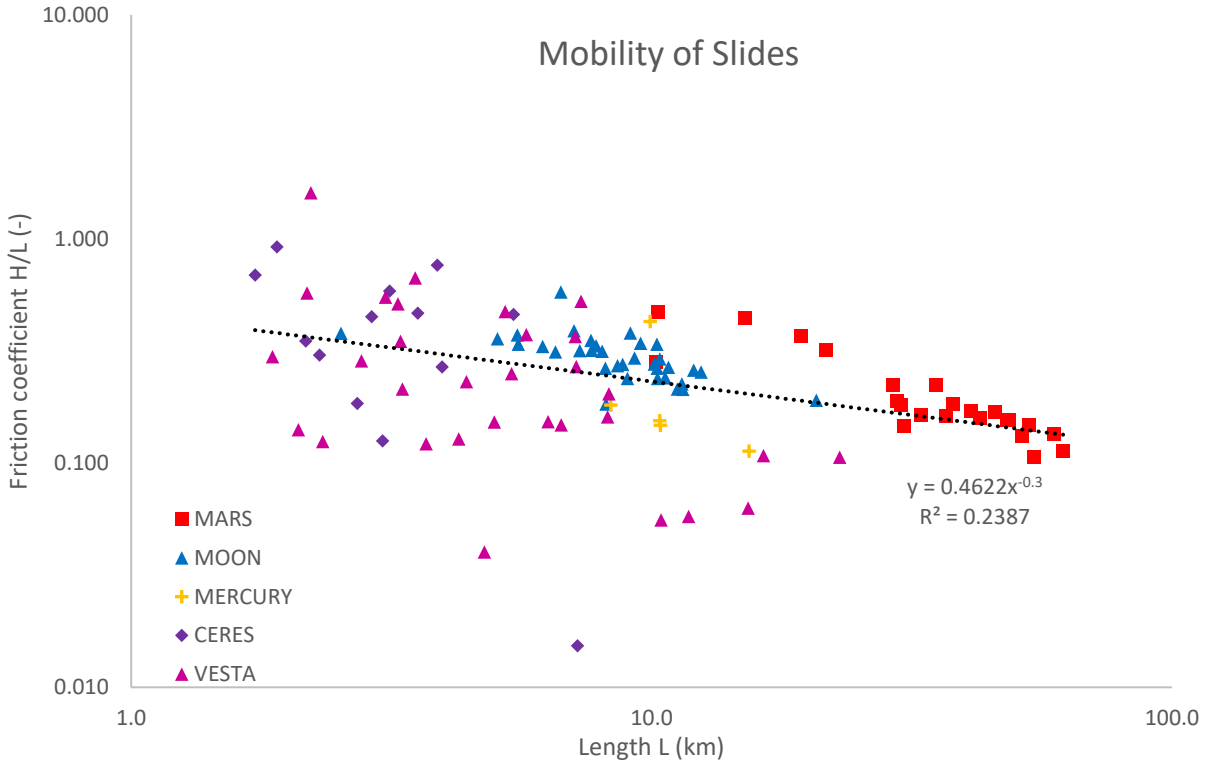

Figure 17: Mobility of slides shown by the dimensionless friction coefficient H/L plotted over runout length L in a log-log plot.

4.2.3 Slumps

Figure 18 below shows the mobility of slumps found on Mars, the Moon, Ceres and Vesta. The available datasets for slump are limited but, regardless, the slump features are quite large, with runouts generally larger than 7 km. Except for two slumps on Ceres, no small slump features were measured. Slides and flows show a much larger range of runout lengths and most of these movement have lengths of 10s of meters.

Despite the small number of measured slumps, a negative trend can be seen in the data. Lunar slumps seem to follow this trend, but for the other bodies too little data is available to be able to see. This means that larger slumps have higher mobility and have longer runout relative to the fall height.

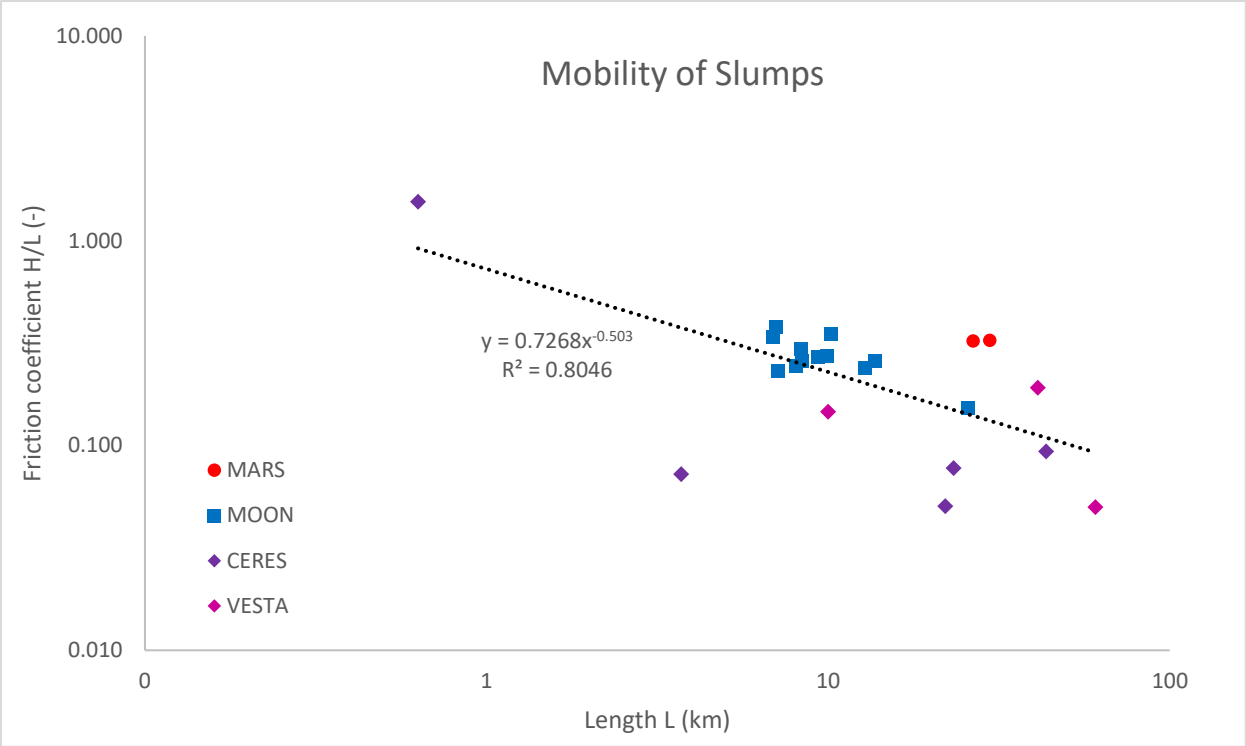

Figure 18: Mobility of slumps shown by the dimensionless friction coefficient H/L plotted over runout length L in a log-log plot.

4.2.3 Data spread and trends

Figure 19 displays the combined data from all movement. We observe that the different motion types have a similar spread regarding mobility. By overlapping the data, we notice a large number of mass wasting features cluster between 5 – 15 km in length and values of 0.1 – 0.5 for the friction coefficient. Here we also see the large spread of flow features compared to the other two motion types. The figure shows that slumps are among the largest features. However, there are also a lot of large slides and flows. Looking back at Figure 16 and Figure 17, we know that the largest flows and slides are found on Mars. If we ignore these, slumps become the largest features. So, apart from a few outliers, slumps are the largest features for all bodies except Mars.

Figure 19: Mobility of all flows, slides and slumps plotted against runout length L. Power functions are fitted for each type.

Chapter 5 – Discussion

5.1 Types of extraterrestrial mass wasting

On the rocky bodies discussed in this research, many different types of movements were found. Based on the classification proposed by Cruden & Varnes (1996), a new mass-wasting classification system is developed consisting of main classes and subclasses. For each body, the features discovered on its surface were classified using the classification system. The results show that several types are present on all the bodies , while others only occur on some bodies (Table 1). In this chapter, the (re)classification of mass wasting features into the specified classes and the main differences between the movement types are discussed.

5.1.1 Classification

In the mass wasting classification, there is a lot of inconsistency in the use of certain terms and definitions. This is the case for mass wasting on Earth (Shanmugam & Wang, 2015), but even more so when celestial bodies are concerned. Researchers often use classification systems based on terrestrial definitions but applied them to their specific research area. And because extraterrestrial mass wasting can be very different from what we know on Earth, new classifications are often introduced specifically to the research topic (Duarte et al., 2019; Quantin et al., 2004; Schmidt et al., 2017). This can be very useful for studying characteristics of mass wasting of a specific type or scale, or even on one celestial body. However, for comparing mass wasting across various bodies, these specific classes lose their value. This requires a more general classification structure like the one based on Cruden & Varnes (1996) proposed in Chapter 2. To integrate data classified otherwise, reclassification is necessary to be able to compare the features. This was done for several datasets used in this review.

Aside from classification structure, the accuracy of classification is an important factor to consider when identifying mass wasting features. Especially when multiple bodies are concerned. The environmental conditions, material type, geological and physical context, and timescale of an event all contribute to the resulting morphology. This means that the same mass movement in two different bodies can result in wildly different morphologies. It is therefore crucial that the classification attributes are not too specific to any one set of conditions, so that similar events on different bodies can be classified as the same movement. On the other hand, the attributes should also not be too vague. This could lead to a situation where two different movement classifications overlap each other. A balance should be found between the two. Still, there will always be mass movements that share attributes from different categories, for example when a slump transitions into a flow-type movement. In some cases, specific intermediate classes can therefore play a vital role in classification systems (Duarte et al., 2019).

The classification system proposed in chapter 2 (see Figure 3) has been constructed based on common attributes found on several bodies. For each movement type, as well as the subclasses of flow, morphological descriptions by the identifying authors were analyzed and compared. Attributes described in multiple studies were used in the classification system. This ensured that the morphological characteristics would not only be found on one specific body but would be more general in the context of all rocky bodies.

5.1.2 Identification bias

Not all movement types have been identified on our targeted bodies. This can be explained by the fact that certain types are present on some bodies but might not even exist on other bodies. The other explanation is that the morphological features left behind by the mass wasting events are not able to be identified. First of all, due to the large size of celestial bodies, searching the entire surface for a

specific morphological feature is an ambitious/demanding task. So only because a feature is not (yet) found, does not mean that a certain mass wasting type does not happen on that body. This means that there is a bias based on the search area. As we saw in Chapter 3, most mass wasting happens in craters due to the steep slopes and loose material. This means that research on mass wasting is generally focused on craters, creating a bias in the findings. Image quality is another important reason some features are not identified. Some features, e.g., pit chains formed by bouncing boulders as a result of rockfalls, are small and difficult to see compared to large slumps or slides. Furthermore, if the image resolution on a body is very coarse, as we see on Mercury with 166 m/pixel, many features smaller than that distance are not identifiable at all. This creates a bias on what features are found on that body.

5.1.3 Comparing presence of mass wasting types

Looking at Table 1, we see that not all features are present on the targeted/selected rocky bodies. Cases where features are not found, and possible reasons are discussed.

Main movement types

Thus far, falls are found on the Moon and Mars because the imagery/data is of high enough quality to identify individual boulders. Kokelaar et al. (2017) reported that boulders down to 1.5 m in diameter can be identified on the Moon. Such high-quality imagery is not available for the other bodies, so identifying individual boulders is only possible if they have a diameter of several times the pixel size. This would mean roughly 100 m sized boulders on Ceres and Vesta and almost kilometer scale boulders on Mercury. Rockfalls do not generally occur on such large scales.

On Mercury, slumps are not identified. Based on how common these features are on other bodies; it should be likely that they also would occur on Mercury. Combined with the fact that they are generally large, makes it strange that this feature is not identified here. A possible explanation for this is the lack of research on mass wasting on this planet. Only a few studies have been conducted here and Brunetti et al. (2015), who found by far the most mass wasting features, had used an oversimplified classification resulting in all features being classified as rockslides. The poor image quality can make it hard to distinguish slide morphology from that of a slump. So perhaps, if more detailed imagery is available, this may reveal that some of the features currently classified as slides, could in fact be slumps.

On the comets, only a few events of rockfalls have been identified, and flows take place as a more continuous process on the flat terrains due to regular outgassing, rather than from individual mass wasting events. We know that outgassing events and mass wasting are related (Pajola et al., 2017), but more research is necessary to fully understand what other types of movement can take place on these icy bodies.

Subclasses of flow

Thus far avalanches, defined as large and high velocity flows, are only found on Mars. A reason for this could be that Mars is the only body capable of generating flows of such a large scale, like the one in Figure 9. On other bodies, the largest features are often slumps or large slides. The large size of these avalanches could be explained due to entrainment caused by sublimation of CO_2 ice in the flow material (de Haas et al., 2019; Schmidt et al., 2017).

Creep features are present on the Moon and Vesta. These features are quite difficult to find because they do not have an obvious morphology like flows, slides and slumps. They are only identifiable by a gentle slope and some small transverse ridges or mounds. Creep may occur on Mars, Mercury and Ceres, but it has not been actively searched for and therefore not identified yet. Another explanation

is that conditions on the Moon and Vesta are just right for the slow gradual transport of regolith, allowing creep features to form.

Channeled flow is found almost everywhere, except on Ceres. However, the abundance of volatiles in the subsurface makes fluidized flow possible here. We see this in the other types of flow on the asteroid. Flows on Ceres seem to prefer sweeping flows over channelized flows, despite the first type being rare, but the reason remains unknown. It is only found on the Moon and Ceres. This is most likely classification related.

Ejecta flows are not found on the Moon and Vesta. However, this flow type is likely to occur on these bodies, since it is directly linked to meteoroid impacts (Xiao & Komatsu, 2013), which do indeed happen on the Moon and Vesta. A reason that this is not identified could be that these flows occur outside of impact craters, while much of the research on flows on these bodies is focused on movements inside craters.

5.2 Morphology: similarities and differences

5.2.1 Comparing morphology

As we saw in Chapter 4, the morphology of mass wasting deposits can vary significantly. One of the reasons for this can be linked to the scale of the feature. Most features vary in size, even on the same body. Especially slides have a wide range of scale, and this affects the deposit morphology. Size can for instance influence the deposition slope. Otto et al. (2013) found that large slides flatten on gentler slopes than young, smaller slides. Small slides that occur in small craters often have a simple shape and a smooth surface (Brunetti et al., 2015), while large slide features often have bumps and ridges on the top surface (Quantin et al., 2004). This is also the case for slumps. Large features often have secondary failures, making the slump morphology more complex (Krohn et al., 2014). Large slides and slumps also can transition into flow-type movement, which happens less with smaller features, since these do not lose cohesion as fast as larger ones (Kokelaar et al., 2017).

The material type of a movement also plays an important role in forming the morphology. Particularly the grain size is a determining factor. This effect can be seen in ejecta flows, which generally consist of fine material and are highly mobile (Duarte et al., 2019; Xiao & Komatsu, 2013). Xiao et al. (2013) also made a distinction between rock slides and debris slides based on fragment size and consolidation state, because the resulting slides showed different behavior and morphology. The material type also includes ice grains within the moving mass. These can partially melt or become slippery, which causes lubricated flow to occur, increasing the mobility of the movement (Schmidt et al., 2017).

Gravity is not only the core reason that mass wasting takes place in the first place, but it also affects many processes related to mass wasting. It determines how strongly the grains are pushed against each other, which can influence cohesion, which determines how easily slides and slumps transition into flows. Furthermore, Kleinhans et al. (2011) found that in a reduced gravity environment from 1 g to 0.1 g, the static angle of repose increases with 5°, and the dynamic angle of repose decreases with 10°. This means that on bodies with reduced gravity, material can remain stable on steeper slopes, while it comes to a stop on a lower angle. This has an impact on the final morphology, so this effect of gravity should be considered when comparing mass wasting features from different gravitational environments.

The most important factor influencing final deposit morphology is the mobility of the moving material. We have seen that predominantly flow-type movements can be mobilized, increasing their runout length significantly. This allows the flows, which have a relatively small volume, to reach much further

distances compared to the more voluminous slides. How a movement can be mobilized is discussed in section 5.3: Mobility.

5.2.2 Specific morphological features

Some features are common on several bodies and their presence indicates similar processes.

Gullies

Gully morphology is present on the Moon (Kokelaar et al., 2017; Senthil Kumar et al., 2013), on Mars (Conway et al., 2019; de Haas et al., 2019; Dundas et al., 2019; Hecht, 2002; Malin & Edgett, 2000) and on Vesta (Krohn et al., 2014; Scully et al., 2015). And everywhere, this feature, containing an alcove, channel and depositional fan, is linked to flow-type movement. Whether this is caused by transient liquid water, like on Vesta (Scully et al., 2015), by dry granular flows (Krohn et al., 2014), or by fluidization due to sublimating volatiles (Conway et al., 2019; de Haas et al., 2019; Dundas et al., 2019).

Outgassing

A process that has been observed on several bodies is outgassing. As a result of sublimating volatiles from subsurface bodies of ice (or evaporating liquid), outgassing disturbs the regolith on the surface and can form depressions or pits. On Vesta, pitted terrain formed by this process is a recognized feature and occurs on crater floors (Scully et al., 2015). This is also found to occur on Mars, for example on debris aprons, and this is linked to an ice-rich ground (Mangold, 2011). On Comet 9P, outgassing also occurs and leaves behind depressions on the surface (Belton & Melosh, 2009).

5.3 Mobility

5.3.1 Fluidization and volatiles

We have seen that mobilization occurs in three different ways. Dry granular flow, lubricated flow and sublimation driven flow. Dry granular flow is mostly observed on bodies with low volatile content, such as Vesta (Parekh et al., 2021). Here, slides are the most common mass wasting type, and these features are mobilized by dry granular flow. No extra fluidization takes place in such movements.

Although very rare, sometimes flows can become lubricated by small amounts if liquid water. This is possible on both Mars and Vesta, where water ice is present. Although unstable in normal climate conditions, transient liquid water can exist under the right temperatures and pressure conditions. This water then has a residence time of up to a few hours on Mars (Conway et al., 2019). On Vesta, it is believed to exist at least long enough to form gully landforms on Vesta (Scully et al., 2015). Another way of forming lubricated flow, is when small grains of ice within a flowing mass partially melt. This reduces the basal friction and causes some fluidization of the movement (Schmidt et al., 2017).

Sublimation of volatiles is the most important mechanism causing fluidization of mass wasting material. This happens because the intergranular friction is reduced by the pressure of the gas produced by the sublimation (de Haas et al., 2019; Mangold, 2011). This reduced friction allows the material to behave more like a fluid. As a result, the detached material flows easily downslope. In some cases, the heat produced by the friction between the grains or between the surface and the flowing mass can lead to more aggressive sublimation. This extra sublimation due to friction mobilizes more material from the surface, causing entrainment (de Haas et al., 2019).

5.3.2 Trends in mobility

Mobility of mass wasting features is quantified by using a coefficient of friction, by calculating the ratio between fall height and runout length *H/L*. The features in the dataset that contained fall height and runout length information were plotted and this resulted in negative trends for *H/L* over *L* plots. This means that for larger (longer) features, the friction coefficient is lower thus the mobility is higher. Here,

only length is discussed as a measure of size. Crosta et al. (2018) propose the same relation but for volume. They state that the friction coefficient *H/L* decreases with increasing volume. The negative trend in friction coefficient is also consistent with the findings of Parekh et al. (2021), who found negative *H/L* over *L* trends for both slides and flow-type movement.

The spread of the data is quite large, especially for the flow data. So large in fact that the natural spread of the data is larger than the spread per body. Unfortunately, this means that we cannot find out if there are any clear differences in mobility between the different bodies. Nevertheless, we can make some observations from the position of the data clusters of each body. For Ceres, we see that the flows have very high mobility and reach very high runout lengths, while flows on Vesta have lower mobility and reach less far. This difference can be linked to the different amounts of volatiles present on the two bodies (Parekh et al., 2021). As mentioned in section 3.6.1, Vesta is a dry body with little volatile substances. Flows on the surface of Vesta therefore experience less fluidization by sublimating volatiles compared to Ceres or Mars, where volatiles are more abundant in the regolith. This results in shorter flows on Vesta. Slides, on the other hand, are surprisingly short on Ceres, while on Vesta they have longer runout lengths. This can be attributed to the fact that slides are the most common feature on Vesta, while they occur less frequently on Ceres, where flows are more common (Parekh et al., 2021).

The natural spread of the data is larger than the spread per body. This means we cannot say anything about the differences in trend or behavior between each body. Subtle differences caused by gravity and atmospheric pressure may be present, but unfortunately cannot be seen in this data.

5.4 Triggers

5.4.1 Preconditioning

Mass wasting occurs when the driving forces are greater than the resistive forces, i.e. the factor of safety is less than 1 and the slope becomes unstable. However, mass wasting can still occur if a slope is marginally stable (Pradhan & Siddique, 2019). In these cases, a final trigger is required that initiates the motion of the material. Here, several triggering mechanisms found in extraterrestrial mass wasting are discussed. Before a movement is triggered, however, preconditioning is often crucial in weakening the slope or 'preparing' the material for movement. Meteoroid impacts not only create slopes for material to flow down over but also severely weaken the target rock (Brunetti et al., 2015; French, 1998; Xiao et al., 2013). Many cracks are formed, making detachment of material easier. Furthermore, the brittle impact melt material that forms during impact is easily shattered, causing mass wasting (Xiao et al., 2013). Sublimation of volatiles is also a preconditioning process, as it weakens regolith slopes. The produced gas increases massively in volume and causes a reduction of friction between the grains, making the slope less stable (de Haas et al., 2019).

5.4.2 Sublimation as a trigger

Sublimation can act as both a preconditioning and triggering mechanism. De Haas et al. (2019) concluded that CO_2 sublimation can trigger flows in Martian gullies, as well as fluidize the flow. Parekh et al. (2021) argue however, that sublimation is not enough to reduce the friction below the point where gravity can initiate motion. Only when movement is started by some other force, can sublimation affect the motion. At least, this is what Parekh et al. (2021) concluded for mass wasting on Ceres and Vesta. On comet 9P, sublimation is able to initiate motion by fluidizing the cometary material on the surface (Belton & Melosh, 2009).

5.4.3 Thermal stress

The weakening of slopes by sublimation is only relevant for granular movements. Fall-type movements are fundamentally different because these movements are about the detachment of singular blocks of

material from a cliff, rather than a granular mass. These are also not triggered by sublimation, but rather by thermal stresses on the rock due to diurnal temperature changes (Pajola et al., 2017; Tesson et al., 2020). This type of stress is also a preconditioning factor for mass wasting on crater walls in general.

5.4.3 Seismic shaking

The most common trigger is seismic shaking (Brunetti et al., 2015; French, 1998; Krohn et al., 2014; Otto et al., 2013; Schultz & Gault, 1975; Tesson et al., 2020; Xiao et al., 2013). Processes like tectonics, volcanism or tidal forces can cause this, but most mass movements are triggered by impact-related seismic shaking. This affects the area surrounding the impact location, but it can also have an effect on larger distances. Large-impact events can cause shaking far away by the propagation of p-waves (Schultz & Gault, 1975). Also on very small scales, impact events can result in mass wasting. Tiny impacts on crater walls can initiate small flows (Crosta et al., 2018; Senthil Kumar et al., 2013). Also related to impacts are ejecta flows. The flow material and initial momentum are products of the impact. Afterwards when the material has settled, flows can be triggered in unstable areas within the ejecta sheet, which are related to the initial flow (Crosta et al., 2018).

5.5 Recommendations for future research

To further enlarge our knowledge about extraterrestrial mass wasting, an effort should be made to fully understand what types of mass wasting are present on the bodies. Specifically, targeted search should be conducted for features that likely exist, but are not yet identified, such as channeled flow on Ceres. Above all, this is the case for Mercury. We know that mass wasting does occur there, but the availability of high-resolution imagery is limited. The BepiColombo mission led by the European Space Agency is currently on its way to the planet and should resolve this issue. On board is the SIMBIO-SYS instrument containing a spectrometer and multiple imagers, including a high-resolution imaging channel with a spatial resolution of 5 m/pixel, a stereo and color imaging channel capable of creating digital terrain models (Flamini et al., 2010). High-resolution imagery should be used to investigate whether slumps are present on the surface and to investigate how flow processes related to volatile sublimation, take place on this planet. Another way mass wasting could be better understood is by using volume-based analysis. Much of the research now is done using length and area measurements with only a few studies using volume calculations (Kokelaar et al., 2017; Quantin et al., 2004). With knowledge about transported volumes and masses, we can learn more about the actual forces acting on the surface, which could have implications for all kinds of surface processes.

Chapter 6 – Conclusions

In this study, extraterrestrial mass wasting on several bodies in the Solar System was investigated. A new classification system was developed to identify mass wasting features in different planetary environments. A dataset was created combining mass wasting data collected from prior research, with 1320 features in total. The morphology was compared and a quantitative analysis of the mobility of the features was performed. Based on this, several conclusions can be drawn.

1. To compare mass wasting events across multiple bodies that have different environments, a general classification system should be used to classify features based on attributes that are universal, and not body-specific, like the one proposed in this review. This classification consists of four main movement types: fall, flow, slide and slump. Five important subclasses for flow-type movements are defined: avalanche, creep, channeled flow, sweeping flow and ejecta flow. When comparing features, the effects of the different environmental characteristics should be considered, and special attention has to be paid to biases related to search area, scale and image data quality.
2. The main movement types have been identified on the following bodies. Falls were identified on the Moon, Mars and on comet 67P. Flows were found on all bodies included in the study, except comet 67P. Slumps were found on the Moon, Mars, Ceres and Vesta. Slides were found on all bodies except the comets (i.e. Moon, Mars, Mercury, Ceres and Vesta). Some subclasses of flows were also found. Avalanches were identified only on Mars, creep was found to occur on the Moon and Vesta. Channeled flow is the most occurring subclass, appearing on the Moon, Mars, Mercury and Vesta. Meanwhile, sweeping flows are only found on the Moon and Ceres. Finally, ejecta flows are found on Mars, Mercury and Ceres.
3. The morphology of mass wasting features is different per movement type or class. Falls have a unique morphology, in the sense that most times the deposit consists of one or a few clasts and in some cases a talus cone. Flows show the most variation in morphology, mainly in runout length, compared to the other classes. Slides are the most common feature and have a very large size range. Slumps are generally the largest features, at least in terms of displaced volume. Within each class, there are similarities and differences in morphology. These differences can almost always be explained by one or more of the following factors: scale of the feature, material type, gravity and most importantly, mobility of the movement.
4. Fluidization of material is a relatively common process in extraterrestrial mass wasting, mainly observed in flow-type movements, but also in slides. Fluidization is necessary to match the flow characteristics that form the observed morphologies of these mass wasting features. Fluidized flows can reach further distances and shape specific landforms like gullies. Three degrees of fluidization exist: dry granular flow (no fluidization), lubricated flow (somewhat fluidized) and sublimation driven flow (fluidized).
5. Volatile substances, if present on a body, are the most important fluidization agent. This can happen in several ways. Specific temperature and pressure conditions can allow transient flow of liquid water where this is normally unstable, this is hypothesized on Mars and Vesta. In the short period before it is vaporized, this causes lubricated flow. Sublimation of volatiles in ice form can cause fluidization of material due to the large volume of gas produced. This lowers intergranular friction and allows dry masses to behave as a fluid, resulting in long runout morphologies. This is called sublimation driven flow.
6. Mobility analysis shows that for larger features with longer runout length the ratio *H/L* decreases, indicating higher mobility. This is true for flows, slides and slumps. Over all, flows have the highest mobility of these types, mainly due to the fluidization processes.

7. Mass wasting can be triggered in multiple ways, but before this can happen, preconditioning factors play an important role in weakening the slope. Meteoroid impacts severely crack the target rock and create much loose granular material and ejecta. Sublimation also acts as a preconditioning factor, lowering the intergranular friction. Sublimation of volatiles can in some cases also act as a triggering mechanism. For rockfalls, thermal stresses can be a trigger. The most common triggering mechanism, however, is (impact-induced) seismic shaking. This affects areas near the impact, but also far away due to p-wave propagation.

References

Aubry, C., Conway, S. J., Malliband, C., Galluzzi, V., & Giacomini, L. (2021). A survey of landforms indicating slope processes in the mid-latitudes of Mercury. *Europlanet Science Congress*, *15*. https://doi.org/10.5194/epsc2021-490ï

Belton, M. J. S., & Melosh, J. (2009). Fluidization and multiphase transport of particulate cometary material as an explanation of the smooth terrains and repetitive outbursts on 9P/Tempel 1. *Icarus*, *200*(1), 280–291. https://doi.org/10.1016/j.icarus.2008.11.012

Blewett, D. T., Chabot, N. L., Denevi, B. W., Ernst, C. M., Head, J. W., Izenberg, N. R., Murchie, S. L., Solomon, S. C., Nittler, L. R., McCoy, T. J., Xiao, Z., Baker, D. M. H., Fassett, C. I., Braden, S. E., Oberst, J., Scholtel, F., Preusker, F., & Hurwitz, D. M. (2011). Hollows on Mercury: MESSENGER Evidence for Geologically Recent Volatile-Related Activity. *Science*, *333*(6051), 1856–1859. https://doi.org/10.1126/science.1211997

Brunetti, M. T., Xiao, Z., Komatsu, G., Peruccacci, S., & Guzzetti, F. (2015). Large rock slides in impact craters on the Moon and Mercury. *Icarus*, *260*, 289–300. https://doi.org/10.1016/j.icarus.2015.07.014

Conway, S. J., De Haas, T., & Harrison, T. N. (2019). Martian gullies: A comprehensive review of observations, mechanisms and insights from Earth analogues. *Geological Society Special Publication*, *467*(1), 7–66. https://doi.org/10.1144/SP467.14

Crosta, G. B., Frattini, P., Valbuzzi, E., & De Blasio, F. V. (2018). Introducing a New Inventory of Large Martian Landslides. *Earth and Space Science*, *5*(4), 89–119. https://doi.org/10.1002/2017EA000324

Cruden, D. M., & Varnes, D. J. (1996). Landslide Types and Processes. In *Transportation Research Board, U.S. National Academy of Sciences, Special Report* (Vol. 247). https://www.researchgate.net/publication/269710331

De Blasio, F. V. (2011). Landslides in Valles Marineris (Mars): A possible role of basal lubrication by sub-surface ice. *Planetary and Space Science*, *59*(13), 1384–1392. https://doi.org/10.1016/j.pss.2011.04.015

de Haas, T., McArdell, B. W., Conway, S. J., McElwaine, J. N., Kleinhans, M. G., Salese, F., & Grindrod, P. M. (2019). Initiation and Flow Conditions of Contemporary Flows in Martian Gullies. *Journal of Geophysical Research: Planets*, *124*(8), 2246–2271. https://doi.org/10.1029/2018JE005899

Diez, A. (2018). Liquid water on Mars. *Science*, *361*(6401), 448–449. https://doi.org/10.1126/science.aau1829

Duarte, K. D., Schmidt, B. E., Chilton, H. T., Hughson, K. H. G., Sizemore, H. G., Ferrier, K. L., Buffo, J. J., Scully, J. E. C., Nathues, A., Platz, T., Landis, M., Byrne, S., Bland, M., Russell, C. T., & Raymond, C. A. (2019). Landslides on Ceres: Diversity and Geologic Context. *Journal of Geophysical Research: Planets*, *124*(12), 3329–3343. https://doi.org/10.1029/2018JE005673

Dundas, C. M., Mcewen, A. S., Diniega, S., Hansen, C. J., Byrne, S., & Mcelwaine, J. N. (2019). The formation of gullies on Mars today. *Geological Society, London, Special Publications*, *467*(1), 67–94. https://doi.org/10.6084/m9.figshare.c.3936886

Filacchione, G., Raponi, A., Capaccioni, F., Ciarniello, M., Tosi, F., Capria, M. T., De Sanctis, M. C., Migliorini, A., Piccioni, G., Cerroni, P., Barucci, M. A., Fornasier, S., Schmitt, B., Quirico, E., Erard, S., Bockelee-Morvan, D., Leyrat, C., Arnold, G., Mennella, V., … Peter, G. (2016). *Seasonal exposure of carbon dioxide ice on the nucleus of comet 67P/Churyumov-Gerasimenko*. https://www.science.org

Flamini, E., Capaccioni, F., Colangeli, L., Cremonese, G., Doressoundiram, A., Josset, J. L., Langevin, Y., Debei, S., Capria, M. T., De Sanctis, M. C., Marinangeli, L., Massironi, M., Mazzotta Epifani, E., Naletto, G., Palumbo, P., Eng, P., Roig, J. F., Caporali, A., Da Deppo, V., … Hello, Y. (2010). SIMBIO-SYS: The spectrometer and imagers integrated observatory system for the BepiColombo planetary orbiter. *Planetary and Space Science*, *58*(1–2), 125–143. https://doi.org/10.1016/j.pss.2009.06.017

French, B. M. (1998). Formation of Impact Craters. In *Traces of Catastrophe: A Handbook of Shock-Metamorphic Effects in Terrestrial Meteorite Impact Structures* (pp. 17–30). Lunar and Planetary Institute. https://www.lpi.usra.edu/publications/books/CB-954/CB-954.intro.html

Hecht, M. H. (2002). Metastability of liquid water on Mars. *Icarus*, *156*(2), 373–386. https://doi.org/10.1006/icar.2001.6794

Housen, K. R., & Wilkening, L. L. (1982). *REGOLITHS ON SMALL BODIES IN THE SOLAR SYSTEM!*

Hugenholtz, C. H. (2008). Frosted granular flow: A new hypothesis for mass wasting in martian gullies. *Icarus*, *197*(1), 65–72. https://doi.org/10.1016/j.icarus.2008.04.010

Hungr, O., Leroueil, S., & Picarelli, L. (2014). The Varnes classification of landslide types, an update. In *Landslides* (Vol. 11, Issue 2, pp. 167–194). Springer Verlag. https://doi.org/10.1007/s10346-013-0436-y

Keller, E. A., & DeVecchio, D. E. (2019). Mass Wasting. In *Natural Hazards* (5th ed., pp. 256–297).

Kleinhans, M. G., Markies, H., De Vet, S. J., In't Veld, A. C., & Postema, F. N. (2011). Static and dynamic angles of repose in loose granular materials under reduced gravity. *Journal of Geophysical Research: Planets*, *116*(11). https://doi.org/10.1029/2011JE003865

Kokelaar, B. P., Bahia, R. S., Joy, K. H., Viroulet, S., & Gray, J. M. N. T. (2017). Granular avalanches on the Moon: Mass-wasting conditions, processes, and features. *Journal of Geophysical Research: Planets*, *122*(9), 1893–1925. https://doi.org/10.1002/2017JE005320

Krohn, K., Jaumann, R., Otto, K., Hoogenboom, T., Wagner, R., Buczkowski, D. L., Garry, B., Williams, D. A., Yingst, R. A., Scully, J., De Sanctis, M. C., Kneissl, T., Schmedemann, N., Kersten, E., Stephan, K., Matz, K. D., Pieters, C. M., Preusker, F., Roatsch, T., … Raymond, C. A. (2014). Mass movement on Vesta at steep scarps and crater rims. *Icarus*, *244*, 120–132. https://doi.org/10.1016/j.icarus.2014.03.013

Lucchetti, A., Pajola, M., Poggiali, G., Semenzato, A., Munaretto, G., Cremonese, G., Brucato, J. R., & Massironi, M. (2021). Volatiles on mercury: The case of hollows and the pyroclastic vent of Tyagaraja crater. *Icarus*, *370*. https://doi.org/10.1016/j.icarus.2021.114694

Lucchetti, A., Penasa, L., Pajola, M., Massironi, M., Brunetti, M. T., Cremonese, G., Oklay, N., Vincent, J. B., Mottola, S., Fornasier, S., Sierks, H., Naletto, G., Lamy, P. L., Rodrigo, R., Koschny, D., Davidsson, B., Barbieri, C., Barucci, M. A., Bertaux, J. L., … Tubiana, C. (2019). The Rocky-Like

Behavior of Cometary Landslides on 67P/Churyumov-Gerasimenko. *Geophysical Research Letters*, *46*(24), 14336–14346. https://doi.org/10.1029/2019GL085132

Malin, M. C. (1992). Preliminary Results From Magellan Cycle 1 Observations. In *JOURNAL OF GEOPHYSICAL RESEARCH* (Vol. 97).

Malin, M. C., & Edgett, K. S. (2000). Evidence for Recent Groundwater Seepage and Surface Runoff on Mars. *Science*, *288*(5475), 2330–2335. https://www.science.org

Malliband, C. C., Conway, S. J., Rothery, D. A., & Balme, M. R. (2019). Potential Identification of Downslope Mass Movements on Mercury Driven by Volatile-Loss. *Lunar and Planetary Science Conference*, *50*, 1804.

Mangold, N. (2011). Ice sublimation as a geomorphic process: A planetary perspective. In *Geomorphology* (Vol. 126, Issues 1–2, pp. 1–17). https://doi.org/10.1016/j.geomorph.2010.11.009

Manheim, M. R., Henriksen, M. R., Robinson, M. S., Kerner, H. R., Karas, B. A., Becker, K. J., Chojnacki, M., Sutton, S. S., & Blewett, D. T. (2022). High-Resolution Regional Digital Elevation Models and Derived Products from MESSENGER MDIS Images. *Remote Sensing*, *14*(15). https://doi.org/10.3390/rs14153564

Moore, J. M., Asphaug, E., Morrison, D., Spencer, J. R., Chapman, C. R., Bierhaus, B., Sullivan, R. J., Chuang, F. C., Klemaszewski, J. E., Greeley, R., Bender, K. C., Geissler, P. E., Helfenstein, P., & Pilcher, C. B. (1999). Mass Movement and Landform Degradation on the Icy Galilean Satellites: Results of the Galileo Nominal Mission. In *Icarus* (Vol. 140). http://www.idealibrary.comon

Orosei, R., Ding, C., Fa, W., Giannopoulos, A., Hérique, A., Kofman, W., Lauro, S. E., Li, C., Pettinelli, E., Su, Y., Xing, S., & Xu, Y. (2020). The global search for liquid water on mars from orbit: Current and future perspectives. In *Life* (Vol. 10, Issue 8, pp. 1–15). MDPI AG. https://doi.org/10.3390/life10080120

Otto, K. A., Jaumann, R., Krohn, K., Matz, K. D., Preusker, F., Roatsch, T., Schenk, P., Scholten, F., Stephan, K., Raymond, C. A., & Russell, C. T. (2013). Mass-wasting features and processes in Vesta's south polar basin Rheasilvia. *Journal of Geophysical Research: Planets*, *118*(11), 2279–2294. https://doi.org/10.1002/2013JE004333

Pajola, M., Höfner, S., Vincent, J. B., Oklay, N., Scholten, F., Preusker, F., Mottola, S., Naletto, G., Fornasier, S., Lowry, S., Feller, C., Hasselmann, P. H., Güttler, C., Tubiana, C., Sierks, H., Barbieri, C., Lamy, P., Rodrigo, R., Koschny, D., … Baratti, E. (2017). The pristine interior of comet 67P revealed by the combined Aswan outburst and cliff collapse. *Nature Astronomy*, *1*. https://doi.org/10.1038/s41550-017-0092

Parekh, R., Otto, K. A., Jaumann, R., Matz, K. D., Roatsch, T., Kersten, E., Elgner, S., & Raymond, C. (2021). Influence of Volatiles on Mass Wasting Processes on Vesta and Ceres. *Journal of Geophysical Research: Planets*, *126*(3). https://doi.org/10.1029/2020JE006573

Piqueux, S., Kleinböhl, A., Hayne, P. O., Heavens, N. G., Kass, D. M., McCleese, D. J., Schofield, J. T., & Shirley, J. H. (2016). Discovery of a widespread low-latitude diurnal CO2frost cycle on Mars. *Journal of Geophysical Research: Planets*, *121*(7), 1174–1189. https://doi.org/10.1002/2016JE005034

Pokorný, P., Mazarico, E., & Schorghofer, N. (2021). Erosion of volatiles by micrometeoroid bombardment on ceres and comparison to the moon and mercury. *Planetary Science Journal*, *2*(3). https://doi.org/10.3847/PSJ/abef04

Pradhan, S. P., & Siddique, T. (2019). Mass wasting: An overview. In S. P. Pradhan, V. Vishal, & T. N. Singh (Eds.), *Advances in Natural and Technological Hazards Research* (Vol. 50, pp. 3–20). Springer Netherlands. https://doi.org/10.1007/978-3-319-77377-3_1

Preusker, F., Oberst, J., Head, J. W., Robinson, M. S., Watters, T. R., & Solomon, S. C. (2012). Topography of Mercury from stereo images: Regional terrain models from MESSENGER orbital mapping. *EPSC Abstracts*, *7*. https://www.researchgate.net/publication/258732248

Preusker, F., Scholten, F., Matz, K. D., Roatsch, T., Hviid, S. F., Mottola, S., Knollenberg, J., Kührt, E., Pajola, M., Oklay, N., Vincent, J. B., Davidsson, B., A'Hearn, M. F., Agarwal, J., Barbieri, C., Barucci, M. A., Bertaux, J. L., Bertini, I., Cremonese, G., … Tubiana, C. (2017). The global meter-level shape model of comet 67P/Churyumov-Gerasimenko. *Astronomy and Astrophysics*, *607*. https://doi.org/10.1051/0004-6361/201731798

Preusker, F., Scholten, F., Matz, K.-D., Elgner, S., Jaumann, R., Roatsch, T., Joy, S. P., Polanskey, C. A., Raymond, C. A., & Russell, C. T. (2016). *Dawn at Ceres - Shape model and rotational state*.

Preusker, F., Scholten, F., Matz, K.-D., Roatsch, T., Jaumann, R., Raymond, C. A., & Russell, C. T. (2012). Topography of Vesta from Dawn FC stereo images. In *European Planetary Science Congress* (Vol. 7). http://meetingorganizer.copernicus.org/EPSC2012/EPSC2012-428-1.pdf

Quantin, C., Allemand, P., & Delacourt, C. (2004). Morphology and geometry of Valles Marineris landslides. *Planetary and Space Science*, *52*(11), 1011–1022. https://doi.org/10.1016/j.pss.2004.07.016

Roatsch, T., Kersten, E., Matz, K. D., Preusker, F., Scholten, F., Elgner, S., Jaumann, R., Raymond, C. A., & Russell, C. T. (2013). High-resolution Vesta Low Altitude Mapping Orbit Atlas derived from Dawn Framing Camera images. *Planetary and Space Science*, *85*, 293–298. https://doi.org/10.1016/j.pss.2013.06.024

Roatsch, T., Kersten, E., Matz, K. D., Preusker, F., Scholten, F., Jaumann, R., Raymond, C. A., & Russell, C. T. (2012). High resolution Vesta High Altitude Mapping Orbit (HAMO) Atlas derived from Dawn framing camera images. *Planetary and Space Science*, *73*(1), 283–286. https://doi.org/10.1016/j.pss.2012.08.021

Roatsch, T., Kersten, E., Matz, K. D., Preusker, F., Scholten, F., Jaumann, R., Raymond, C. A., & Russell, C. T. (2016). High-resolution Ceres High Altitude Mapping Orbit atlas derived from Dawn Framing Camera images. *Planetary and Space Science*, *129*, 103–107. https://doi.org/10.1016/j.pss.2016.05.011

Roatsch, T., Kersten, E., Matz, K. D., Preusker, F., Scholten, F., Jaumann, R., Raymond, C. A., & Russell, C. T. (2017). High-resolution Ceres Low Altitude Mapping Orbit Atlas derived from Dawn Framing Camera images. *Planetary and Space Science*, *140*, 74–79. https://doi.org/10.1016/j.pss.2017.04.008

Roelofs, L., Conway, S. J., van Dam, B., van Eijk, A., Merrison, J. P., Iversen, J. J., Sylvest, M., Patel, M. R., Markies, H., van Maarseveen, M., McElwaine, J., Kleinhans, M. G., & de Haas, T. (2024). The Dynamics of CO2-Driven Granular Flows in Gullies on Mars. *Journal of Geophysical Research: Planets*, *129*(6). https://doi.org/10.1029/2024JE008319

Russell, C. T., & Raymond, C. A. (2011). The Dawn mission to Vesta and Ceres. *Space Science Reviews*, *163*(1–4), 3–23. https://doi.org/10.1007/s11214-011-9836-2

Schmidt, B. E., Hughson, K. H. G., Chilton, H. T., Scully, J. E. C., Platz, T., Nathues, A., Sizemore, H., Bland, M. T., Byrne, S., Marchi, S., O'Brien, D. P., Schorghofer, N., Hiesinger, H., Jaumann, R., Pasckert, J. H., Lawrence, J. D., Buzckowski, D., Castillo-Rogez, J. C., Sykes, M. V., … Raymond, C. A. (2017). Geomorphological evidence for ground ice on dwarf planet Ceres. *Nature Geoscience*, *10*(5), 338–343. https://doi.org/10.1038/ngeo2936

Schultz, P. H., & Gault, D. E. (1975). Seismic Effects from Major Basin Formations on the Moon and Mercury. *The Moon*, *12*, 159–177.

Scully, J. E. C., Russell, C. T., Yin, A., Jaumann, R., Carey, E., Castillo-Rogez, J., McSween, H. Y., Raymond, C. A., Reddy, V., & Le Corre, L. (2015). Geomorphological evidence for transient water flow on Vesta. *Earth and Planetary Science Letters*, *411*, 151–163. https://doi.org/10.1016/j.epsl.2014.12.004

Senthil Kumar, P., Keerthi, V., Senthil Kumar, A., Mustard, J., Gopala Krishna, B., Amitabh, Ostrach, L. R., Kring, D. A., Kiran Kumar, A. S., & Goswami, J. N. (2013). Gullies and landslides on the Moon: Evidence for dry-granular flows. *Journal of Geophysical Research: Planets*, *118*(2), 206–223. https://doi.org/10.1002/jgre.20043

Shanmugam, G., & Wang, Y. (Ed.). (2015). The landslide problem. *Journal of Palaeogeography*, *4*(2), 109–166. https://doi.org/10.3724/SP.J.1261.2015.00071

Steckloff, J. K., Johnson, B. C., Bowling, T., Jay Melosh, H., Minton, D., Lisse, C. M., & Battams, K. (2015). Dynamic sublimation pressure and the catastrophic breakup of Comet ISON. *Icarus*, *258*, 430–437. https://doi.org/10.1016/j.icarus.2015.06.032

Tesson, P. A., Conway, S. J., Mangold, N., Ciazela, J., Lewis, S. R., & Mège, D. (2020). Evidence for thermal-stress-induced rockfalls on Mars impact crater slopes. *Icarus*, *342*. https://doi.org/10.1016/j.icarus.2019.113503

Varnes, D. J. (1978). Slope Movement Types and Processes. In R. L. Schuster & R. J. Krizek (Eds.), *Landslides: Analysis and Control* (Special Report 176, pp. 11–33). Transportation Research Board, National Academy of Sciences.

Williams, D. R. (2016, April 18). *Solar System Small Worlds [Fact Sheet]*. NSSDCA, NASA. https://nssdc.gsfc.nasa.gov/planetary/factsheet/galileanfact_table.html

Williams, D. R. (2024, January 11). *Mars [Fact Sheet]*. NSSDCA, NASA. https://nssdc.gsfc.nasa.gov/planetary/factsheet/marsfact.html

Xiao, Z., & Komatsu, G. (2013). Impact craters with ejecta flows and central pits on Mercury. *Planetary and Space Science*, *82–83*, 62–78. https://doi.org/10.1016/j.pss.2013.03.015

Xiao, Z., Zeng, Z., Ding, N., & Molaro, J. (2013). Mass wasting features on the Moon - how active is the lunar surface? *Earth and Planetary Science Letters*, *376*, 1–11. https://doi.org/10.1016/j.epsl.2013.06.015

Appendices

A1: Imagery and resolutions

Table 2: Imagery data with resolution and corresponding mission and instrument (sources are grouped per body). Below is the relevant surface imagery of every rocky body discussed. It includes the mission and science instrument, the resolution (if available) and the image type. Table 3 contains the same information but related to elevation data such as local and global digital elevation models.

Table 2: Imagery data with resolution and corresponding mission and instrument (sources are grouped per body).

Body	Instrument	Resolution (m/p)	Type	Size / source
The Moon	LO1-LO5	60	Global mosaic	17 GB [1]
	LROC-WAC	100	Global mosaic	5.5 GB [4]
	LROC-NAC	0.5	Local & polar mosaics	- [10]
Mars	Viking-VIS (MDIM2.1)	232	Global mosaic (color)	12 GB [11]
	MGS-MOC (NAC)	1.5 – 12	Local images	- [14]
	MRO-CTX	5.0	Global mosaic	11.5 TB [8]
	MRO-HiRISE	0.30	Local images	- [12]
	MRO-HiRISE	0.25	Local mosaic (Jezero crater)	6.9 GB [9]
Mercury	Mariner 10	≥ 90	Flyby mosaics	- [2]
	MESSENGER-WAC	665	Global mosaic (color)	761 MB [4]
	MESSENGER-WAC/NAC	166	Global mosaic (morphology)	2.1 GB [4]
	MESSENGER-WAC/NAC	166	Global mosaic (low incidence)	1.9 GB [4]
Ceres	Dawn-FC (HAMO)	140	Global mosaic	214 MB [2]/ (Roatsch et al., 2016)
	Dawn-FC (LAMO)	35	Global mosaic	(Roatsch et al., 2017)
Vesta	Dawn-FC (HAMO)	60	Near-global mosaic	341 MB [1] / (Roatsch et al., 2012)
	Dawn-FC (LAMO)	20	Near-global mosaic	1.3 GB [2] / (Roatsch et al., 2013)
Comet 67P	Rosetta-OSIRIS/NavCam	-	Many individual images	- [4]
Comet 9P	Deep Impact-HRI/MRI/ITS	-	Many individual images	- [3]
	Stardust NExT-Navigation Camera	-	Many individual images	- [3]

Table 3: Elevation data with resolution and corresponding mission and instrument (sources are grouped per body).

Body	Instrument	Resolution (m/p)	Type	Size / source
The Moon	LROC-WAC	100	Global DTM	± 9 GB [7]
	LROC-LOLA	118	Global DEM	8 GB [8]
Mars	MGS-MOLA / MEX-HRSC	200	Global DEM	11 GB [2]
	MRO-HiRISE	1.0	Local DTM (Jezero crater)	1.8 GB [10]
	MRO-HiRISE	1.0	Multiple local DTMs	Variable [13]
Mercury	MESSENGER-WAC/NAC	665	Global DEM	506 [6]
	MESSENGER-WAC/NAC	78 - 500	Local DTMs	(Manheim et al., 2022)
	MESSENGER-WAC/NAC	250	Local DTM	(Preusker, Oberst, et al., 2012)
Ceres	Dawn-FC (HAMO)	135	Global DTM	446 MB [3] / (Preusker et al., 2016)
Vesta	Dawn-FC (HAMO)	100	Near-global DTM	(Roatsch et al., 2012)
Comet 67P	Rosetta-NAC	-	Global Shape Model	(Preusker et al., 2017)

Comet 9P	Stardust NExT – Navigation Camera	± 2.5	3D-image (Deep Impact site)	2.68 MB [5]

A2: Relevant space missions and resulting imagery

The Moon

Missions

Lunar Orbiter (LO I – LO V) – *NASA 1966 & 1967*

The Lunar Orbiter program consisted of five imaging satellites launched in 1966 through 1967 that provided global coverage of the lunar surface. The images captured by these spacecrafts were the first to be taken from lunar orbit. This was done so that potential landing sites for the Apollo program could be examined. [2, 3]

Imaging system: The Lunar Orbiters had a dual-lens camera. It used a high-resolution narrow angle lens and a medium-resolution wide angle lens to capture images on the same roll of film, simultaneously. [1]

Lunar Reconnaissance Orbiter (LRO) – *2009*

The LRO mission is a more modern lunar mission, launched in 2009. The objective of this mission, similar to its predecessors, was to map the surface of the moon in order to prepare for future human landings, this time with a 0.5 m/pixel resolution and in a polar orbit. Alongside mosaic images, the mission aimed to map global topography. Furthermore, the presence of water ice in permanently shadowed craters on the south pole was investigated. [3] The mission would have ended after one year, but the spacecraft since has continued operation around the moon with extended mission objectives. [9]

LROC: The camera system on board is called the Lunar Reconnaissance Orbiter Camera and contains multiple sensors. One of these is the wide-angle camera (WAC), which has a resolution of 100 m/pixel. A global lunar DTM has been constructed with this camera, with 100 m x 100 m resolution (GLD100). The system also contains two narrow angle cameras (NAC), both with resolutions of 0.5 m/pixel, used for high resolution images of the surface. [5]

LOLA: The Lunar Orbiter Laser Altimeter is an instrument that measures the elevation of the lunar surface based on the travel time of laser pulses. The pulse is split into five beams that create swaths spaces 1.25 from each other at the equator. Due to the polar orbit, the coverage of LOLA is better at the poles. [6]

Imagery

Mosaics: A global mosaic of the lunar surface is available with 59 m/pixel resolution, which was constructed using various Lunar Orbiter spacecraft covering different areas (III, IV & V) [1]. Later, a 100 m/pixel resolution global mosaic was constructed with LROC-WAC images [4]. The LROC-NAC images are used for detailed mosaic images of specific areas of interest, as well as the polar regions. [9]

Elevation model: From the LROC-WAC images, a global DTM is constructed with a 100 m/pixel resolution, divided into 10 TIFF files covering four sections of both hemispheres up to 60° and the two poles [7]. From the LOLA data, another global DEM was constructed with a resolution of 118 m/pixel (at the equator). The elevations were calculated relative to the lunar reference radius of 1737.4 km. Where shadows in the LROC-WAC images limited DTM construction in the polar regions, the LOLA based DEM provides accurate data there. [7, 8]

Mars

Missions

Viking 1 & 2 missions – *NASA 1975*

The Viking missions were two identical spacecraft consisting of an orbiter and a lander. Both were launched in 1975 and both landers reached the surface in 1975. The Viking 1 lander conducted the first successful landing on Mars. The main objectives of the orbiters were to survey the surface to identify the landing sites and bring the landers to the planet to take measurements. [13]

VIS: The Visual Imaging Subsystem consisted of two cameras that made images of the surface with resolutions ranging from 150 to 300 m/pixel. Specific areas of interest were imaged with 8 m/pixel resolution. [13]

Mars Global Surveyor (MGS) – *NASA 1996*

The Mars Global Surveyor, or MGS was launched in November 1996 and began its observation of Mars in 1999. The mission ended in 2006. The probe has a near polar orbit, making the North to South (DEM) measurements of higher quality than the East to West measurements, since data needs less computation to be sequential (Quantin et al., 2004). The mission helped with selecting a landing site for future rover missions, and even found evidence of flowing water in gullies. [1]

MOLA: The Mars Orbiter Laser Altimeter was an instrument that provided altimetry data by sending infrared pulses to the Martian surface. This enabled the construction of topographic maps with accuracies of 463 m/pixel and later 200 m/pixel and a vertical precision of 30 cm. The instrument further acted as a passive radiometer at a wavelength of 1064 nm. [1, 2]

MOC: The Mars Orbiter Camera is a dual-mode camera system. Similar to the LROC system, it as a wide-angle camera (WAC) and a narrow angle camera (NAC). The wide-angle camera shows a colored fish-eye perspective of the planet with 7.5 km/pixel resolution, allowing for daily global monitoring. Many WAC images in sequence create a time lapse animation, with which large scale features such as storms or large sand dunes can be tracked. The WAC also obtained context images for the narrow angle camera with 240 m/pixel resolution. The narrow angle camera created high resolution greyscale images with resolutions from 1.5 to 12 m/pixel, with which geological studies could be conducted. [1, 3]

Mars Express spacecraft (MEX) – *ESA 2003*

The first European mission to Mars, the Mars Express mission (MEX), was launched in 2003 and entered its near polar target orbit in January 2004. Its objectives included a detailed study of the chemical composition of the atmosphere, mapping mineral composition of the surface, finding evidence of past water and, most importantly, mapping the surface of Mars in high detail and in 3D. The mission also included study of the moon Phobos. The Beagle 2 lander was also a part of the mission, but unfortunately it failed to deploy correctly. [4]

HRSC: The High-Resolution Stereo Camera produces full color images of Mars with a resolution of 10 m/pixel. Areas of interest can be imaged with 2 m/pixel resolution. The stereo camera can produce 3D images in full color, with a 50 m/pixel grid size and a vertical accuracy of 10 m. [2,4]

VMC: The Visual Monitoring Camera was originally intended to be used for confirming the Beagle 2 separation but has since been used for capturing images of the planet from horizon to horizon. This view is used to track large scale storms. [4]

Mars Reconnaissance Orbiter (MRO) – *NASA 2005*

The Mars Reconnaissance Orbiter (MRO) was launched in 2005, has been orbiting Mars since 2006, and is still active today. It has 6 science instruments on board, of which the relevant ones are listed below. The main objectives of this mission include characterizing the atmosphere and climate, investigating water and ice in the subsurface, and mapping the surface in high resolution. This detailed mapping was done for the identification of several objectives, such as water-related landforms, stratigraphic and compositional evidence of water, and potential future landing sites. The orbiter was further used as a communication relay between Marian surface missions and Earth. [7]

HiRISE: High Resolution Imaging Science Experiment is a high-resolution camera. Its spectral range of 400 – 1000 nm allows it to capture light in the visual spectrum as well as near infrared (B, G, R & NIR). The resolution, or ground sample distance (GSD) is 30 cm/pixel from an altitude of 300 km. This allows the identification of objects of roughly 1 meter in size, like boulders. [5, 6]

CTX: The Context Camera produces 6 m/pixel resolution greyscale images in 500-800 nm wavelength (visible light). The purpose of this camera is to provide context to high-resolution observations by other instruments like HiRISE and CRISM. For this reason, the images are made simultaneously with the HiRISE instrument, so that they can be easily linked together. [5, 7]

CRISM: The Compact Reconnaissance Imaging Spectrometer for Mars is used for the identification of water-related minerals on a global scale, but also at specific locations in higher detail. [7]

Imagery

Mosaics: The Viking missions made global surface observations of 150 – 300 m/pixel resolution, as well as local observations with 8 m/pixel resolution. From these observations a detailed black and white mosaic was made, which was later combined with original Viking color images to form a global full color mosaic with a 232 m/pixel resolution [11, 13]. The Bruce Murray Laboratory for Planetary Visualization, which is a part of the California Institute of Technology, produced a global mosaic of Mars based on the MRO-CTX images. This mosaic covers 99.5% of the planet with a resolution of 5 m/pixel [8]. The HiRISE images are of very high quality and although they are not often used in large scale mosaics due to their high detail, they provide invaluable data individually [12]. This being said, for the Mars2020 mission that featured the landing of the Perseverance rover in the Jezero crater, an orthorectified mosaic with 0.25 m/pixel resolution was constructed to map hazards in the landing area. [9]

Elevation models: With the MOLA (MGS) instrument, a global DEM was constructed with a resolution of 463 m/pixel. Later, this DEM was combined with data from the HRSC (MEX) camera to form a new DEM with a resolution of 200 m/pixel [2]. Using the HiRISE camera on the MRO, a 1 m/pixel DTM was constructed of the Mars2020 landing site (Jezero crater), alongside the orthomosaic mentioned previously [10]. With the MRO-HiRISE images, many small-scale high resolution DTMs are created from stereo image pairs, with resolutions of 1.0 m/pixel [12].

Mercury

Missions

Mariner 10 – *NASA 1973*

The Mariner 10 mission performed a flyby pas Mercury and Venus flyby and was launched in 1973. This was the first mission to Mercury, so it made the first actual pictures of the surface, and the first measurements of temperatures and magnetic field. During the first encounter of the planet, it was determined that Mercury does not have a measurable atmosphere. In total, the spacecraft made three flybys, the closest of which was 5768 km, and returned 2700 pictures covering almost half the planet. [1]

MESSENGER – *NASA 2004*

The MErcury Surface Space ENvironment GEochemistry and Ranging (MESSENGER) mission to Mercury was a part of NASA's Discovery Program. It was the first spacecraft to orbit the planet and map it in its entirety. It was launched in 2004 and entered orbit in 2011, where it made observations for four years until the mission ended with a controlled impact in 2015. [3]

MDIS: The Mercury Dual Imaging System is a camera system on board of MESSENGER, and it has an average resolution of 250 m/pixel. It contains a multispectral wide-angle camera (WAC), capturing visible to near-infrared light (395 to 1040 nm). It also contains a narrow angle camera (NAC), which made monochrome images with a resolution of up to 10 m/pixel (Blewett et al., 2011). [5]

MLA: The Mercury Laser Altimeter provides accurate altitude measurements using an infrared laser pulse, calculating the distance based on two-way travel time. The accuracy of the measured altitude was 30 cm, and this data served as reference for DEMs created with MDIS data [5]. Due to the orbit of MESSENGER, the southern hemisphere was more difficult to reach with this instrument, so data was less accurate here (Preusker, Oberst, et al., 2012).

Imagery

Mosaics: The Mariner 10 observations resulted in the construction of multiple mosaics with varying resolutions of up to 90 m/pixel [2].

The MESSENGER MDIS imagery was used to construct multiple global mosaics. One of these was the 'surface morphology base map' with an average resolution of 166 m/pixel or better [4,5]. Alongside this map, a 'color base map' covering eight different narrow-band color filters was created using only the WAC instrument. This map had a 665 km/pixel resolution. Additionally, a 'stereo base map' was created using images from the WAC instrument with a different angle than used in the morphology base map. Both have non-vertical solar illumination so that shadows would indicate morphology. This map had an average resolution of 166 m/pixel and allowed the construction of a stereo DTM. Finally, a low incidence angle mosaic was constructed to minimize shadows and thus better visualize reflectance properties of the surface. This also has an average resolution of 166 m/pixel. [4,5]

Elevation models: With the MDIS camera system, a global DEM was constructed with a resolution of 665 m/pixel. The elevation of points in this DEM is relative to the reference sphere with a radius of 2439.400 km [6]. High resolution regional DEMs were created from MDIS images combined with data from the MLA for geodetic reference. This was done for 57 DEMs covering nine areas of interest. The horizontal resolution of these DEMs ranges from 78 m/pixel to 500 m/pixel. The vertical resolution is smaller than the DEM pixel scale (Manheim et al., 2022). Furthermore, from the stereo images created by the MDIS-WAC mentioned earlier, Preusker, Oberst, et al. (2012) created a regional DTM showing the possibility of accurate elevation models even in places where the MLA does not provide sufficient data.

Ceres

Missions

Dawn Mission – *NASA 2007*

Like MESSENGER, the Dawn mission was a part of the NASA's Discovery Program and launched on September 27th, 2007. The mission targeted, for the first time, the two largest bodies in the asteroid belt. First it orbited the asteroid Vesta for 14 months and then left for the dwarf planet Ceres, where it stayed in orbit for three years. It was the first spacecraft to orbit two extra-terrestrial bodies, as well as the first to orbit a dwarf planet. The objective of the Dawn mission was to gain understanding about

these protoplanets, as they provide insight in the early development of planets. The mission ended with a controlled impact into the surface of Ceres in November 2018. [1]

VIR: The Visual and Infrared spectrometer is a camera system that makes observations in two channels. One covering visual light with wavelengths between 250 and 1000 nm and another covering infrared light with wavelengths between 1000 and 5000 nm. The VIR is used to determine mineralogical compositions based on spectral profiles. (Russell & Raymond, 2011) [1]

GRaND: The Gamma Ray and Neutron Detector is used for investigating the elemental composition of the top meter of the subsurface. This instrument can be used to determine if a body is rich in water ice or other volatiles (Russell & Raymond, 2011).

FC: The Framing Camera is used for detailed observation of the surface. It covers wavelengths from visual light to near infrared and has a broadband clear filter and seven narrowband filters (400 - 1000 nm). The framing camera provides multiple stereo coverage by changing its observation geometry. This camera observes the shape and surface characteristics of both protoplanets with resolutions of 25 m/pixel and 62 m/pixel for Vesta and Ceres, respectively. The camera was used in both high and low altitude mapping orbits, HAMO and LAMO, for different phases of the mission. (Russell & Raymond, 2011) [1]

Imagery

Mosaic: The Dawn HAMO mosaic of Ceres has a resolution of 140 m/pixel. At high latitudes, these images are hard to interpret, and they begin to behave strangely and give different values [2]. During the LAMO phase of the mission, images were collected with which a 35 m/pixel global mosaic was constructed (Roatsch et al., 2017). The framing camera using the clear filter was used to provide extra mosaics for both HAMO and LAMO [4].

Elevation model: The DAWN global DTM of Ceres has a resolution of 135 m/pixel with ±10 m vertical accuracy and is derived from stereo imagery pairing. The elevation is taken relative to a reference biaxial ellipsoid with dimensions 482 x 482 x 446 km (Preusker et al., 2016). [3]

Vesta

Missions

NASA's Dawn mission discussed earlier also visited Vesta. See the previous section for information on this mission.

Imagery

Mosaic: The Dawn HAMO mosaic of Vesta has a resolution of 60 m/pixel. Unfortunately, the northern regions of Vesta are largely in shadow because of the northern winter during the LAMO phase of the Dawn mission (Parekh et al., 2021; Roatsch et al., 2012). [1]

During the LAMO phase of the Dawn mission, high resolution imagery was collected and used to construct a global mosaic with a resolution of 20 m/pixel (Roatsch et al., 2013). [2]

Elevation model: The DAWN global DTM of Vesta has a resolution of ±100 m/pixel with ±5 m vertical accuracy and is derived from stereo imagery pairing from images taken during the HAMO mission phase. The elevations are relative to a biaxial ellipsoid with dimensions 285 x 285 x 229 km (Preusker, Scholten, et al., 2012).

C67P

Missions

Rosetta - Philae – *ESA 2004*

The Rosetta - Philae mission, also just called Rosetta, was a combined orbiter – lander mission conducted by the European Space Agency. The objective was to orbit a comet for the first time, land the Philae probe on the surface, and study the nucleus. The spacecraft was launched in March of 2004 and reached the comet in August 2014, when it entered orbit. On the way, Rosetta made observations of the Deep Impact event at comet 9P/Tempel 1, discussed later. In November 2014, the Philae probe landed on the surface. The mission ended two years later with a controlled impact on the surface. [1,2]

OSIRIS: The Optical, Spectroscopic, and InfraRed Imaging System is the main imaging system of the orbiter. It has narrow-angle camera (NAC) and a wide-angle camera (WAC). The NAC has a spectral range of 250 to 1000 nm, using 12 filters. It was used to observe the surface of the nucleus from different altitudes resulting in different resolutions up to 2 cm/pixel (from 1 km). The WAC was primarily used for observing dust and gas emissions around the nucleus using its 14 filters offering a spectral range of 240 to 720 nm. From an altitude of 100 km, the NAC and WAC have resolutions of 1.86 m/pixel and 10.1 m/pixel, respectively. [2]

NavCam: The Philae lander also had a navigation camera, called NavCam. This camera was mainly intended for locating certain stars and constellations for navigational purposes.

Other instruments: The spacecraft also contained many other instruments, including an ultraviolet imaging spectrometer ALICE, a visible and infrared mapping spectrometer VIRTIS and a microwave instrument MIRO. [3]

Imagery

With the OSIRIS imaging system, many photographs of the surface have been made with varying extents and resolutions. The WAC mainly took photos of the outline of the comet, showing its odd two lobed shape, while the NAC made detailed observations of the surface and its features. The NavCam also provided images of the comets' surface. [4]

Using photogrammetry, the NAC images were used to create a detailed shape model of the comet. This allowed for measurements of the comets' volume and density. Although this model is complete, the data was collected over a period of 18 months so inaccuracies may be present due to a changing surface. (Preusker et al., 2017)

C9P

Missions

Deep Impact – *NASA 2005*

The Deep Impact mission was launched in January of 2005 and its objective was to hit comet 9P/Tempel 1 with a small impactor and observe the effect with a flyby spacecraft. After the mission concluded in August of 2005, it completed a flyby of another comet (103P/Hartley 2) in 2010 before communication was lost in 2013. [1]

HRI: The High-Resolution Instrument is the main camera on the spacecraft. It has both a multispectral camera with a filter wheel and an infrared spectrometer. At a distance of 700 km, their resolutions are 2 m/pixel and 10 m/pixel, respectively. Even though the spacecraft included star trackers, this camera also served as a navigation aid. [1,2]

MRI: The Medium Resolution Instrument acts like a backup for the HRI. It collects visible light images with 10 m/pixel resolution from 700 km. At closest approach, roughly 500 km, the MRI covers an area 1.2 times the diameter of the comet nucleus with a 7 m/pixel resolution. This allows it to capture context images for the detailed HRI data, as well as images of the impact ejecta. Like the HRI, this instrument also helped with navigation. [1,2]

ITS: The Impactor Targeting Sensor was the main camera on the impactor and was used for navigating the object to the nucleus. It was very similar to the MRI, except it didn't have a filter wheel. The maximum resolution of the camera was 0.5 m/pixel at its closest distance before the impact. [2]

Stardust NExT – *NASA 1999*

The Stardust mission was launched in February 1999 and was planned to fly past asteroid 5535 Annefrank and comet 81P/Wild 2. Its objective was to collect and return interstellar dust particles and comet coma particles. After the mission successfully concluded with the sample return in 2006, the extended mission New Exploration of Tempel 1 (NExT) began. In February 2011, the spacecraft flew past comet 9P/Tempel 1 at a distance of 181 km and collected images. On these images the Deep Impact crater was finally confirmed. [4]

Navigation Camera: This camera, though used primarily for navigation, was also used to capture images of the comets and asteroids it flew past. For each of these, 72 images were taken [4]

Imagery

No image mosaics are created of the comet, but many of the HRI and ITS images show a detailed view of the entire comet nucleus. The ITS images from the descent phase show higher resolution images where some surface features can be seen. Images captured by Stardust NExT show the Deep Impact mission's impact site with a resolution of roughly 2.5 m/pixel. A 3D image has also been constructed of the area. [3,5]

Non-literary sources A1 and A2:

Moon:

[1] https://astrogeology.usgs.gov/search/map/Moon/Lunar-Orbiter/Lunar_LO_MR_Mosaic_Global_59m;
[2] https://www.nasa.gov/lunar-orbiters/;
[3] https://en.wikipedia.org/wiki/Lunar_Orbiter_program;
[4] https://astrogeology.usgs.gov/search/map/Moon/LRO/LROC_WAC/Lunar_LRO_LROC-WAC_Mosaic_global_100m_June2013;
[5] https://www.lroc.asu.edu/about;
[6] https://science.nasa.gov/mission/lro/lola/;
[7] https://wms.lroc.asu.edu/lroc/view_rdr/WAC_GLD100; [8] https://astrogeology.usgs.gov/search/details/Moon/LRO/LOLA/Lunar_LRO_LOLA_Global_LDEM_118m_Mar2014/cub;
[9] https://www.lroc.asu.edu/about/objectives;
[10] https://www.lroc.asu.edu/images

Mars:

[1] https://science.nasa.gov/mission/mars-global-surveyor/;
[2] https://astrogeology.usgs.gov/search/map/Mars/Topography/HRSC_MOLA_Blend/Mars_HRSC_MOLA_BlendDEM_Global_200mp;
[3] https://www.msss.com/all_projects/mgs-mars-orbiter-camera.php;
[4] https://www.esa.int/Science_Exploration/Space_Science/Mars_Express;
[5] https://science.nasa.gov/mission/mars-reconnaissance-orbiter/;
[6] https://www.uahirise.org/specs/;
[7] https://science.nasa.gov/resource/mars-reconnaissance-orbiter-fact-sheet/
[8] https://murray-lab.caltech.edu/CTX/index.html
[9] https://astrogeology.usgs.gov/search/map/Mars/Mars2020/JEZ_hirise_soc_006_orthoMosaic_25cm_Eqc_latTs0_lon0_first
[10] https://astrogeology.usgs.gov/search/map/Mars/Mars2020/JEZ_hirise_soc_006_DTM_MOLAtopography_DeltaGeoid_1m_Eqc_latTs0_lon0_blend40;
[11] https://astrogeology.usgs.gov/search/map/Mars/Viking/MDIM21/Mars_Viking_MDIM21_ClrMosaic_global_232m;

[12] https://www.uahirise.org/;
[13] https://science.nasa.gov/mission/viking/
[14] https://www.msss.com/msss_images/index.html

Mercury:

[1] https://science.nasa.gov/mission/mariner-10;
[2] https://photojournal.jpl.nasa.gov/spacecraft/Mariner%2B10;
[3] https://science.nasa.gov/mission/messenger/;
[4] https://messenger.jhuapl.edu/Explore/Images.html#global-mosaics;
[5] https://messenger.jhuapl.edu/About/Spacecraft-and-Instruments.html;
[6] https://astrogeology.usgs.gov/search/map/Mercury/Topography/MESSENGER/Mercury_Messenger_USGS_DEM_Global_665m_v2

Ceres:

[1] https://science.nasa.gov/mission/dawn/;
[2] https://astrogeology.usgs.gov/search/map/Ceres/Dawn/DLR/FramingCamera/Ceres_Dawn_FC_DLR_global_59ppd_Feb2016;
[3] https://astrogeology.usgs.gov/search/map/Ceres/Dawn/DLR/FramingCamera/Ceres_Dawn_FC_HAMO_DTM_DLR_Global_60ppd_Oct2016;
[4] https://sbn.psi.edu/pds/resource/dawn/dwncfcmosaics.html

Vesta:

[1] https://astrogeology.usgs.gov/search/map/Vesta/Dawn/DLR/HAMO/Vesta_Dawn_FC_HAMO_Mosaic_Global_74ppd.cub;
[2] http://dawn_gis.dlr.de/atlas_dir/lamo.html

Comet 67P:

[1] https://www.esa.int/Science_Exploration/Space_Science/Rosetta_overview;
[2] https://www.mps.mpg.de/en/rosetta/osiris;
[3] https://www.esa.int/Science_Exploration/Space_Science/Rosetta/Rosetta_factsheet;
[4] https://imagearchives.esac.esa.int/index.php?/category/1;

Comet 9P:

[1] https://science.nasa.gov/mission/deep-impact-epoxi/;
[2] https://deepimpact.astro.umd.edu/tech/index.html;
[3] https://photojournal.jpl.nasa.gov/target/Other?subselect=Mission%3ADeep+Impact%3ATarget%3ATempel+1;
[4] https://science.nasa.gov/mission/stardust;
[5] https://photojournal.jpl.nasa.gov/catalog/PIA13872

A3 Global distributions of mass wasting

Here, global maps are presented with the distribution and classification of mass wasting features for the Moon, Mars, Mercury, Ceres and Vesta. The individual maps are also uploaded separately in higher quality as PDF files.

A3.1 Mass wasting map of the Moon

Map containing all mass wasting features on the Moon. In the legend, colors indicate movement type and shapes indicate the different authors. The background is a 100 m/p global mosaic based on LROC-WAC imagery in simple cylindrical projection. The elevation layer is a 118 m/p global DEM based on LRO-LOLA data.

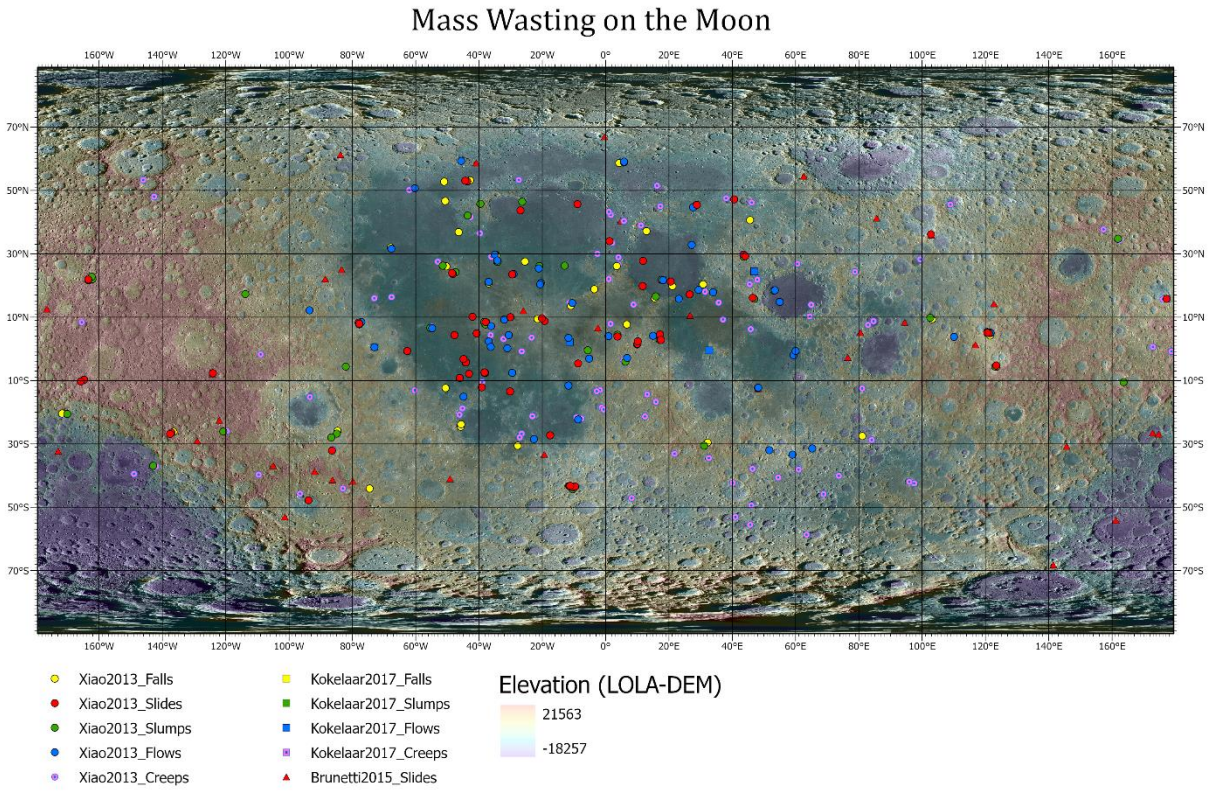

A3.2 Mass wasting map of Mars

Map containing all mass wasting features on Mars. In the legend, colors indicate movement type and shapes indicate the different authors. The background is a 232 m/p global mosaic based on Viking MDIM2.1 imagery in simple cylindrical projection. The elevation layer is a 200 m/p global DEM based on MGS MOLA data.

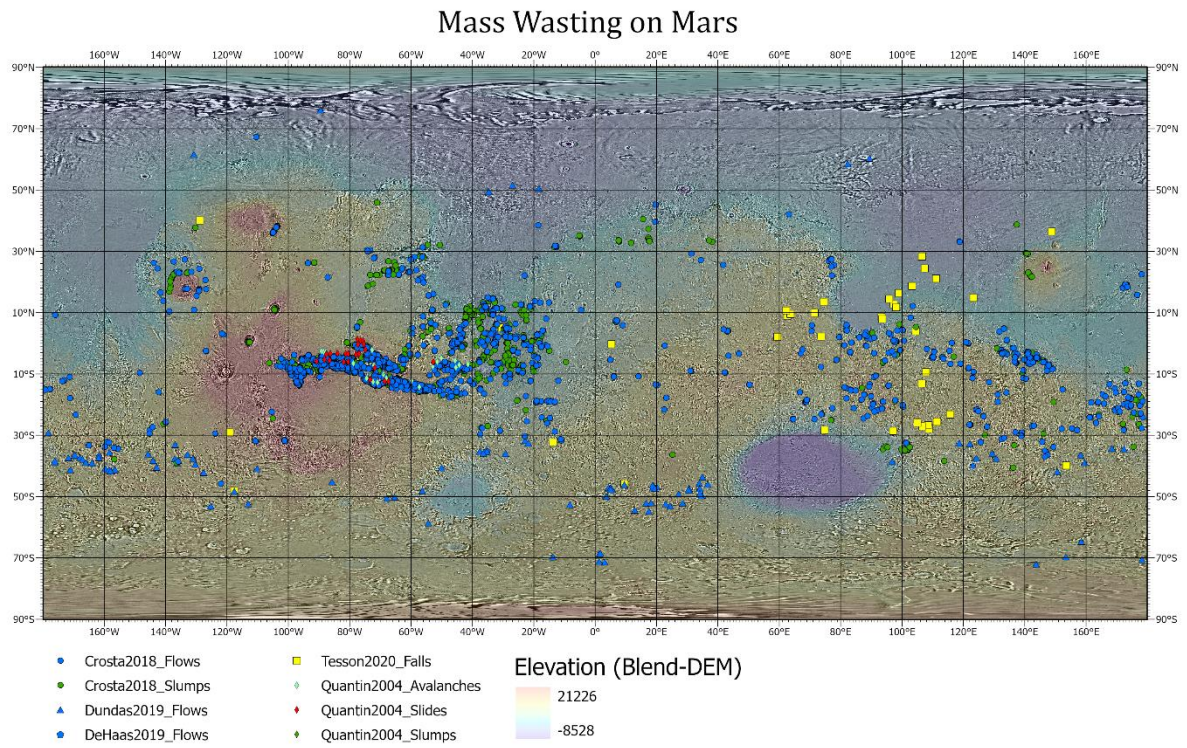

A3.3 Mass wasting map of Mercury

Map containing all mass wasting features on Mercury. In the legend, colors indicate movement type and shapes indicate the different authors. The background is a 250 m/p global mosaic based on MESSENGER MDIS NAC and WAC imagery in equirectangular projection. The elevation layer is a 665 m/p global DEM based on MESSENGER MDIS NAC and WAC data.

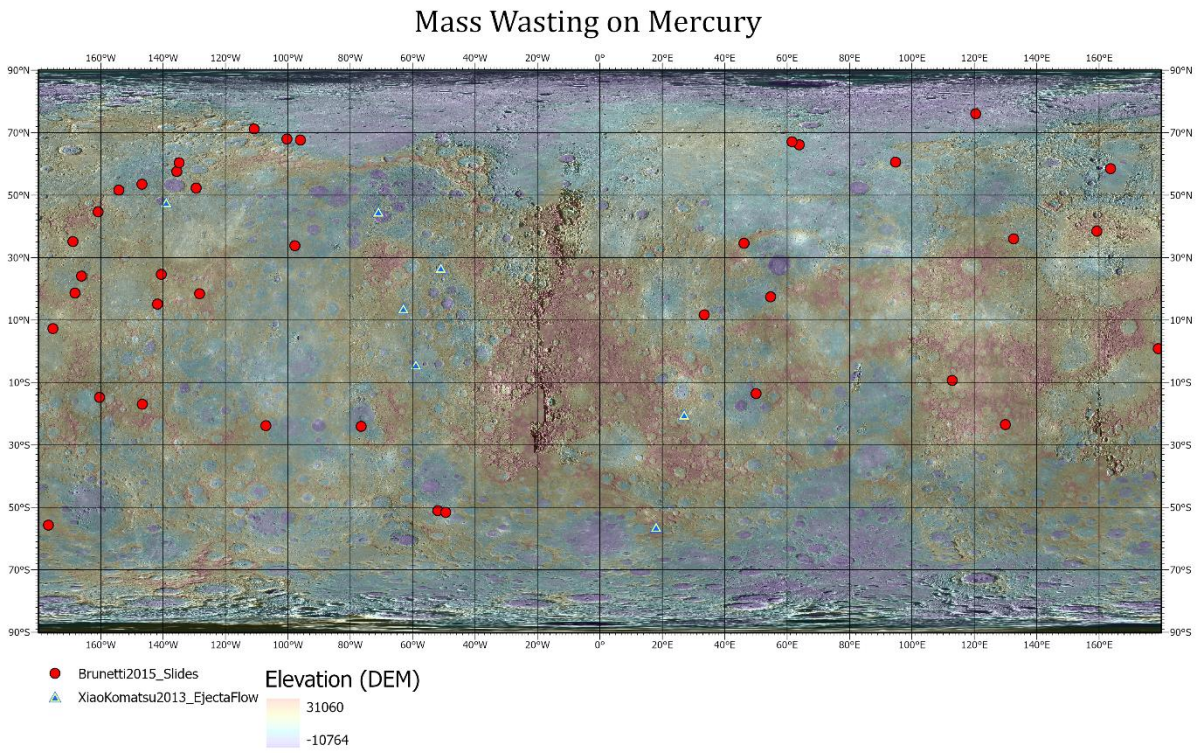

A3.4 Mass wasting map of Ceres

Map containing all mass wasting features on Ceres. In the legend, colors indicate movement type and shapes indicate the different authors. The background is a 140 m/p global mosaic based on Dawn Framing Camera HAMO imagery in simple cylindrical projection. The elevation layer is a 135 m/p global DEM based on Framing Camera HAMO data.

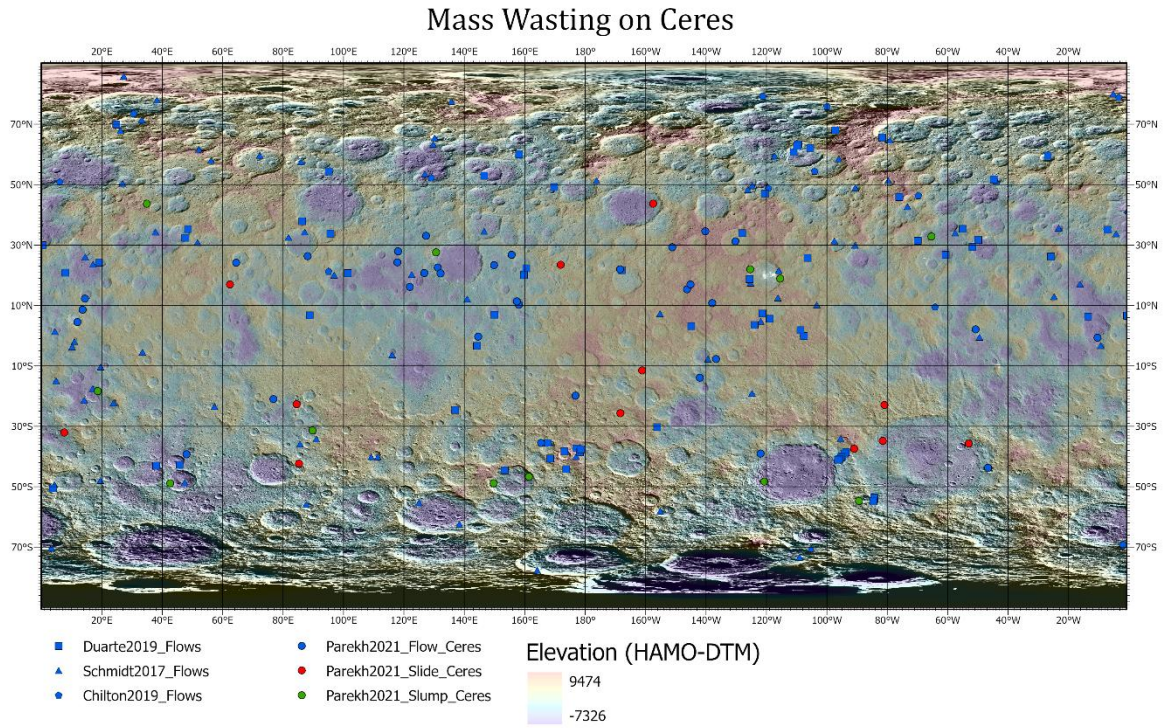

A3.5 Mass wasting map of Vesta

Map containing all mass wasting features on Vesta. In the legend, colors indicate movement type and shapes indicate the different authors. The background is a 60 m/p near-global mosaic based on Dawn Framing Camera HAMO imagery in simple cylindrical projection. The elevation layer is a 100 m/p near-global DTM based on Framing Camera HAMO data. Due to the position of the asteroid during data collection, the northern hemisphere is partly covered in shadow.

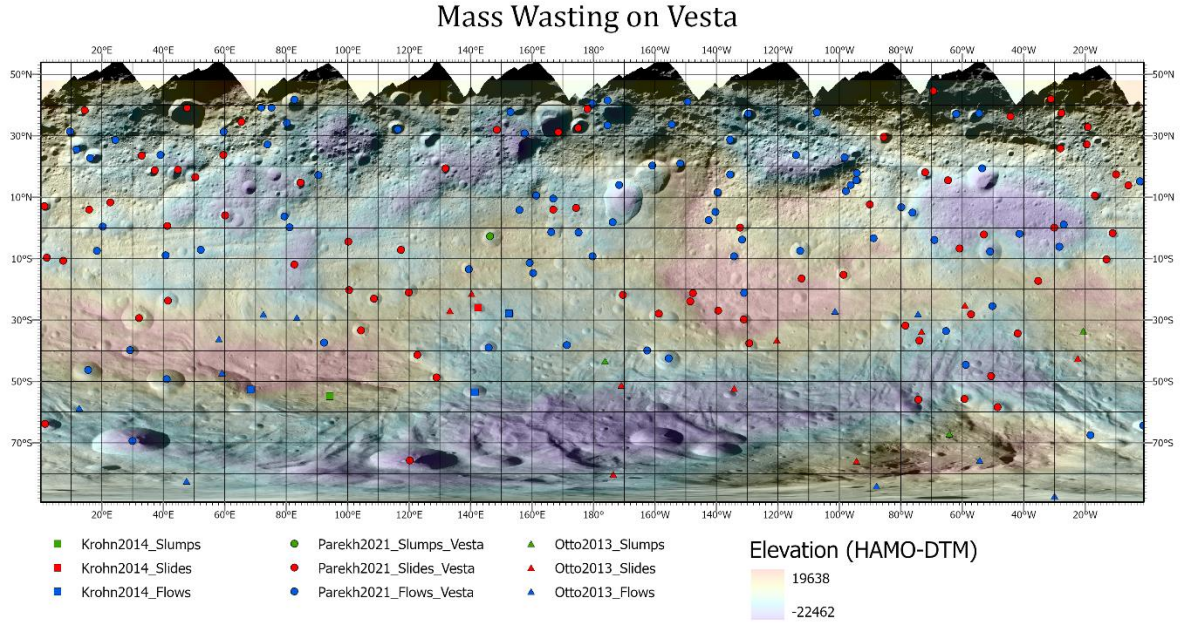

A4 Dataset extraterrestrial mass wasting

A dataset of all the collected mass wasting features on the bodies discussed in this review is uploaded separately with the name: “Mass_Wasting_Data.xlsx”. This dataset contains data from several authors, as well as measurements carried out using the NASA Trek services or using ArcGIS pro. For each feature, if available, the following information is given in the spreadsheet:

- ID: The ID of the feature consists of two letters indicating the body, followed by a three-digit number.
- Latitude: Latitude in degrees, from -90° to 90°
- Longitude: Longitude in degrees, from -180° (west) to 180° (east)
- Crater / basin / chasma: Short description of the location of the feature, like the name of the crater in which it was found.
- Classification / *reclassification*: The movement class. If the feature was reclassified to fit the classes discussed in chapter 2, this is written in italics.
- Crater diameter: Diameter of the host crater, in km.
- Slope information: If available, the slope measured in degrees (°) of two slope sections.
    - Initiation slope
    - Deposition slope
- Area: Planimetric area of the feature, given in km^2.
- Volume: Volume of the displaced material, in km^3.
- Runout length: Length of the feature, from detachment point (often crater rim) to furthest deposit. Given in km.
- Fall height: Elevation difference between detachment point and furthest deposit, in km.
- Friction coefficient: The friction coefficient as a measurement of mobility. This is calculated by dividing the fall height *H* by the runout length *L*. This is a dimensionless coefficient. If the value is calculated within the datasheet, this is indicated by bold text.
- Boulder transport: Indication if boulder transport is observed within the feature.
- Article: Article where the data was taken from.
- Name in source: The name of the feature in the source article or dataset.
- Spacecraft / Mission: The mission that gathered the data used to identify the feature.
- Sensor: The sensor that captured the image used for identification.
- Additional information: Extra notes relevant to the specific feature or data.